Impulsive noise detection and mitigation in communication systems

by

Reza Barazideh

B.S., Amirkabir University of Technology, Iran, 2006

M.S., Shahed University, Iran, 2009

AN ABSTRACT OF A DISSERTATION

submitted in partial fulfillment of the
requirements for the degree

DOCTOR OF PHILOSOPHY

Department of Electrical and Computer Engineering
Carl R. Ice College of Engineering

KANSAS STATE UNIVERSITY
Manhattan, Kansas

2019

Abstract

Impulsive noise is a widespread and rapidly growing source of harmful interference in many applications such as vehicular communications, power line communication (PLC), underwater acoustic (UWA) communication, and Internet of Things (IoT). Noise of this type may originate from a variety of sources such as motors, high efficiency lighting, and even other wireless systems such as pulse-type or frequency-modulated continuous wave (FMCW) radars. Impulsive interference can reduce signal quality to the point of reception failure and increase bit errors resulting in degradation in system reliability. Multicarrier transmission techniques and, in particular, orthogonal frequency division multiplexing (OFDM), is proposed to cope with the frequency selectivity of the propagation channel. Although, OFDM provides some level of robustness against impulsivity by spreading the power of impulsive noise over multiple subcarriers, its performance degrades dramatically if the power of impulsive noise exceeds a certain threshold.

Many mitigation techniques focus on reducing the interference before it reaches the receiver. In the context of this dissertation, the emphasis is on the reduction of interference that has already entered the signal path. Specifically, this dissertation aims to develop approaches to effectively detect and mitigate the severe impact of the impulsive noise. Here, we investigate two different categories of impulsive noise suppression techniques that can be used as a stand-alone solution or combined with other interference reduction techniques.

First, we design and develop Blind Adaptive Intermittently Nonlinear Filters (BAINFs) for analog-domain mitigation of impulsive noise. The idea behind using analog domain mitigation is that insufficient processing bandwidth severely limits the effectiveness of digital nonlinear interference mitigation techniques. Therefore, the suppression of non-Gaussian noise in the analog domain before the analog to digital converter (ADC) where the outliers are more distinguishable can be helpful. The BAINFs can be implemented in many

structures and we propose some sample realizations of BAINFs that can be used in different applications. In this dissertation, we consider PLC and UWA communication systems as case studies. The performance of the proposed BAINFs in these systems is quantified analytically and with experimental data.

Secondly, in the classic threshold based outlier detection approaches, determining the optimum threshold is the main challenge as this threshold will vary in response to channel conditions and model mismatches. As always, there is a compromise between detection and false alarm probability in the traditional threshold based methods. To overcome this drawback, we propose a two stage impulsive noise mitigation approach. In the first stage, a machine learning approach such as a deep neural network (DNN) is used to detect the instances of impulsivity. Then, the detected impulsive noise can be mitigated in the suppression stage to alleviate the harmful effects of outliers. The robustness of the proposed DNN-based approach under (i) mismatch between impulsive noise models considered for training and testing, and (ii) bursty impulsive environment when the receiver is empowered with interleaving technique is evaluated.

Impulsive noise detection and mitigation in communication systems

by

Reza Barazideh

B.S., Amirkabir University of Technology, Iran, 2006

M.S., Shahed University, Iran, 2009

A DISSERTATION

submitted in partial fulfillment of the
requirements for the degree

DOCTOR OF PHILOSOPHY

Department of Electrical and Computer Engineering
Carl R. Ice College of Engineering

KANSAS STATE UNIVERSITY
Manhattan, Kansas

2019

Approved by:

Co-Major Professor
Dr. Balasubramaniam Natarajan

Approved by:

Co-Major Professor
Dr. Alexei V.Nikitin

Copyright

Abstract

Impulsive noise is a widespread and rapidly growing source of harmful interference in many applications such as vehicular communications, power line communication (PLC), underwater acoustic (UWA) communication, and Internet of Things (IoT). Noise of this type may originate from a variety of sources such as motors, high efficiency lighting, and even other wireless systems such as pulse-type or frequency-modulated continuous wave (FMCW) radars. Impulsive interference can reduce signal quality to the point of reception failure and increase bit errors resulting in degradation in system reliability. Multicarrier transmission techniques and, in particular, orthogonal frequency division multiplexing (OFDM), is proposed to cope with the frequency selectivity of the propagation channel. Although, OFDM provides some level of robustness against impulsivity by spreading the power of impulsive noise over multiple subcarriers, its performance degrades dramatically if the power of impulsive noise exceeds a certain threshold.

Many mitigation techniques focus on reducing the interference before it reaches the receiver. In the context of this dissertation, the emphasis is on the reduction of interference that has already entered the signal path. Specifically, this dissertation aims to develop approaches to effectively detect and mitigate the severe impact of the impulsive noise. Here, we investigate two different categories of impulsive noise suppression techniques that can be used as a stand-alone solution or combined with other interference reduction techniques.

First, we design and develop Blind Adaptive Intermittently Nonlinear Filters (BAINFs) for analog-domain mitigation of impulsive noise. The idea behind using analog domain mitigation is that insufficient processing bandwidth severely limits the effectiveness of digital nonlinear interference mitigation techniques. Therefore, the suppression of non-Gaussian noise in the analog domain before the analog to digital converter (ADC) where the outliers are more distinguishable can be helpful. The BAINFs can be implemented in many

structures and we propose some sample realizations of BAINFs that can be used in different applications. In this dissertation, we consider PLC and UWA communication systems as case studies. The performance of the proposed BAINFs in these systems is quantified analytically and with experimental data.

Secondly, in the classic threshold based outlier detection approaches, determining the optimum threshold is the main challenge as this threshold will vary in response to channel conditions and model mismatches. As always, there is a compromise between detection and false alarm probability in the traditional threshold based methods. To overcome this drawback, we propose a two stage impulsive noise mitigation approach. In the first stage, a machine learning approach such as a deep neural network (DNN) is used to detect the instances of impulsivity. Then, the detected impulsive noise can be mitigated in the suppression stage to alleviate the harmful effects of outliers. The robustness of the proposed DNN-based approach under (i) mismatch between impulsive noise models considered for training and testing, and (ii) bursty impulsive environment when the receiver is empowered with interleaving technique is evaluated.

Contents

List of Figures

List of Tables

Acknowledgments

I would like to express my deep gratitude to my advisors, Prof. Balasubramaniam Natarajan and Dr. Alexei V.Nikitin, for their guidance and encouragement. Special thanks to Dr. Bala for giving me the opportunity and freedom in this research journey to learn new things. You supported me greatly and were always willing to help me in all situations.

My sincere gratitude to my advisory committee members Dr. Bill Kuhn, Dr. Steve Warren, and Dr. Nathan Albin for their time and constructive comments and feedback that helped me to improve my dissertation.

I am grateful for having the opportunity to work with Dr. Zhaohui Wang and Wensheng Sun and thanks for their time and insightful comments that helped me improve my works.

I would also like to thank my officemates at WiCom group Solmaz Niknam, Alaleh Alivar, Hazhar S. Karimi, Kumar S. Jhala, and Wenji Zhang who brought lots of joy and pleasure to the office and made it feels like home.

I am also grateful to have my parents and family for their never ending love, kindness and unquestioned support. There are not enough words to describe how thankful I am to have them. Thank you for always being there for me. Special thanks to my father for always encouraging me in this endeavour.

I am very fortunate for having Solmaz, my love and my life partner by my side. You are the most amazing person in my life. Thank you for taking care of me beyond my dreams and expectations. Thank you for always supporting me through thick and thin.

Dedication

To my love, Solmaz, for her faith in me and all the happiness and joy she's brought to my life. And my family for their endless encouragement.

Acronyms

AC	Alternating Current
ACDL	Adaptive canonical differential limiter
ADC	Analog to digital convertor
ANDL	Adaptive nonlinear differential limiter
ANP	Analog nonlinear preprocessor
αSGN(m)	Alpha sub-Gaussian noise with memory order m
AWGN	Additive white Gaussian noise
BAINFs	Blind Adaptive Intermittently Nonlinear Filters
BB-PLC	Broadband power-line communication
BER	Bit error rate
BG	Bernouli-Gaussian
BPSK	Binary phase shift keying
CFO	Carrier frequency offset
CLT	Central Limit Theorem
CMTF	Clipped Mean Tracking Filter
CP	Cyclic prefix
CS	Compressive sensing
DFT	Discrete Fourier transform
DNN	Deep neural network
FDI	Frequency-domain interleaving
FEC	Forward error correction
FFT	Fast fourier transform
FMCW	Frequency-modulated continuous wave
GM	Gaussian Mixture
HFM	Hyperbolic frequency-modulated
IC	Integrated circuit
ICI	inter-carrier-interference
IDFT	Inverse discrete Fourier transform
IQR	Interquartile range
ISI	Inter-symbol interference
LDPC	Low-density parity-check
LFM	Linear frequency-modulated

LMMSE	Linear minimum mean squared error
LMP	Locally most powerful
LS	Least squares
LTE	Long term evolution
MANP	Memoryless Analog Nonlinear Preprocessor
MCA	Middleton Class A
MF	Matched filter
MMSE	Minimum mean square error
MSE	Mean square error
NB-PLC	Narrowband power-line communication
OFDM	Orthogonal frequency-division multiplexing
OTA	Operational transconductance amplifier
PAPR	Peak to average power ratio
PDF	Probability density function
PLC	power-line communication
PRIME	Power-line intelligent metering evolution
PSD	Power spectrum density
PSK	Phase shift keying
QAM	Quadrature amplitude modulation
QPSK	Quadrature phase shift keying
QTFs	Quartile Tracking Filters
ReLU	Rectified linear unit
RF	Radio Frequency
RL	Reinforcement learning
ROAD	Rank-Ordered Absolute Differences
SαS	Symmetric Alpha Stable
SBL	sparse Bayesian learning
SINR	Signal to thermal plus impulsive noise ratio (SINR)
SIR	Signal to interference ratio
SNR	Signal to noise ratio
TDI	Time-domain interleaving
UWA	Underwater acoustic
V2G	Vehicular to grid
WAVE	Wireless Access in Vehicular Environments
WSαSN	White symmetric alpha-stable noise
ZP	Zero padding

Chapter 1

Introduction

1.1 Overview and Motivation

Noise is a fundamental consideration in the design of any communication and data acquisition system and manifests in different forms. It is well known that the performance of systems can be severely limited by Gaussian, non-Gaussian, and impulsive interference[4]. Impulsive or narrowband interference can reduce signal quality to the point of reception failure or increase bit errors which degrade the system and result in lower data rates. In the presence of interference the transmitter needs to increase output power which increases its interference to nearby receivers and reduces the battery life of a device.

Technogenic noise is a widespread and rapidly growing source of harmful interference within various electronic devices, systems, and services[5–7]. This interference originates from various sources such as mutual interference of multiple devices integrated in a system (for example, a smartphone equipped with WiFi, Bluetooth, GPS, and many other devices)[8]. In addition, electrical equipment and electronics in a car, home and office, dense urban and industrial environments, increasingly crowded wireless spectrum, mutual radar-radar and radar-communications interference, are other sources of technogenic impulsive noise. In the acoustic domain, impulsive noise can be initiated by natural sources such as marine mammals and crustal movement of earthquakes at the sea bed in underwater systems[9–11].

The prevalence of such noise varies with location and frequency band and is intensifying with the proliferation of handheld electronic devices, especially in densely populated areas. One method to address this problem is to reduce the interference at its source.

Interference reduction approaches can be classified as either static methods (e.g. layout and shielding, spectrum allocation) that avoid interference through device design or network planning, or as adaptive techniques (e.g. controlling/managing protocols such as resource allocation[12] along with adaptive loading[13–15], beam forming[16;17], interference alignment and/or cancelation[18;19]) that estimate and cancel interference during data transmission[20]. These methods typically require careful engineering using detailed knowledge of the system and its interactions with the environment. In this regard one can model the interference by using a stochastic geometry tool[21–24] and take advantage of the provided model at the transmitter to reduce the interfering nodes in the network.

The other method to address interference is to mitigate it at the receiver. In the context of this dissertation, the emphasis is on the reduction of interference that has already entered the signal path. Since a signal of interest typically occupies a different and/or narrower frequency range than the noise, linear filters are applied to the incoming mixture of the signal and the noise in order to reduce the frequency range of the mixture to that of the desired signal. This reduces the power of the interference to a fraction of the total, limited to the frequency range of the signal. Although linear filters or matched filters are optimal in purely Gaussian (e.g. thermal) noise, they cannot increase the passband signal to noise ratio (SNR) in the presence of impulsive noise. On the other hand, nonlinear filters can improve the quality of a signal that is affected by non-Gaussian interference such as intermittent technogenic noise[25]. Fig. 1.1 demonstrates the performance of linear and nonlinear receivers in an impulsive environment[1]. As shown, both approaches provide effectively equivalent performance when thermal noise dominates the impulsive noise. However, the superiority of the Blind Adaptive Intermittently Nonlinear Filter (BAINF) is highlighted when the impulsive noise is dominant where a BAINF offers more than 7 dB gains relative to linear receiver.

Multicarrier transmission techniques have been proposed to cope with the frequency

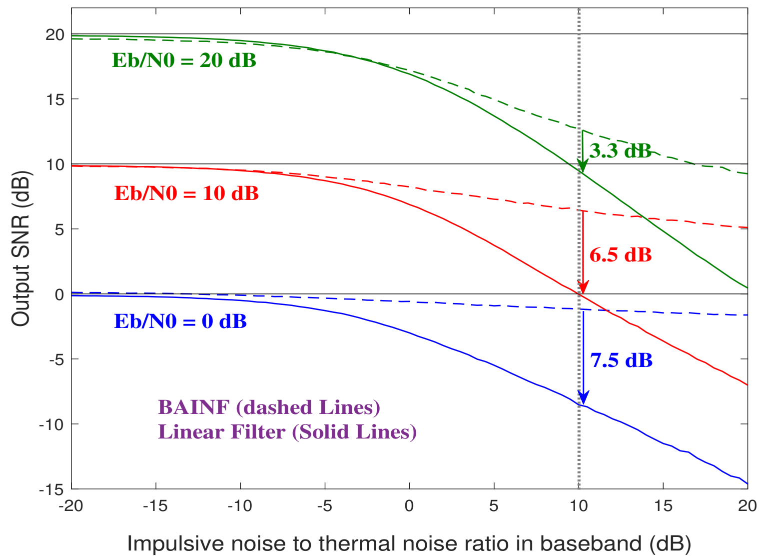

Fig. 1.1: SNR comparison of linear and nonlinear receiver [1].

selectivity of the propagation channel in many applications [26]. Particularly, orthogonal frequency-division multiplexing (OFDM) is widely used in broadband high data rate standards such as IEEE 802.11n and long term evolution (LTE), underwater acoustic (UWA) communication along with IEEE 1901.2 and power-line intelligent metering evolution (PRIME) standards [27], [28] for power-line communication (PLC). Since OFDM employs a larger symbol duration (i.e., narrowband subcarriers), the energy of impulsive noise is naturally spread over all subcarriers. While this provides some level of robustness against impulsivity, system performance can still degrade if impulsive noise power exceeds a certain threshold [29]. Therefore, the vulnerability of OFDM in an impulsive noise environment favors the use of impulsive noise mitigation approaches.

To meet the increasing demand for reducing impulsive noise, many techniques have been explored in prior efforts. For example, robust iterative channel decoding techniques have been used to ameliorate bit error rate (BER) in impulsive environments [30;31]. It has been shown that coding techniques are mostly effective in single carrier schemes and there is not much gain in OFDM systems [32] in the presence of severe impulsive noise. In addition, frequency or time domain interleaving [33–35] without mitigation techniques are not effective in highly impulsive environments.

In general, impulsive noise mitigation techniques in OFDM systems can be divided into two classes. In the first class, the sparsity of the impulsive noise and the structure of OFDM signal are exploited[10]. In this class, first, an estimation of the impulsive noise is derived from the null and/or pilot subcarriers, and then the estimated impulsive noise is subtracted from the received signals. For example, compressive sensing (CS) techniques are used to estimate the impulsive noise by measurements on null subcarriers of OFDM[36],[37]. In[7] a non-parametric algorithm is proposed by extension of[36] to a sparse Bayesian learning (SBL) approach[38]. A combination of factor-graph-based receiver and message-passing technique[39] is proposed in[40] to mitigate impulsive noise.

In the second class of impulsive noise mitigation techniques, the high amplitude and short duration of the impulsive noise are considered as the main parameters for impulsive noise detection and cancelation. Conventional memoryless nonlinear approaches such as clipping[41] and blanking[42] are the most common methods in this class. In addition, joint blanking-clipping[43], linear combination of blanking and clipping[44], deep clipping[45], and multiple-threshold blanking/clipping[46] are proposed to improve the performance of blanking and clipping at extra computational complexity cost. However, the performance of threshold-based nonlinear approaches is highly sensitive to the thresholds which are usually derived experimentally. In[47], a threshold optimization method based on the Neyman-Pearson criterion is proposed. As shown in[48], the performance of all these methods degrades dramatically in severe impulsive environments.

1.2 Research Approach

To address the aforementioned interference issues, this dissertation aims at the development of approaches to effectively detect and mitigate the impact of the impulsive noise. To do so, we investigate two different categories of impulsive noise suppression techniques that can be used as a stand-alone solution or combined with other interference reduction techniques.

First, we study Blind Adaptive Intermittently Nonlinear Filters (BAINFs) for analog-domain mitigation of the impulsive noise. Secondly, we propose a machine learning based approach that learns from the observed signals to detect and separate the contaminated signal with impulsive noise.

The idea behind using analog domain mitigation is that a highly impulsive signal will become less impulsive after bandlimited filtering of the signal in the receiver chain. Since insufficient processing bandwidth severely limits the effectiveness of digital nonlinear interference mitigation techniques, suppression of non-Gaussian interference in the analog domain before the analog to digital convertor (ADC) can be helpful. On the other hand, in the threshold based outlier detection approaches, determining the optimum threshold is the main challenge, as this threshold will vary in response to channel conditions and model mismatches. As always, there is a compromise between detection and false alarm probability in the traditional threshold based methods. To overcome the aforementioned drawback, machine learning based approaches are invoked in this dissertation.

In this regard, there are key research questions that need to be addressed

Question 1: How to develop a realization of BAINF which is compatible with existing linear receivers and can be deployed either as a stand-alone low-cost real-time solution or combined with other interference reduction techniques?

Question 2: How to solidify and further advance the theoretical foundations of a proposed BAINF to address many key fundamental questions regarding both the design and performance of the BAINF.

Question 3: How the idea and different realization of BAINFs can be applied in different applications with diverse sources of interference and enabling receivers resistant to impulsive noise independent of the modulation schemes and communication protocols.

Question 4: How a realization of a BAINF can be implemented practically to offer a robust means to establish the sensitivity range even when the noise is non-stationary?

Question 5: What would be the performance of the proposed BAINF in a practical experimental setup?

Question 6: How and why is machine learning applicable and suitable for impulsive noise detection?

1.3 Contributions

In order to address the aforementioned questions, this dissertation contributes to the state of the art across multiple domains as listed below:

Contribution 1: A realization of the BAINF as an Adaptive Nonlinear Differential Limiter (ANDL) is investigated to mitigate the impulsive noise in the analog domain before the ADC. The proposed ANDL is constructed from a linear analog filter by applying a feedback-based nonlinearity, controlled by a single parameter called resolution parameter. Therefore, the ANDL can be perceived as a time varying linear filter that its time parameter changes based on the amplitude of the incoming signal. Adaptation in ANDL is performed by adjusting the resolution parameter to work efficiently in the presence of various types of impulsive noise without prior knowledge of the noise distribution. In this context, the traditional matched filter construction needs to be modified to ensure distortion-less processing of the desired signal. This contribution is discussed in detail in chapter 2 and in the following article:

[49] **R. Barazideh**, B. Natarajan, A. V. Nikitin, and R. L. Davidchack , "Performance of Analog Nonlinear Filtering for Impulsive Noise Mitigation in OFDM-based PLC Systems," *IEEE Latincom, 2017*, Nov 2017, pp. 1-6.

Contribution 2: The theoretical performance of the ANDL is quantified by deriving a closed-form analytical bound for the average SNR at the output of the filter. The calculation is based on the idea that the ANDL can be perceived as a time-variant linear filter whose bandwidth is modified based on the intensity of the impulsive noise. Moreover, by linearizing the filter time parameter variations, we treat the ANDL as a set of linear filters where the exact operating filter at a given time depends upon the magnitude of the outliers. This contribution is discussed in detail in chapter 3 and in the following article:

[50] **R. Barazideh**, B. Natarajan, A. V. Nikitin, and S. Niknam "Performance Analysis of Analog Intermittently Nonlinear Filter in the Presence of Impulsive Noise," in *IEEE Trans. Veh. Technol.*, vol. 68, no. 4, pp. 3565-3573, April 2019.

Contribution 3: A practical implementation of BAINF as an Adaptive Canonical Differential Limiter (ACDL) is proposed to mitigate impulsive noises in OFDM-based PLC receivers. The ACDL is constructed from a Clipped Mean Tracking Filter (CMTF) and Quartile Tracking Filters (QTFs). The QTFs help to determine a real-time sensitivity range that excludes outliers. This range is fed into the CMTF which is responsible for mitigating impulsive noise. The CMTF is a nonlinear analog filter, and its nonlinearity is controlled by the aforementioned range. Proper selection of this range ensures the improvement of the desired signal quality in the impulsive environment. This contribution is discussed in detail in chapter 4 and in the following article:

[1] **R. Barazideh**, A. V. Nikitin, and B. Natarajan , "Practical Implementation of Adaptive Analog Nonlinear Filtering For Impulsive Noise Mitigation," *IEEE Int. Conf. on Commun. (ICC)*, May 2018, pp. 1-7.

Contribution 4: We propose a receiver structure that deals efficiently with both impulsive noise and Doppler shift channel impairments in coded OFDM-based UWA communication systems. First, an Analog Nonlinear Preprocessor (ANP) is proposed to efficiently detect and mitigate impulsive noise in the analog domain. The proposed ANP exhibits intermittent nonlinearity when there is impulsivity. Next, the impact of impulsive noise on a two-step Doppler shift compensation approach is quantified. Specifically, the ability of the ANP to improve robustness of Doppler shift compensation in the presence of impulsive noise is highlighted. In addition, a memoryless version of the ANP as Memoryless Analog Nonlinear Preprocessor (MANP) is proposed to mitigate the effect of the impulsive noise in the real-data experiments. These contributions are discussed in detail in chapters 5 and 6 and in the following articles:

[51] **R. Barazideh**, S. Niknam, B. Natarajan, and A. V. Nikitin "Intermittently Nonlinear Impulsive Noise Mitigation and Doppler Shift Compensation in UWA-OFDM Systems," *IEEE Access*, vol. 7, pp. 36590-36599, 2019.

[3] **R. Barazideh**, W. Sun, B. Natarajan, A. V. Nikitin, Z. Wang "Impulsive Noise Mitigation in Underwater Acoustic Communication Systems: Experimental Studies," *IEEE Computing and Communication Workshop and Conference (CCWC)*, Jan 2019, pp. 0880-0885.

Contribution 5: We propose a two stage impulsive noise mitigation approach for OFDM-based communication systems. In the first stage, a deep neural network (DNN) is used to detect the instances of impulsivity. Then, the detected impulsive noise is blanked in the suppression stage to alleviate the harmful effects of outliers. Moreover, the robustness of the proposed DNN-based approach is evaluated under (i) a mismatch between impulsive noise models considered for training and testing, and (ii) a bursty impulsive environment when the receiver is empowered with interleaving techniques. This contribution is discussed in detail in chapter 7 and in the following article:

[52] **R. Barazideh**, S. Niknam, and B. Natarajan "Impulsive Noise Detection in OFDM-based System: A Deep Learning Perspective," *IEEE Computing and Communication Workshop and Conference (CCWC)*, Jan 2019, pp. 0937-0942.

1.4 Dissertation Outline

The remainder of this dissertation is organized as follows. The ANDL along with its performance in PLC system is illusterated in chapter 2. We develop the theoretical performance of the proposed ANDL in chapter 3. A practical implementation of the ACDL is proposed in chapter 4, where its performance is evaluated in a PLC system. In chapter 5 another realization of BAINF as an ANP is proposed, where its performance is evaluated in the coded OFDM-based UWA communication systems. A memoryless version of the ANP as MANP is provided in chapter 6 to capture the performance of the MANP with experimental data. An approach based on machine learning for impulsive noise detection is provided in chapter 7. Finally, concluding remarks and direction for future work are provided in chapter 8.

Chapter 2

Analog Nonlinear Filtering for Impulsive Noise Mitigation in OFDM-based PLC Systems

Impulsive noise can severely impact the BER performance of OFDM-based communication systems. In this chapter, we analyze an adaptive nonlinear analog front end filter that mitigates various types of impulsive noise without detrimental effects such as self-interference and out-of-band power leakage caused by other nonlinear approaches like clipping and blanking. Our proposed Adaptive Nonlinear Differential Limiter (ANDL) is constructed from a linear analog filter by applying a feedback-based nonlinearity, controlled by a single resolution parameter. We present a simple practical method to find the value of this resolution parameter that ensures the mitigation of impulsive noise without impacting the desired OFDM signal. In this context, the structure of the matched filter in the receiver is modified to compensate for the filtering effect of the ANDL in the linear regime. Unlike many prior approaches for impulsive noise mitigation that assume a statistical noise model, ANDL is blind to the exact nature of the noise distribution and is designed to be fully compatible with existing linear front end filters. We demonstrate the potency of ANDL by simulating an OFDM-based narrowband PLC compliant with the IEEE standards. We show that the proposed ANDL outperforms other approaches in reducing the BER in impulsive noise environments.

2.1 Introduction

Smart Grid is a concept that enables wide-area monitoring, two-way communications, and fault detection in power grids, by exploiting multiple types of communications technologies, ranging from wireless to wireline [53]. Thanks to the ubiquitousness of the powerline infrastructure, low deployment costs, and its wide frequency band, PLC has become a choice for a variety of smart grid applications [7]. In particular, there has been increasing demand in developing narrowband PLC (NB-PLC) systems in the 3-500 kHz band, offering data rates up to 800 kbps [53]. In order to achieve such data rates, multicarrier modulation techniques such as OFDM are preferred due to their robust performance in frequency-selective channels [48].

Since the powerline infrastructure is originally designed for power delivery and not for data communications, OFDM-based PLC solutions face many challenges such as noise, impedance mismatching and attenuation. Powerline noise typically generated by electrical devices connected to the powerlines and coupled to the grid via conduction and radiation is a major issue in PLC [54]. Due to its technogenic (man-made) nature, this noise is typically non-Gaussian and impulsive, as has been verified by field measurements. Therefore, PLC noise can be modelled as a combination of two terms: (i) thermal noise which is assumed to be additive white Gaussian noise (AWGN), and (ii) the impulsive noise that may be synchronous or asynchronous relative to the main frequency [55]. In [56] and IEEE P1901.2 standard [27], it is shown that in NB-PLC, the dominant non-Gaussian noise is a quasi-periodic impulsive noise (*cyclostationary noise*). Such noise occurs periodically with half the AC (Alternating Current) cycle with a duration ranging from hundreds of microseconds to a few milliseconds. However, it has been also claimed that asynchronous impulsive noise is simultaneously present in the higher frequency bands of NB-PLC [7],[25]. It is observed that the primary noise component in broadband PLC (BB-PLC) in the 1.8-250 MHz band which offers data rates up to 200 Mbps [57;58] is asynchronous and impulsive with short duration, i.e., high power impulses (up to 50 dB above thermal noise power [57]) with random arrivals.

The reduction in the sub-channel SNR in highly impulsive noise environments such as PLC can be too severe to handle by forward error correction (FEC) and frequency-domain interleaving (FDI) [33] or time-domain interleaving (TDI) [34]. Various approaches to deal with impulsive noise in OFDM have been proposed in prior works. Many of those approaches assume a statistical model of the impulsive noise and use parametric methods in the receiver to mitigate impulsive noise. Considering a specific statistical noise model, one can design a periodically switching moving average noise whitening filter [59], linear minimum mean square error (MMSE) equalizer in the frequency domain [60] or iterative decoder [61] to mitigate cyclostationary noise. Such parametric methods require the overhead of training and parameter estimation. In addition, difficulty in parameter estimation and model mismatch degrade the system performance in time varying non-stationary noise.

Alternately, nonlinear approaches can be implemented in order to suppress the effect of impulsive noise. The performance of memoryless digital nonlinear methods such as clipping [41], blanking [42], and combined blanking-clipping [43] have been investigated in prior literature. It has been shown that for these methods, good performance is achieved only for asynchronous impulsive noise, and for high signal to interference ratio (SIR) [48]. To address the challenge of severe impulsive noise conditions, a two-stage nulling algorithm based on iterative channel estimation is proposed in [62]. However, all these digital nonlinear approaches are implemented after the ADC. The main drawback of these approaches lies in the fact that during the process of analog to digital conversion, the signal bandwidth is typically reduced by required anti-aliasing filters and an initially impulsive broadband noise will appear less impulsive [63]-[8]. This makes the removal of impulsivity much harder by digital filters. Although, such problems can be overcome by increasing the sampling rate, it increases complexity and cost, making it inefficient for real-time implementation [25],[64].

In this chapter, we propose an impulsive noise mitigation approach in the analog domain before the ADC by using an ANDL as a blind adaptive analog nonlinear filter. In this technique, the adaptation is done by adjusting a single resolution parameter to work efficiently in the presence of various types of impulsive noise (asynchronous and cyclostationary impulsive noise, or combination of both) without the detailed knowledge of the noise distribution. In

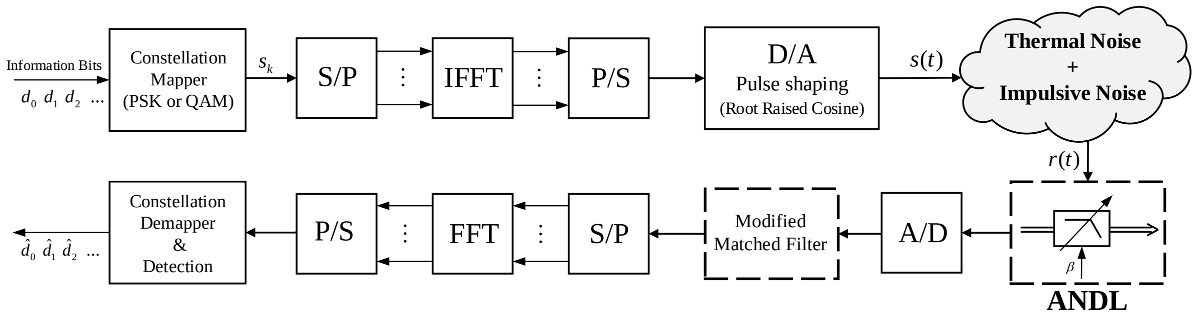

Fig. 2.1: System Model

order to compensate the insertion effect of the ANDL in the linear regime, the structure of the matched filter in the receiver is modified. Since ANDL is nonlinear, their effects on the desired signal are totally different than on the impulsive noise. This feature allows the filter to increase SNR in the desired bandwidth by reducing the spectral density of non-Gaussian noise without significantly affecting the desired signal. Analog structure of this method allows us to use ANDL either as a stand-alone approach, or in combination with other digital impulsive noise reduction approaches.

2.2 System and Noise Models

We consider an OFDM system with complex baseband equivalent representation shown in Fig. 2.1. In this system, information bits are independently and uniformly generated and mapped into baseband symbols s_k based on phase shift keying (PSK) or quadrature amplitude modulation (QAM) scheme with Gray coding. The symbols s_k are sent through an OFDM modulator which employs an inverse discrete Fourier transform (IDFT) (implemented by inverse fast Fourier transform (IFFT)) to transmit the symbols over orthogonal subcarriers. The output analog signal envelope in time domain can be written as

$$s(t) = \frac{1}{\sqrt{N}} \sum_{k=0}^{N-1} s_k \, \mathrm{e}^{j\frac{2\pi k t}{T}} p(t), \quad 0 < t < T, \tag{2.1}$$

where N is the number of subcarriers, T is duration of one OFDM symbol and $p(t)$ denotes the root-raised-cosine pulse shape with a roll-off factor, $\rho = 0.25$. It is assumed that the number of subcarriers is large enough so that Central Limit Theorem (CLT) can be invoked to show that the real and imaginary parts of the OFDM signal $s(t)$ can be modeled as Gaussian random variables. In general, for different applications, we can construct an OFDM symbol with M non-data subcarriers and $N - M$ data subcariers. The non-data subcarriers are either pilots for channel estimation and synchronization, or nulled for spectral shaping and inter-carrier interference reduction. Without loss of generality, the power of the transmitted signal is normalized to unity, i.e., $\sigma_s^2 = 1$. Since the primary focus of this chapter is to study the impact of impulsive noise on OFDM performance, we consider a simple additive noise channel model where the received signal corresponds to

$$r(t) = s(t) + w(t) + i(t). \tag{2.2}$$

Here, $s(t)$ denotes the desired signal with variance σ_s^2, $w(t)$ is complex Gaussian noise with mean zero and variance σ_w^2, and $i(t)$ represents the impulsive noise which is not Gaussian. The receiver involves a typical OFDM demodulator as shown in Fig. 2.1. This traditional receiver structure is modified in order to deal with impulsive noise $i(t)$. Unlike most conventional impulsive noise mitigation approaches which are applied after the ADC, the proposed ANDL is implemented before the ADC. In the following, we begin with a review of the impulse noise models commonly encountered in PLC systems.

2.2.1 Impulsive Noise Models

Two types of impulsive noise that are dominant in the 3–500 KHz band for NB-PLC and in the 1.8–250 MHz band for BB-PLC are cyclostationary impulsive noise and asynchronous impulsive noise, respectively[7]. Since both types of impulsive noise are presented in the NB-PLC[7],[25], our impulsive noise model consists of both cyclostationary and asynchronous impulsive noises.

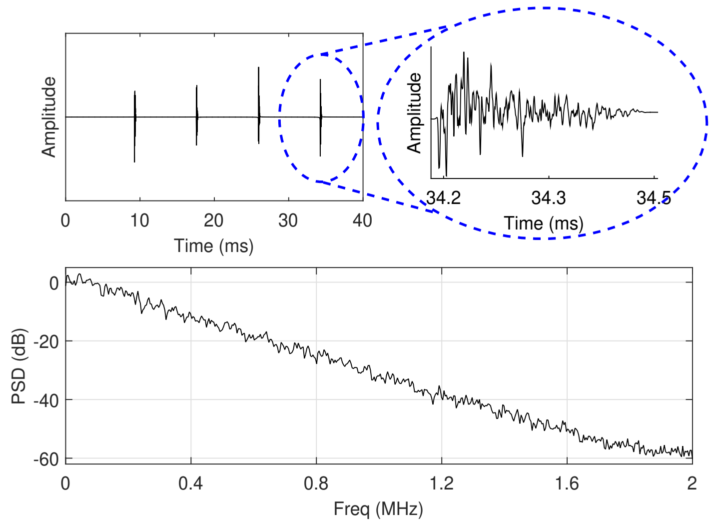

Fig. 2.2: Cyclostationary impulsive noise

Cyclostationary impulsive noise

This type of impulsive noise has a duration ranging from hundreds of microseconds to a few milliseconds[7],[25]. Based on field measurements[65], the dominant part of this noise is a strong and narrow exponentially decaying noise burst that occurs periodically with half the AC cycle ($f_{\mathrm{AC}} = 60Hz$). Therefore, we can model such noise as

$$i_{\mathrm{cs}}(t) = A_{\mathrm{cs}}\,\nu(t)\sum_{k=1}^{\infty}\exp\left(\frac{-t+\frac{k}{2f_{\mathrm{AC}}}}{\tau_{\mathrm{cs}}}\right)\theta\left(t-\frac{k}{2f_{\mathrm{AC}}}\right), \tag{2.3}$$

where A_{cs} is a constant, τ_{cs} is a decaying time parameter, $\nu(t)$ is complex white Gaussian noise process with zero mean and variance one, and $\theta(t)$ is a Heaviside step function. The spectral density of this noise is shaped based on the measured spectrum of impulsivity in practice (power spectrum density (PSD) decaying at an approximate rate of 30 dB per 1 MHz)[65]. The resulting time domain and frequency domain representation of this noise are depicted in Fig. 2.2.

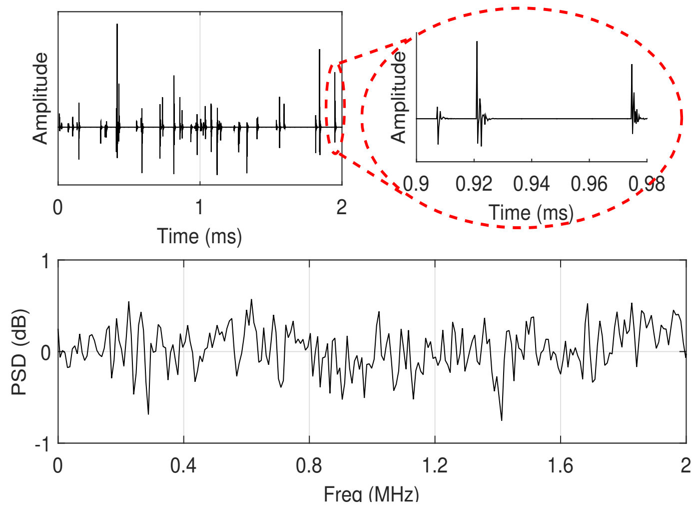

Fig. 2.3: Asynchronous impulsive noise

Asynchronous impulsive noise

This type of impulsive noise consists of short duration and high power impulses with random arrival. Mathematically, we have

$$i_{\mathrm{as}}(t) = \nu(t)\sum_{k=1}^{\infty} A_k\,\theta(t-t_k)\,\mathrm{e}^{\frac{-t+t_k}{\tau_{\mathrm{as}}}}\,, \tag{2.4}$$

where A_k is the amplitude of k^{th} pulse, t_k is a arrival time of a poisson process with parameter λ, and τ_{as} is decaying time parameter and has a duration about few microseconds. The time domain and frequency domain representation of this noise is depicted in Fig. 2.3.

2.3 Adaptive Nonlinear Differential Limiter (ANDL) Design

In this section, we provide an introduction to the basics of the ANDL and the method that can be used to find an effective value for the resolution parameter of the filter to mitigate impulsive noise.

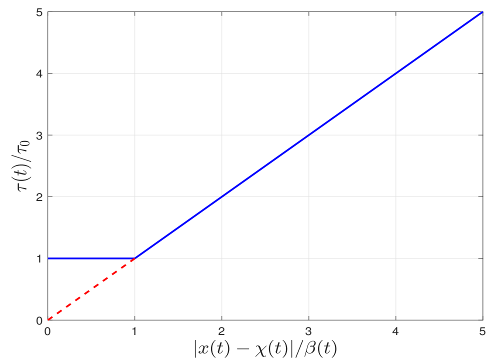

Fig. 2.4: ANDL time parameter $\tau(t) = \tau(|x(t) - \chi(t)|)$.

2.3.1 ANDL Formulation

ANDL is a blind adaptive analog nonlinear filter that can be perceived as a 1st order time varying linear filter with the time parameter $\tau(t)$, that depends on the magnitude of the difference between the input and the output, as discussed in our previous work[25]. Thus, we have

$$\chi(t) = x(t) - \tau(|x(t) - \chi(t)|)\,\dot{\chi}(t)\,, \tag{2.5}$$

where $x(t)$ and $\chi(t)$ are the input and output of the filter, respectively, and the dot denotes the first time derivative. As illustrated in Fig. 2.4, the time parameter $\tau(t) = \tau(|x(t) - \chi(t)|)$ is given by

$$\tau(|x(t) - \chi(t)|) = \tau_0 \times \begin{cases} 1 & |x(t) - \chi(t)| \le \beta(t) \\ \frac{|x(t)-\chi(t)|}{\beta(t)} & \text{otherwise} \end{cases}\,, \tag{2.6}$$

where τ_0 is a fixed time constant that ensures the desired bandwidth and $\beta(t)$ is the resolution parameter of the filter and should be determined to mitigate the impulsive noise efficiently. Although in general the ANDL is a nonlinear filter, it behaves like a linear filter as long as there are no outliers and the magnitude of the difference signal $|x(t) - \chi(t)|$ remains within a certain range determined by the resolution parameter. However, when outliers are encountered, the proper selection of resolution parameter ensures that the magnitude of the corresponding outliers are suppressed by the nonlinear response of the ANDL.

2.3.2 Resolution Parameter Calculation

The configuration of the ANDL consists of a feedback mechanism that monitors the peakedness of the signal plus noise mixture and provides a time-dependent resolution parameter $\beta(t)$ which ensures improvement in the quality of non-stationary signals under time-varying noise conditions. The idea is to pick an effective value of $\beta(t)$ that allows the signal of interest to completely go through the nonlinear filter without any suppression and at the same time mitigate the impulsive noise, maximally. For implementation simplicity, we assume that SNR variations are slower relative to the OFDM symbol duration. Therefore, we can fix the resolution parameter $\beta(t)=\beta$ for each OFDM symbol duration and allow it to change across symbols. The lower bound of the resolution parameter can be found based on difference signal $|x(t) - \chi(t)|$ in case of no impulsive noise. An estimate of the difference signal can be obtained by passing signal $s(t) + w(t)$ through a linear highpass filter with the time constant τ_0. Let $z(t)$ be given by a differential equation for the 1st order highpass filter. Then, we have

$$z(t) = \tau_0 \left[\dot{s}(t) + \dot{w}(t) - \dot{z}(t)\right], \tag{2.7}$$

Lemma 1 provides a lower bound for the choice of resolution parameter β.

Lemma 1. *The efficient value of the resolution parameter $\beta_{\text{eff},\xi}$ for $(1-\xi)$ level distortionless filtering of the transmitted OFDM signal in thermal noise is $\text{erf}^{-1}(1-\xi)\sqrt{2}\sigma_z$, where σ_z^2 is the variance of $z(t)$ and ξ is a sufficiently small constant.*

Proof. Since $s(t)$ and $w(t)$ are independent, for a sufficiently large N it follows from the CLT that $z(t)$ is a complex Gaussian random variable with zero mean and variance σ_z^2. From equations (2.5) and (2.6), the ANDL preserves its linear behavior for $|z(t)| \le \beta$. Therefore, for $(1-\xi)$ distortionless filtering of the transmitted OFDM signal in thermal noise, we require that

$$\Pr\left(|z(t)| > \beta\right) \le \xi \ll 1. \tag{2.8}$$

Since $z(t)$ is Gaussian, we have

$$\Pr(|z(t)| > \beta) = 1 - \operatorname{erf}\left(\frac{\beta}{\sigma_z\sqrt{2}}\right) \leq \xi, \tag{2.9}$$

where erf(.) is the error function. Solving equation (2.9) with respect to β, we obtain

$$\beta_{\text{eff},\xi} \geq \operatorname{erf}^{-1}(1-\xi)\sqrt{2}\sigma_z. \tag{2.10}$$

■

In practice, a choice of $\xi = 4.68 \times 10^{-3}$ leads to $\beta \geq 2\sqrt{2}\,\sigma_z$, i.e., $\beta_{\text{eff}} = 2\sqrt{2}\,\sigma_z$ and we use sample variance instead of statistical variance σ_z^2 as it can be computed online and can track possible nonstationary behavior.

2.3.3 Matched filter Modification

In the absence of the ANDL in the signal chain, the matched filter (MF) following the ADC would have the impulse response $h[k]$ that can be viewed as a digitally sampled continuous-time impulse response $h(t)$ as shown in panel II of Fig. 2.5. Since our proposed filter should not have any negative impact when there is no impulsive noise, it is essential to modify the MF to compensate for the ANDL in a linear chain. We proposed a modification in the digital domain because it is simpler and does not need any extra components. In case of no impulsive noise ANDL acts like a 1st order linear lowpass filter with time constant τ_0. Therefore, the relation between the input $x(t)$ and the output $\chi(t)$ can be expressed as

$$x(t) = \chi(t) + \tau_0\dot{\chi}(t). \tag{2.11}$$

In the linear regime we want to have same result either with or without ANDL (Panels 1 and 2 in Fig. 2.5). Thus, the output of modified matched filter with the input $\chi(t)$ should

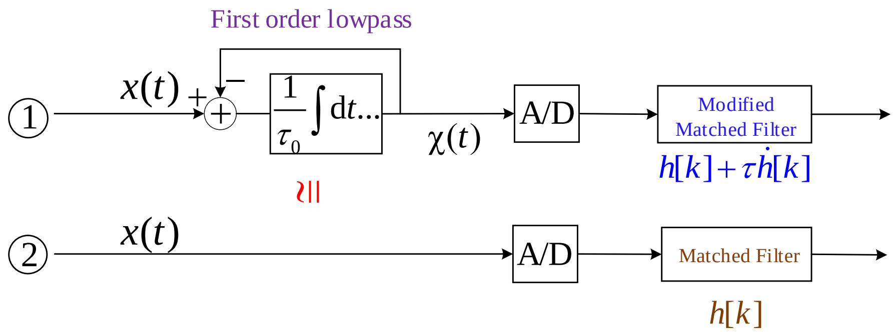

Fig. 2.5: Simplified block diagram of the ANDL operating in linear regime. Adapted from [2].

be equal to the output of MF with the input $x(t)$. Therefore, we have

$$\begin{aligned}\chi(t) * h_{\text{mod}}(t) &= x(t) * h(t) \\ &= (\chi(t) + \tau_0\dot{\chi}(t)) * h(t),\end{aligned} \tag{2.12}$$

where the asterisk denotes convolution and the impulse response $h_{\text{mod}}[k]$ of the modified matched filter in the digital domain can be expressed as

$$h_{\text{mod}}[k] = h[k] + \tau_0\dot{h}[k]. \tag{2.13}$$

In the presence of ANDL the compensation of the modified matched filter on the BER performance of a OFDM system with binary phase shift keying (BPSK) modulation is shown in Fig. 2.6. As it can be seen the effect of ANDL in linear chain completely alleviated by the modified matched filter which means that our proposed filter does not harm the desired signal in case of no impulsive noise.

2.4 Simulation results

In this section, as a specific example we consider an OFDM-based NB-PLC in PRIME. Based on IEEE P1901.2 standard the sampling frequency has been chosen as $f_s = 250$ kHz and

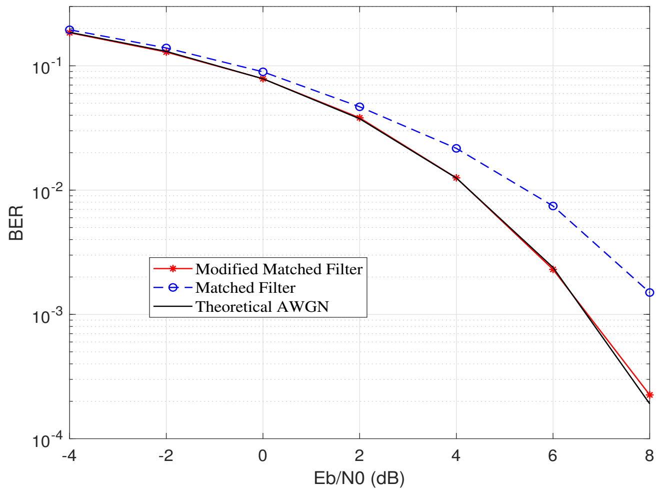

Fig. 2.6: Performance comparison between matched filter and modified matched filter in the presence of ANDL for BPSK modulation.

the fast fourier transform (FFT) size is $N = 512$, i.e, the subcarrier spacing $f = 488$ Hz. As carriers $N = 86 - 182$ are occupied for data transmission based on the PRIME model, the desired signal is located in the frequency range 42-89 kHz[28].

The system is investigated in a noise environment that is typical for NB-PLC and it consists of three components (1) thermal noise (with PSD decaying at rate of 30 dB per 1 MHz) (2) periodic cyclostationary exponentially decaying component with the repetition frequency at twice the AC line frequency and duration ranging from hundreds of microseconds to a few milliseconds, and (3) asynchronous random impulsive noise with normally distributed amplitudes captured by a poisson arrival process with parameter λ.

We use first order ANDL, with τ_0=$1/(4\pi f_0)$ and corner frequency f_0=89 kHz, which is followed by a 2nd order linear filter with the time parameter $\tau = 2 \times \tau_0$ and the quality factor $Q = 1$. It is important to note that in the considered system model, the matched filter can take the role of the linear filter. When $\beta \to \infty$ this ANDL becomes a 3rd order Butterworth filter with cutoff frequency twice the highest frequency of the desired signal. All simulations have been performed for BPSK modulation and the cyclostationary impulsive noise is simulated as a damped sinusoid based on (2.3) and it lasts for $200\mu s$ (one tenth of OFDM symbol). The asynchronous impulsive noise is added to the transmitted signal with

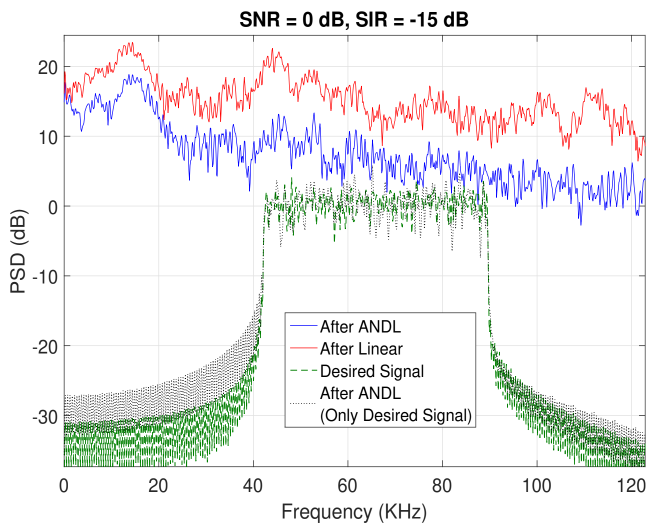

Fig. 2.7: Power Spectral Density.

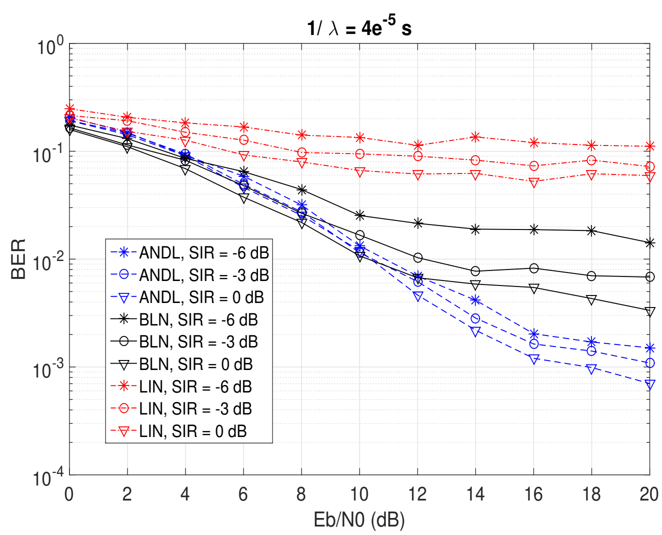

Fig. 2.8: BER versus SNR with fixed SIR.

different probability of impulsivity based on (2.4) which lasts for $2\mu s$. Since the cyclostationary noise is dominant in the NB-PLC, we set the power of this component three times higher than the asynchronous impulsive noise. We mimic the analog domain by oversampling the transmitted OFDM signal by factor 40 and downsampling after ANDL. In the following, BER of the OFDM system is used as the metric to evaluate the performance of ANDL in comparison with other conventional approaches such as linear filtering and blanking. Since, the noise is essentially stationary in the system, we can pick the effective β based on lemma 1 for a fixed SNR leading to a classic ANDL implementation.

Fig. 2.7 shows the PSD for a given signal to thermal plus impulsive noise ratio (SINR) after impulsive noise mitigation filter. It is evident that we have significant impulsive noise suppression in passband with the ANDL compared to the suppression offered by a linear filter. This figure also shows that when there is no impulsive noise, the ANDL does not distort our desired signal in the passband. This disproportional effect of ANDL over the impulsive noise and desired signal in the passband results in significant SNR improvement at the receiver.

To demonstrate the robustness of the ANDL to different types of impulsive noise, we consider the case when both asynchronous and cyclostationary impulsive noise impact the signal simultaneously. The BER performance of proposed approach for different values of SIR versus SNR is shown in Fig. 2.8. We compare the ANDL performance with blanking and the optimal threshold for blanking is found based on an exhaustive numerical search. Fig. 2.8 shows that the ANDL based reception results in better BER performance relative to blanking and linear filter especially in high SNR. The BER performance of the system for a given SINR versus SNR is shown in Fig. 2.9. Since SINR is fixed, we have more impulsivity when thermal noise is low (i.e., high SNR region). Fig. 2.9 shows that the performance of blanking and linear filter remains almost unchanged while the ANDL shows a significant improvement in high SNR region. This result highlights the effectiveness of the ANDL in severe impulsive noise environments.

The importance of choosing optimum resolution parameter β is shown in Fig. 2.10. This figure shows the ANDL performance for different values of β for given amount of impulsive noise. We can see that the best performance is observed when β is selected based on lemma 1. As we deviate from this choice, the performance degradation is gradual and in many cases still superior to the linear filter performance (captured by setting β to a high value).

2.5 Summary

In this chapter, the ANDL is proposed to mitigate asynchronous and cyclostationary impulsive noises in OFDM-based PLC receiver. In addition, a practical method to find an effective

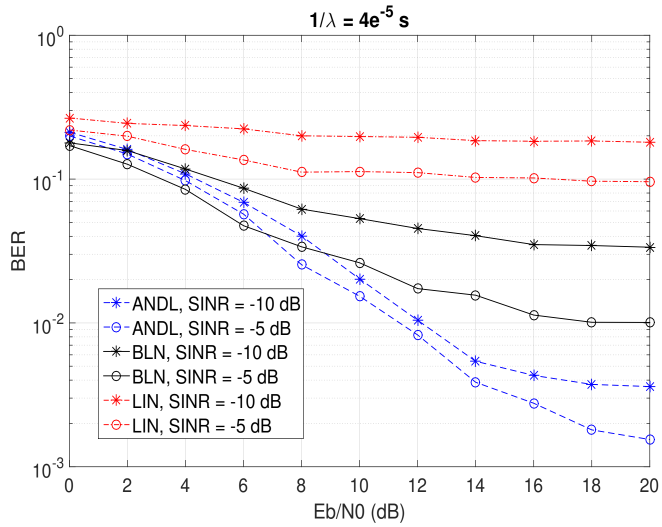

Fig. 2.9: BER versus SNR with fixed SINR.

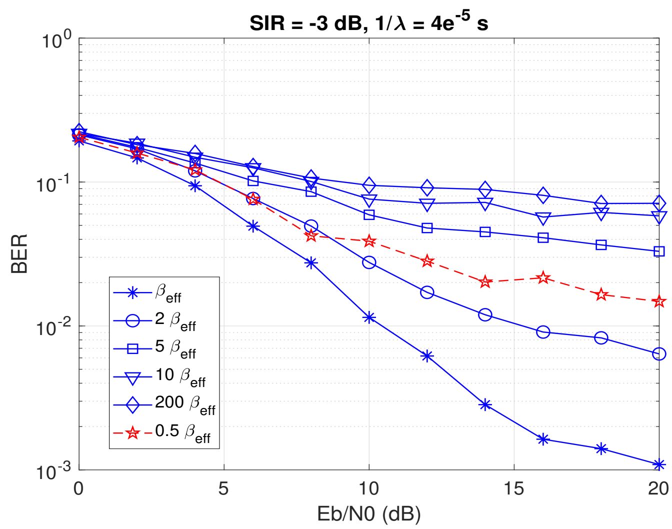

Fig. 2.10: Effect of resolution parameter on ANDL performance.

value for the resolution parameter of ANDL is presented. In this context, the structure of the matched filter in the receiver is modified to compensate the filtering effect of the ANDL in the linear regime. We demonstrate the ability of ANDL to significantly reduce the PSD of impulsive noise in the signal passband without having prior knowledge of the statistical noise model or its parameters. The results show that ANDL can provide improvement in the overall signal quality ranging from distortionless behavior for low impulsive noise conditions to significant improvement in BER performance in the presence of strong impulsive component. It also has been shown that the performance of ANDL can be enhanced by careful selection of resolution parameter. It is important to note that ANDL can be deployed either as a stand-alone low-cost real-time solution for impulsive noise mitigation, or combined with other interference reduction techniques.

Chapter 3

Theoretical Performance of ANDL in the Presence of Impulsive Noise

As it has been mentioned in chapter 2, the proposed ANDL is implemented in the analog domain where the broader acquisition bandwidth makes outliers more detectable and consequently it is easier to remove them. While the proposed ANDL behaves like a linear filter when there is no outlier, it exhibits intermittent nonlinearity in response to impulsive noise. In this chapter, we quantify the performance of the ANDL by deriving a closed-form analytical bound for the average SNR at the output of the filter. The calculation is based on the idea that the ANDL can be perceived as a time-variant linear filter whose bandwidth is modified based on the intensity of the impulsive noise. In addition, by linearizing the filter time parameter variations, we treat the ANDL as a set of linear filters where the exact operating filter at a given time depends upon the magnitude of the outliers. The theoretical average BER is validated through simulations and the performance gains relative to classical methods such as blanking and clipping are quantified.

3.1 Introduction

Multicarrier transmission techniques such as OFDM is widely used in many applications in vehicular communications ranging from wired communication such as PLC in Home-Plug Green PHY standard for vehicular to grid (V2G) communications [66] to wireless communications such as 802.11p Wireless Access in Vehicular Environments (WAVE) standard [67], and UWA communication [68]. However, OFDM provides some level of robustness against impulsivity, system performance can still degrade if the impulsive noise exceeds a certain threshold and its effect gets spread over all subcarriers [29]. Taking an OFDM-based system as an example, this chapter analytically quantifies the performance of the ANDL in the presence of impulsive noise. Here, we introduce a proper model for impulsive noise which captures its characteristics in analog domain while maintaining equivalency with the common models used in discrete domain. In order to reduce the complexity of the analytical derivations, the proposed ANDL is simplified. However, we show that this simplification does not degrade the performance of the proposed filter. Finally, the BER performance of the ANDL is analytically quantified by approximating the ANDL as a set of linear filters. Here, the exact linear filter that operates at a given time depends upon the magnitude of the outliers. Then, a closed-form analytical bound is derived for the average SNR at the output of the proposed filter and the analytical BER performance is validated by simulation.

3.2 System and Noise Models

The system model considered in this chapter is the same as Fig. 2.1. Therefore, under perfect synchronization, the received signal in an additive noise channel is given by

$$r(t) = s(t) + w(t) + i(t). \tag{3.1}$$

Here, $s(t)$ denotes the desired OFDM signal with variance σ_s^2 and bandwidth B_s; $w(t)$ is complex Gaussian noise with mean zero and variance σ_w^2; and $i(t)$ represents the impulsive noise with mean zero and variance $\sigma_i^2 \gg \sigma_w^2$. According to the structure of the receiver in

Fig. 2.1, the proposed ANDL is implemented before the ADC as a front end filter and the matched filter is modified to compensate the filtering effect of the ANDL in linear regime. In the following, we begin with a review of the impulse noise model.

3.2.1 Impulsive Noise Model

The widely used impulsive noise models assume the presence or absence of a strong noise component as the realization of two mutually exclusive events [48]. To analyze and evaluate system performance, we propose a model that captures characteristics of an impulsive noise in the analog domain. The considered impulsive noise consists of short duration high powered impulses with random arrivals and corresponds to

$$i(t) = \nu(t) \sum_{k=1}^{\infty} B_k \left[\theta(t - t_k) - \theta(t - t_k - \tau_{as})\right], \tag{3.2}$$

where, $\nu(t)$ represents complex white Gaussian noise process with zero mean; B_k is the amplitude of k^{th} pulse and modeled by Gaussian random variable; t_k is a arrival time of a Poisson process with parameter λ; $\theta(t)$ denotes the Heaviside unit step function, and τ_{as} is the duration of impulsive noise. In general the duration τ_{as} can change randomly for each burst but here, for simplicity, we assume a fixed average duration for all bursts. However, it is important to note that the method and results presented in this work can be easily extended to the case when the impulsive noise duration is random. The resulting time and frequency domains representation of this noise in analog domain is depicted in Fig. 3.1.

Note that, while (3.2) captures a bursty impulsive noise with random amplitude in analog domain, it also can represent Bernouli-Gaussian (BG) impulsive noise model in time duration

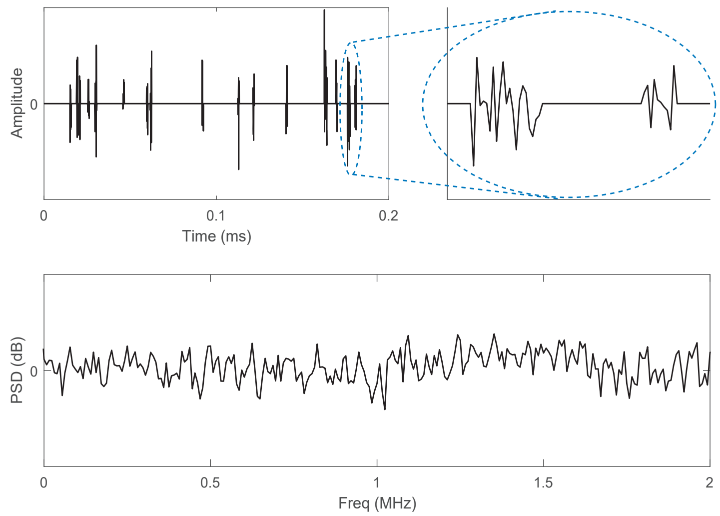

Fig. 3.1: Asynchronous impulsive noise

T with average success probability ϵ given by

$$\begin{aligned}
\varepsilon &= \left[\sum_{k=0}^{\infty} \frac{\mathrm{e}^{-\lambda T}(\lambda T)^k}{k!} k\tau_{as}\right] \Bigg/ T \\
&= \lambda\tau_{\mathrm{as}} \left[\sum_{k=1}^{\infty} \frac{\mathrm{e}^{-\lambda T}(\lambda T)^{k-1}}{(k-1)!}\right] \\
&= \lambda\tau_{\mathrm{as}} \left[\sum_{k=0}^{\infty} \frac{\mathrm{e}^{-\lambda T}(\lambda T)^{k}}{k!}\right] \\
&= \lambda\tau_{\mathrm{as}}. \qquad (3.3)
\end{aligned}$$

In the next section, we discuss the design and implementation of ANDL in detail.

3.3 Fundamentals of ANDL

An introduction to the fundamentals of the ANDL and finding an efficient value for the resolution parameter is provided in this section.

3.3.1 ANDL Design

ANDL is a blind adaptive intermittently nonlinear filter that, can be perceived as a first order time varying linear filter. According to the basic concept of the proposed ANDL [25;49], the time parameter $\tau(t)$ varies proportionally with the magnitude of the difference signal between input and output of the filter. Therefore, we have

$$\chi(t) = x(t) - \tau(|x(t) - \chi(t)|)\,\dot{\chi}(t)\,, \tag{3.4}$$

where $x(t)$ and $\chi(t)$ are the input and output of the filter, respectively, and $\dot{\chi}(t)$ denotes the first time derivative of $\chi(t)$. As shown in Fig. 3.2, the time parameter $\tau(t) = \tau(|x(t) - \chi(t)|)$ is given by

$$\tau(|x(t) - \chi(t)|) = \tau_0 \times \begin{cases} 1 & |x(t) - \chi(t)| \leq \beta(t) \\ \frac{|x(t)-\chi(t)|}{\beta(t)} & \text{otherwise} \end{cases}\,, \tag{3.5}$$

where τ_0 is a fixed time constant and $\beta(t)$ is the resolution parameter of the filter. The value of $\beta(t)$ should be determined properly in order to mitigate the impulsive noise efficiently. In general, the ANDL is an intermittent nonlinear filter and behaves linearly, when the magnitude of the difference signal $|x(t) - \chi(t)|$ remains within a certain range determined by the resolution parameter $\beta(t)$. This allows us to avoid instabilities that are often associated with nonlinear filtering. However, in case of outliers, the proper selection of $\beta(t)$ leads the ANDL to the nonlinear regime to suppress the outliers. Based on (3.5), ANDL is extremely aggressive toward high amplitude impulsive noise, i.e., larger spikes in the input signal will result in a greater suppression at the output. According to the structure of ANDL, the objective is to determine a time-dependent resolution parameter $\beta(t)$ that enhances the quality of non-stationary signals under time-varying noise conditions. Therefore, an efficient value of $\beta(t)$ should allow to maximize the suppression of the impulsive noise without distorting the signal of interest. It is assumed that the power of thermal noise is fixed over one OFDM symbol duration. Therefore, the resolution parameter is constant ($\beta(t)$=β) in the duration of each OFDM symbol and it only changes across symbols. A proper value of

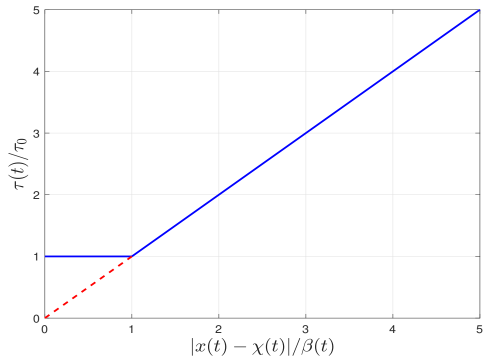

Fig. 3.2: ANDL time parameter $\tau(t) = \tau(|x(t) - \chi(t)|)$.

resolution parameter β can be found based on 2.10. Note that, the matched filter is also modified based on 2.13 to compensate for the ANDL in the linear regime.

3.4 Linear Approximation of The ANDL

Now that we have summarized the structure and operation of the ANDL, in this section we derive analytical expressions for the average SNR at the ANDL output.In order to characterize the theoretical performance of the ANDL we employ a linear approximation.

3.4.1 Time Parameter $\tau(t)$ Approximation

According to (3.5), the proposed ANDL enters the nonlinear regime only at the time of incoming impulsive noise where the difference signal $|x(t) - \chi(t)|$ would be approximately equal to $|x(t)|$. Therefore, the time parameter of the ANDL in (3.5) can be approximated as

$$\tau(\kappa|x(t)|) = \tau_0 \times \begin{cases} 1 & \text{for} \quad \kappa|x(t)| \leq \beta_0 \\ \frac{\kappa|x(t)|}{\beta_0} & \text{otherwise} \end{cases}, \tag{3.6}$$

where $\beta_0 = \beta_{\text{eff},\zeta}$, and κ is a positive constant that can be used to tune the modified ANDL for various impulsive noise models. In order to find the theoretical performance we approximate the ANDL by combination of n linear filters as illustrated in Fig. 3.3. Here, the time constant

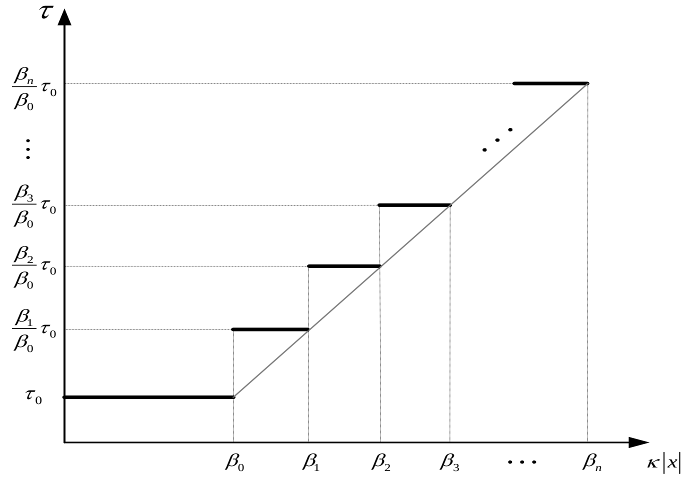

Fig. 3.3: ANDL time parameter $\tau = \tau(\kappa|x|)$.

of each individual linear filter can be expressed as

$$\tau(t) = \begin{cases} \tau_0, & \kappa|x(t)| < \beta_0 \\ \tau_1 = \frac{\beta_1}{\beta_0}\tau_0, & \beta_0 < \kappa|x(t)| < \beta_1 \\ \vdots & \\ \tau_k = \frac{\beta_k}{\beta_0}\tau_0, & \beta_{k-1} < \kappa|x(t)| < \beta_k \end{cases} . \tag{3.7}$$

As can be seen in Fig. 3.4, the performance of the approximated ANDL in (3.6) with $\kappa = 1$ is almost the same as the primary ANDL in (3.5). Fig. 3.4 also shows that the approximation with a combination of n linear filters results in performance equivalent to the (3.5). Theoretically, we have the best approximation when $n \to \infty$ where the difference between two consecutive filters $\triangle\beta = \beta_k - \beta_{k-1}$, $1 \leq k \leq n$ is small and the values of β_k are optimized. In this work, for simplicity, the linearization is performed assuming a constant $\triangle\beta$. Fig. 3.4 shows that in practice, a reasonable value of n and $\triangle\beta$ that guarantee $\beta_n = \beta_0 + n\triangle\beta > max|x(t)|$ (cover the entire range of $|x(t)|$) ensures the accuracy of the approximation.

In our ANDL structure, the received signal passes through a broadband lowpass filter to limit the input noise power while ensuring that the impulsive noise is not excessively spread out in time. Considering a sufficiently broadband front end filter, the input signal $x(t)$ for

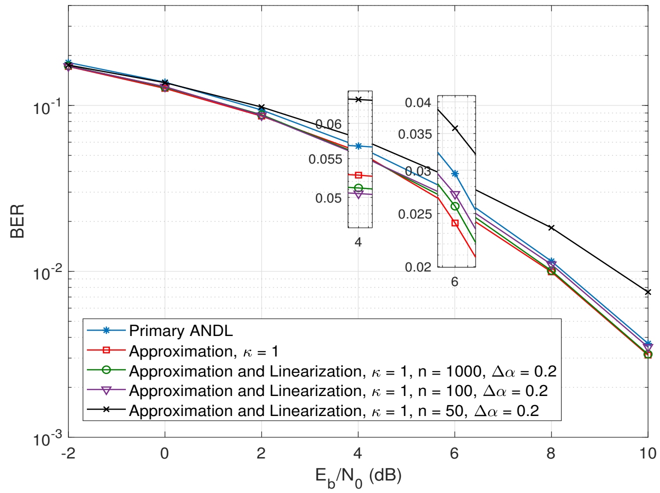

Fig. 3.4: Linear approximation of ANDL. SIR $= 0$ dB, $\lambda = 2B_s$, $\tau_{as} = 1\mu$s.

ANDL can be represented by a stationary mixture of two Gaussian components weighted by $1-\varepsilon$ and ε. Therefore, the probability density function (PDF) of the input signal $x(t)$ can be expressed via a Gaussian Mixture (GM) model given by

$$f_X(x) = (1-\varepsilon)\phi_{x_1}(0,\sigma_1^2) + \varepsilon\phi_{x_2}(0,\sigma_2^2), \tag{3.8}$$

where

$$\begin{aligned} x_1(t) &= s(t) + w(t) \sim \mathcal{N}(0, \sigma_1^2 = \sigma_s^2 + \sigma_w^2) \\ x_2(t) &= s(t) + w(t) + i(t) \sim \mathcal{N}(0, \sigma_2^2 = \sigma_s^2 + \sigma_w^2 + \sigma_i^2), \end{aligned} \tag{3.9}$$

and $\phi_x(.)$ is the Gaussian PDF defined by

$$\phi_x(\mu, \sigma^2) = \frac{1}{\sqrt{2\pi}\sigma} \mathrm{e}^{-\frac{(x-\mu)^2}{2\sigma^2}}. \tag{3.10}$$

Based on the GM model and according to (3.7), the average filtering effect of the ANDL can be computed via an averaged time parameter τ corresponding to

$$\mathbb{E}[\tau] = (1-\varepsilon)\sum_{k=0}^{n} p_{k,1}\tau_k + \varepsilon\sum_{k=0}^{n} p_{k,2}\tau_k, \tag{3.11}$$

where,

$$p_{k,1} = \begin{cases} \Pr(0 < \kappa \left| x_1(t) \right| < \beta_0), & k = 0 \\ \Pr(\beta_{k-1} < \kappa \left| x_1(t) \right| < \beta_k), & k = 1, ..., n \end{cases}$$
$$= \begin{cases} 1 - \operatorname{erfc}\left(\frac{\beta_0}{\sqrt{2}\kappa\sigma_1}\right), & k = 0 \\ \operatorname{erfc}\left(\frac{\beta_{k-1}}{\sqrt{2}\kappa\sigma_1}\right) - \operatorname{erfc}\left(\frac{\beta_k}{\sqrt{2}\kappa\sigma_1}\right), & k = 1, ..., n \end{cases}, \tag{3.12}$$

and

$$p_{k,2} = \begin{cases} \Pr(0 < \kappa \left| x_2(t) \right| < \beta_0), & k = 0 \\ \Pr(\beta_{k-1} < \kappa \left| x_2(t) \right| < \beta_k), & k = 1, ..., n \end{cases}$$
$$= \begin{cases} 1 - \operatorname{erfc}\left(\frac{\beta_0}{\sqrt{2}\kappa\sigma_2}\right), & k = 0 \\ \operatorname{erfc}\left(\frac{\beta_{k-1}}{\sqrt{2}\kappa\sigma_2}\right) - \operatorname{erfc}\left(\frac{\beta_k}{\sqrt{2}\kappa\sigma_2}\right), & k = 1, ..., n \end{cases}. \tag{3.13}$$

Here, erfc(.) represents the complementary error function.

3.4.2 Output of the ANDL

Considering (3.7), the ANDL can be approximated by a weighted combination of n linear filters with each of them functioning with probabilities corresponding to (3.12) and (3.13). Thus, the average output of the filter based on a mixture model input can be expressed as

$$\chi(t) = \begin{cases} \chi_1(t), & \text{with probability } 1 - \varepsilon \\ \chi_2(t), & \text{with probability } \varepsilon \end{cases}, \tag{3.14}$$

where

$$\begin{aligned} \chi_1(t) &= \sum_{k=0}^{n} p_{k,1} \left\{ [s(t) + w(t)] * h_k(t) \right\}, \\ \chi_2(t) &= \sum_{k=0}^{n} p_{k,2} \left\{ [s(t) + w(t) + i(t)] * h_k(t) \right\}. \end{aligned} \tag{3.15}$$

Here, $h_k(t)$ is a first order linear lowpass filter with time constant τ_k. In order to quantify

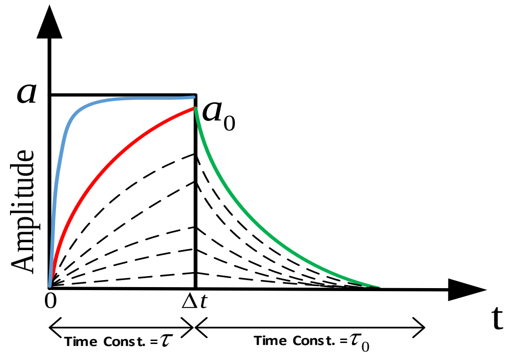

Fig. 3.5: Step Response of the ANDL.

the output power of each individual filter, we consider square pulses as an input (if not, each shape can be approximated by summation of narrower square pulses). According to Fig. 3.5, the output of the proposed ANDL consists of two parts $y_1(t)$ (red line) and $y_2(t)$ (green line) which are given by

$$
\begin{aligned}
y_1(t)\,\big|_{(\tau,a)} &= a(1-e^{-\frac{t}{\tau}}), \qquad 0 \le t \le \Delta t \\
y_2(t)\,\big|_{(\tau_0,a)} &= a_0 e^{-\frac{(t-\Delta t)}{\tau_0}}, \qquad\qquad t \ge \Delta t,
\end{aligned}
\tag{3.16}
$$

where τ is the time parameter for $y_1(t)$ (i.e., τ_k in k^{th} region of (3.7)); τ_0 represents the time constant and it is determined based on the bandwidth of desired signal; Δt is duration of square pulse with amplitude a, and $a_0 = a(1-e^{-\frac{\Delta t}{\tau}})$. Note that $\tau = \tau_0$ when there is no impulsive noise. Thus, given τ, τ_0 and a, the corresponding output power after lowpass filtering for a single pulse is given by

$$
\begin{aligned}
P\,\big|_{(\tau,a)} = (P_1+P_2)\,\big|_{(\tau,a)} &= \int_0^{\Delta t} |y_1|^2 dt + \int_{\Delta t}^{\infty} |y_2|^2 dt \\
&= \int_0^{\Delta t} \left|a(1-e^{-\frac{t}{\tau}})\right|^2 dt + \int_{\Delta t}^{\infty} \left|a_0 e^{-\frac{(t-\Delta t)}{\tau_0}}\right|^2 dt \\
&= a^2\left[\Delta t - \frac{\tau}{2}e^{-\frac{2\Delta t}{\tau}} + 2\tau e^{-\frac{\Delta t}{\tau}} - 3\frac{\tau}{2}\right] + a_0^2\frac{\tau_0}{2}.
\end{aligned}
$$

This amount of power is the total residual power after filtering which consists of power of the desired signal, thermal, and impulsive noises. In order to find their individual contributions, we use average residual power for desired signal and thermal noise but for impulsive noise we calculate the residual power for each region in Fig. 3.3, separately. Since the ANDL is approximated by a set of linear filters and the amplitude variation of the desired signal is much smaller than impulsive noise variation (lower bandwidth), the average residual power of desired signal can be determined by averaging over τ and a, that is

$$P_s = \mathbb{E}_{\tau,a}[P\,|_{\tau,a}] = \int\int P\,\Big|_{(\tau,a)}\,.f_T(\tau).f_A(a)\,d\tau da. \tag{3.17}$$

In the case of the desired signal, random variable a corresponds to $|s(t)|$ which has a folded-normal distribution ($s(t)$ has Gaussian distribution). Therefore, we have

$$P_s = \mathbb{E}^2\left[|s(t)|\right]\left((1-\varepsilon)\sum_{k=0}^{n} p_{k,1}P\,\Big|_{(\tau_k,1)} + \varepsilon\sum_{k=0}^{n} p_{k,2}P\,\Big|_{(\tau_k,1)}\right), \tag{3.18}$$

where

$$\mathbb{E}[|s(t)|] = \sigma_s\sqrt{\frac{2}{\pi}}e^{(-\mu_s^2/2\sigma_s^2)} + \mu_s(1-2\phi(\frac{-\mu_s}{\sigma_s})). \tag{3.19}$$

Similarly, in the case of thermal noise, the random variable a corresponds to $|w(t)|$ and we have

$$P_w = \mathbb{E}^2\left[|w(t)|\right]\left((1-\varepsilon)\sum_{k=0}^{n} p_{k,1}P\,\Big|_{(\tau_k,1)} + \varepsilon\sum_{k=0}^{n} p_{k,2}P\,\Big|_{(\tau_k,1)}\right), \tag{3.20}$$

where

$$\mathbb{E}[|w(t)|] = \sigma_w\sqrt{\frac{2}{\pi}}e^{(-\mu_w^2/2\sigma_w^2)} + \mu_w(1-2\phi(\frac{-\mu_w}{\sigma_w})). \tag{3.21}$$

The amplitude variation of the impulsive noise is much larger than the amplitude variation of the desired signal and thermal noise. However, it is possible that some impulsive noise may be buried within the desired signal and thermal noise. If that is the case, then there will be no way to distinguish between impulsive noise and the other components of the received signal in a band limited system. This problem highlights the advantage of the proposed ANDL which is implemented in the analog domain where a wide acquisition bandwidth makes the impulsive noise more distinguishable. Thus, the absolute value of impulsive noise is more likely to be larger than the resolution parameter. Consequently, the impulsive noise will encounter a filter with large τ proportional to its amplitude as shown by dashed lines in Fig. 3.5. Therefore, we find the average amplitude of impulsive noise in each region of Fig. 3.3 and for simplicity we pick the center of each region except in the first region where β_0 is picked as a representative of the amplitude of impulsive noise. Thus, we have

$$\mathbb{E}[|i_k|] = \begin{cases} \beta_0, & k = 0 \\ \beta_0 + \frac{(2k-1)\Delta\beta}{2}, & k = 1, ..., n \end{cases}, \tag{3.22}$$

and the average residual power of impulsive noise after the linearized ANDL is given by

$$P_i = \varepsilon \sum_{k=0}^{n} \mathbb{E}^2[|i_k|].p_{k,2}.P \left|_{(\tau_k,1)}\right. . \tag{3.23}$$

Finally, the average output SNR can be expressed as

$$\mathrm{SNR}_{\mathrm{avg}} = \frac{P_s}{P_w + P_i}. \tag{3.24}$$

Therefore, the average BER can be bounded using Jensen's inequality. For example, for BPSK $\mathrm{BER}_{\mathrm{avg}} \leq Q(\sqrt{2\,\mathrm{SNR}_{\mathrm{avg}}})$ where $Q(.)$ is the Q-function.

3.5 Simulation results

In this section, the analytical results derived in the previous sections are validated through simulations. In addition, SNR and BER of an OFDM system with BPSK modulation are used to compare the performance of the proposed analog nonlinear filter to other conventional approaches such as linear filtering, blanking and clipping. As a specific example, an OFDM-based system with signal bandwidth $B_s = 100\,kHz$ and $N = 512$ subcarriers is chosen as a reference, but the conclusions can be extended to any OFDM system as long as the number of subcarriers is large enough to satisfy the Gaussian signal assumption. The system is investigated in an additive noise environment that consists of two components: (i) thermal noise, (ii) asynchronous random impulsive noise with normally distributed amplitudes captured by a Poisson arrival process with parameter λ and time duration τ_{as}. To mitigate the impulsive noise, a first order ANDL with τ_0=1/(4πB_s) is used. It is important to note that when $\beta \to \infty$ the ANDL becomes a first order linear lowpass filter and a modified matched filter is used to alleviate the filtering effect of ANDL in the linear regime. To emulate the analog signals in the simulation, the digitization rate is chosen to be significantly higher (by about two orders of magnitude, i.e., a factor of 10^2) than the ADC sampling rate. Note that in all simulations, (i) the optimum thresholds for blanking and clipping are found based on an exhaustive numerical search, (ii) the resolution parameter $\beta(t)$ for ANDL is determined based on expression 2.10 with low computational complexity, and (iii) $\kappa = 1$, $\Delta\beta = 0.2$, and the number of quantization levels n is determined according to the dynamic range of incoming signal and considered $\Delta\beta$. Fig. 4.4 shows the properties of the signal in time and frequency domain, and its amplitude distribution for different methods of impulsive noise mitigation. In Fig. 4.4, the black dashed lines (shaded area) represent the desired signal (without noise), and the colored solid lines represent the signal+noise mixtures. The leftmost panels show the time domain traces, the rightmost panels show the PSD, and the middle panels show the PDF of amplitude. From the panels of the last row, it is clear that the ANDL efficiently reduces the spectral density of the impulsive noise in the signal passband without significantly affecting the signal of interest. By comparing the panels of row LIN (Linear), CLP (Clipping) and BLN (Blanking) with row ANDL (specially PSDs panels), it can be seen that the achieved improvement due to ANDL in the quality of the baseband signal is significant. In the following, the aforementioned improvement is shown in terms of SNR and BER.

The SNR performance for linear filter, ANDL, blanking, and clipping in various noise compositions is compared in Fig. 4.5. According to Fig. 4.5, all approaches provide effectively equivalent performance when thermal noise dominates the impulsive noise. However, the

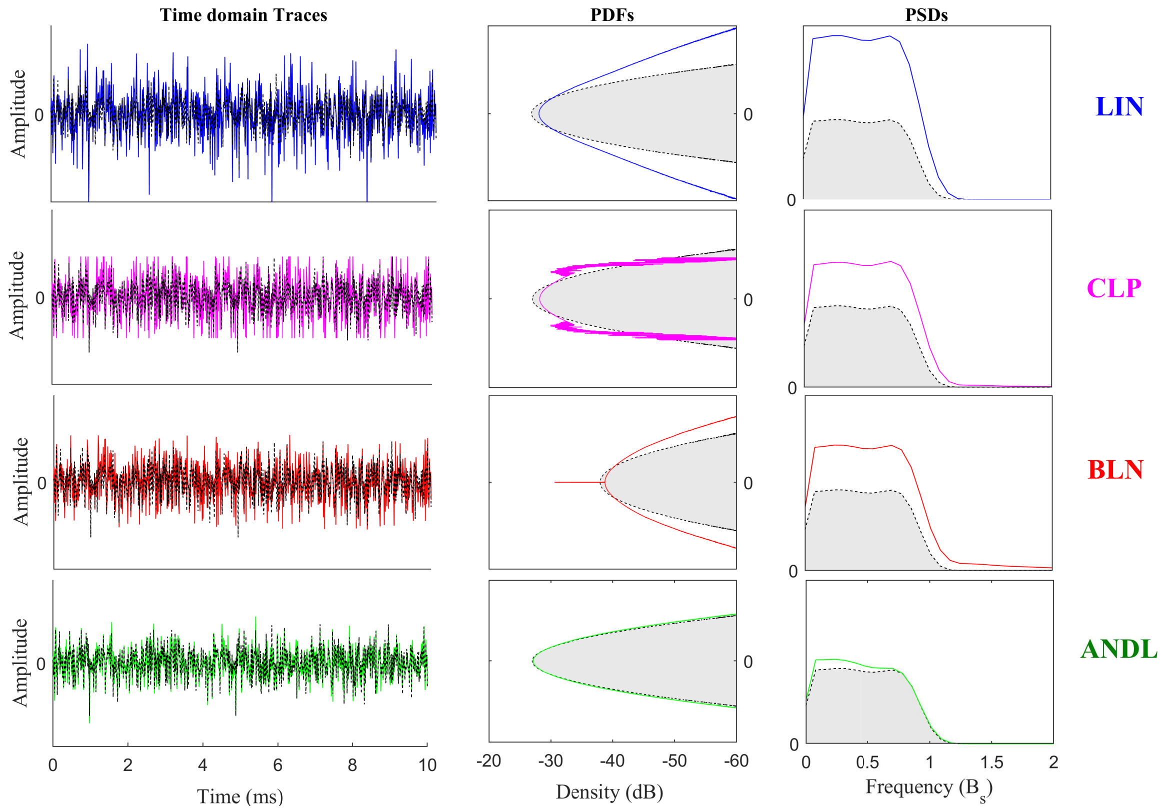

Fig. 3.6: Comparison of different approaches in time and frequency domain. $E_b/N_0 = 10$ dB, SIR $= 0$ dB, $\lambda = B_s$.

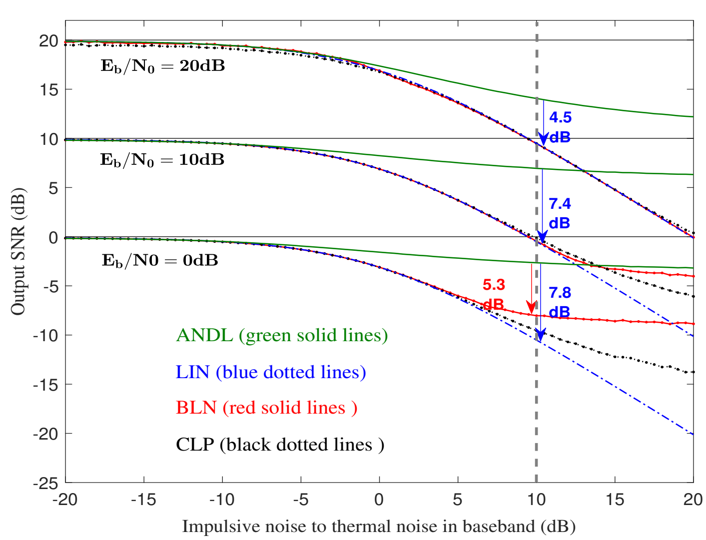

Fig. 3.7: Comparison of output SNR for different approaches. $\lambda = 2B_s$.

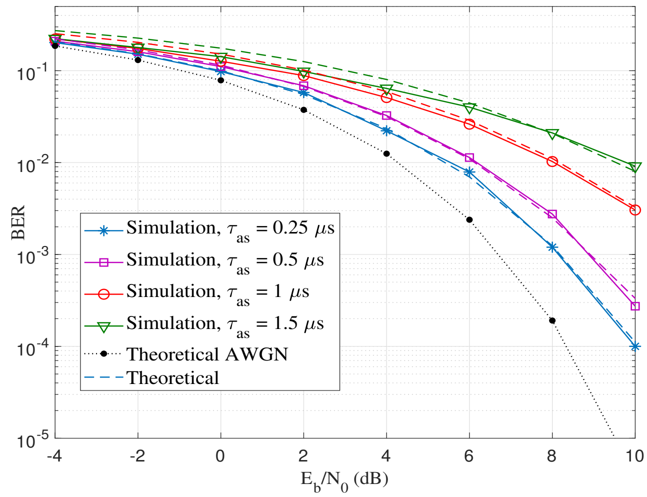

Fig. 3.8: BER versus E_b/N_0. SIR $= 0$ dB, $\lambda = 2B_s$.

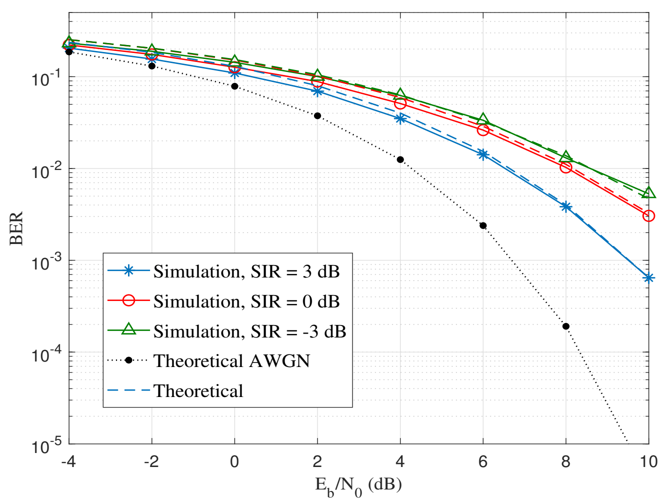

Fig. 3.9: BER versus E_b/N_0. $\lambda = 2B_s$, $\tau_{as} = 1\mu$s.

superiority of the ANDL is highlighted when the impulsive noise is dominant and in low SNR (SNR less than zero) its performance is almost insensitive to further increase in the impulsive noise power. The potency of the ANDL in impulsive noise environment is validated by both simulation and theoretical results. The BER performance of the ANDL in fixed SIR and different duration of impulsive noise versus Eb/N0 is shown in Fig. 3.8. As expected, we have better performance in short duration impulsive noise. Fig. 3.9 shows the BER performance of the ANDL in fixed duration of impulsive noise and different values of SIR

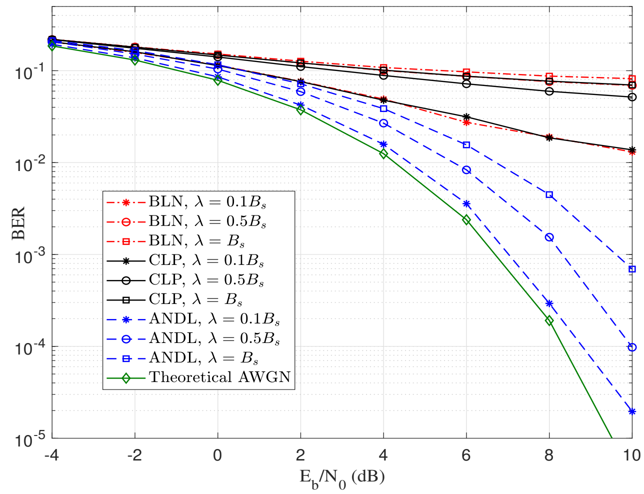

Fig. 3.10: BER comparison of ANDL, BLN, and CLP versus E_b/N_0 for different values of λ. SIR = 0 dB, $\tau_{as} = 1\mu$s.

versus Eb/N0. As shown in Fig. 3.8 and Fig. 3.9, the theoretical results are well aligned with simulation in different scenarios which validate our theoretical calculations.

Fig. 3.10 compares the BER performance of ANDL with blanking and clipping for different levels of impulsivity (λ) with $\tau_{as} = 1\mu$s. Fig. 3.10 shows that blanking and clipping are very vulnerable to impulsivity level and their performance is dramatically poor in high impulsive environment. Although, the performance loss of the ANDL with increasing the impulsivity level is also noticeable, still outperforms other approaches in all scenarios. In Fig. 3.11, the BER performance of ANDL for different values of SIR in highly impulsive environments ($\lambda = 2B_s$) is compared with blanking and clipping. Fig. 3.11 shows that both blanking and clipping have poor performance and ANDL outperforms them especially at high SNR. The potency of ANDL in reducing the PSD of impulsive noise in the signal passband is due to the fact that unlike other nonlinear methods, ANDL is implemented in the analog domain where the outliers are still broadband and distinguishable. Therefore, in highly impulsive environment as shown in Fig. 3.11, ANDL is highly preferable to digital approaches such as blanking and clipping.

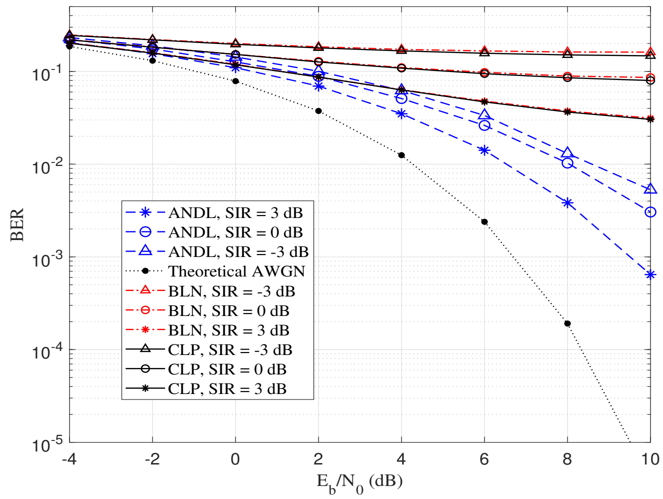

Fig. 3.11: BER comparison of ANDL, BLN, and CLP versus E_b/N_0 for different values of SIR. $\lambda = 2B_s$, $\tau_{as} = 1\mu$s.

3.6 Summary

In this chapter, ANDL is proposed to mitigate impulsive noise in OFDM-based systems. In addition, an approximation of the ANDL using a piecewise combination of linear filters is used to derive closed-form analytical expressions for the average SNR at the output of the proposed filter. We also show that the theoretical BER results are well aligned with simulation results for different compositions of noise. The theoretical analysis and simulation results show that the ANDL ensures significant improvement in SNR and BER performance in the presence of strong impulsive noise component. Moreover, the ANDL outperforms other conventional outlier mitigation methods that exploit amplitude distribution such as blanking and clipping by providing lower BER in impulsive noise environments. It is important to note that the proposed ANDL is totally blind and can be deployed in real-time applications for both sparse and bursty impulsive noise scenarios.

Chapter 4

Practical Implementation of Adaptive Analog Nonlinear Filtering For Impulsive Noise Mitigation

In chapter 3 we study the analytical performance of a realization of BAINFs as ANDL. In this chapter, we investigate another realization of BAINFs and its practical implementation consideration. We propose a practical blind adaptive analog nonlinear filter to efficiently detect and mitigate impulsive noise. Specially, we design an Adaptive Canonical Differential Limiter (ACDL) which is constructed from a Clipped Mean Tracking Filter (CMTF) and Quartile Tracking Filters (QTFs). The QTFs help to determine a real-time range that excludes outliers. This range is fed into the CMTF which is responsible for mitigating impulsive noise. The CMTF is a nonlinear analog filter and its nonlinearity is controlled by the aforementioned range. Proper selection of this range ensures the improvement of the desired signal quality in impulsive environment. It is important to note that the proposed ACDL behaves like a linear filter in case of no impulsive noise. The performance improvement of the proposed ACDL is due to the fact that unlike other nonlinear methods, the ACDL is implemented in the analog domain where the outliers are still broadband and distinguishable. Simulation results in PRIME (OFDM-based narrowband PLC system) demonstrate the superior BER performance of ACDL relative to other nonlinear approaches such as blanking and clipping in impulsive noise environments.

4.1 Introduction

With the pervasive reach of powerline infrastructure, low deployment costs, and its wide frequency band, PLC has become a strong candidate for a variety of smart grid applications [53]. High speed communication over powerlines has recently attracted considerable interest and offer a very interesting alternative to wireless communication systems. The ability to support high data rates in PLC requires multicarrier protocols such as OFDM [48]. The two major issues in OFDM-based PLC are: (1) impedance mismatch that is due to the fact that the powerline infrastructure is originally designed for power delivery and not for communications [53], and (2) noise that typically consists of two parts: the thermal noise, which is assumed to be additive Gaussian noise, and impulsive noise that may be synchronous or asynchronous relative to the main frequency [27;47].

In chapter 2 and chapter 3, ANDL is proposed to mitigate impulsive noise in analog domain before the ADC [49;50]. In previous chapters, we studied the basics of the ANDL and the SNR and BER performance of the ANDL in a practical OFDM-based system is investigated. Although, in [49] a simple method is proposed to determine an effective value for the resolution parameter that maximizes signal quality while mitigating the impulsive noise, finding the resolution parameter in real-time and practical implementation of the filter are still a open problem that we address in this chapter.

In this chapter, the ACDL is proposed to mitigate the effect of impulsive noise in PLC system without knowledge of the noise distribution. The effects of this filter on the desired signal are totally different relative to that on the impulsive noise because of nonlinearity of this filter. Therefore, SNR in the desired bandwidth will increase by reducing the spectral density of non-Gaussian noise without significantly affecting the desired signal. We validate the performance of the ACDL by measuring the SNR and the BER of a practical PLC system. In addition, we highlight the preference of our approach rather than other conventional

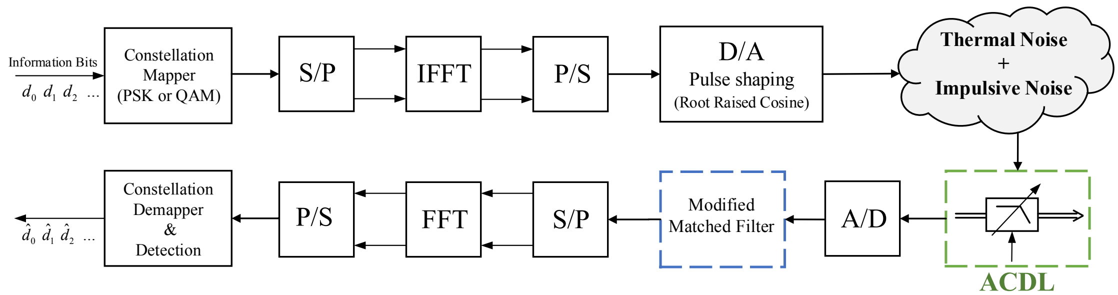

Fig. 4.1: System model block diagram.

approaches such as blanking, clipping and linear filtering.

4.2 System Model

The considered OFDM-based system is shown in Fig. 4.1. Therefore, like previous chapters, under perfect synchronization, the received signal in an additive noise channel is given by

$$r(t) = s(t) + w(t) + i(t). \tag{4.1}$$

Here, $s(t)$ denotes the desired signal with variance σ_s^2, $w(t)$ is complex Gaussian noise with mean zero and variance σ_w^2, and $i(t)$ represents the impulsive noise which is not Gaussian and it is assumed that $s(t)$, $w(t)$, and $i(t)$ are mutually independent. In general, the model in (4.1) can be expanded to include channel attenuation (fading) effect. However, since the goal of this chapter is to demonstrate a novel approach to mitigation of impulsive noise, we restrict ourselves to additive noise channel model in (4.1). It is important to note that the proposed ACDL approach is applicable to alternate channel model as well. As shown in Fig. 4.1, the conventional structure of the receiver is modified in order to deal with impulsive noise $i(t)$ and the proposed filter is implemented before the ADC as a front end filter. Like chapter 2, the Non-Gaussian noise $i(t)$ consists of both cyclostationary impulsive noise and asynchronous impulsive noise that can be modeled based on 2.3 and 2.4, respectively. In the next section, we discuss the ACDL design and implementation in detail.

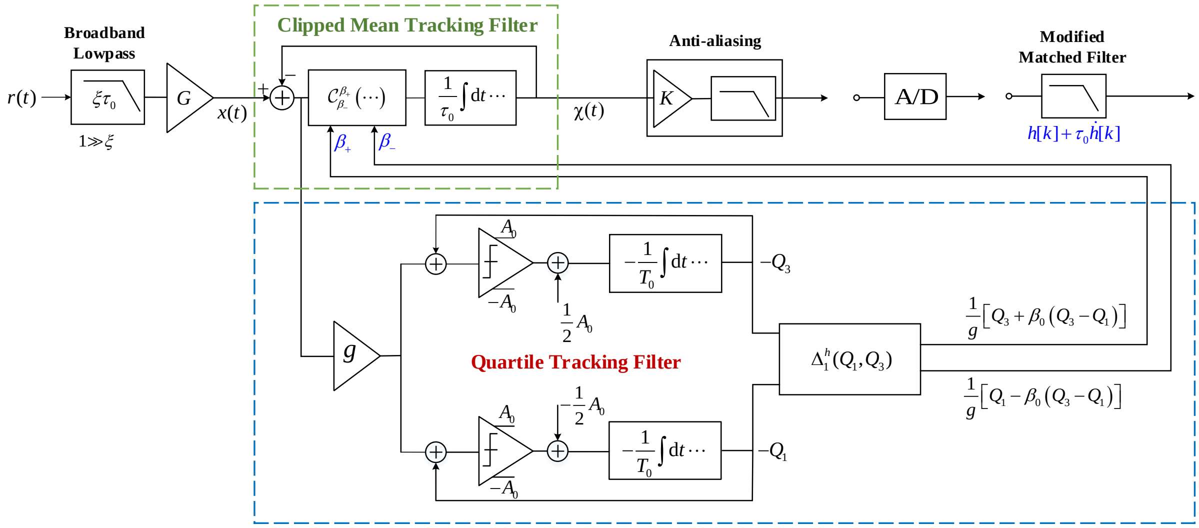

Fig. 4.2: Practical implementation of ACDL. Adapted from [2].

4.3 Practical Implementation of Adaptive Canonical Differential Limiter (ACDL)

The principal block diagram of the ACDL is shown in Fig. 4.2. Without loss of generality, it is assumed that the output ranges of the active components (active filters, integrators, and comparators), as well as the input range of the ADC, are limited to a certain finite range, e.g., to the power supply range $\pm V_c$. The time parameter τ_0 is such that $1/2\pi\tau_0$ is equal to the corner frequency of the anti-aliasing filter (e.g., approximately twice the bandwidth of the signal of the interest B_x), and the time constant T_0 is two-to-three orders of the magnitude larger than B_x^{-1}. The purpose of the front-end lowpass filter is to limit the input noise power and at the same time its bandwidth should remain sufficiently wide (i.e. $\xi \ll 1$), so that the impulsive noise is not excessively spread out in time. In general, we can assume that the gain K is constant and is largely depended on the value of the parameter ξ (e.g. $K \sim \sqrt{\xi}$), and the gains G and g are adjusted in order to fully utilise the available output ranges of the active components, and the input range of the ADC. For instance, G and g may be chosen to ensure that the average absolute value of the output signal (i.e., observed at point IV) is approximately $V_c/10$, and the difference $Q_3 - Q_1$ is $2V_c/5$.

4.3.1 Clipped Mean Tracking Filter (CMTF)

The role of the CMTF is to mitigate outliers from the input signal and at the same time it should be designed to behave like a linear filter in the absence of outliers. As shown in the block diagram of the CMTF in Fig. 4.2, the input $x(t)$ and the output $\chi(t)$ signals can be related by the following 1st order nonlinear differential equation

$$\frac{\mathrm{d}}{\mathrm{d}t}\chi(t) = \frac{1}{\tau_0}\mathcal{C}_{\beta_-}^{\beta_+}\left(x(t) - \chi(t)\right), \tag{4.2}$$

where the clipping function $\mathcal{C}_{\beta_-}^{\beta_+}(x)$ is defined as

$$\mathcal{C}_{\beta_-}^{\beta_+}(x) = \begin{cases} \beta_+ & for \quad x > \beta_+ \\ \beta_- & for \quad x < \beta_- \\ x & otherwise \end{cases}, \tag{4.3}$$

where $\beta+$ and $\beta-$ are the upper and lower clipping values, respectively. Note that for the clipping values such that $\beta_- \leq x(t) - \chi(t) \leq \beta_+$ for all t, equation (4.2) describes a 1st order linear lowpass filter with corner frequency $1/2\pi\tau_0$, and the filter shown in Fig. 4.2 operates in a linear regime. However, when the values of the difference signal $x(t) - \chi(t)$ are outside of the interval $[\beta_-, \beta_+]$, the rate of change of $\chi(t)$ is limited to either β_-/τ_0 or β_+/τ_0 and no longer depends on the magnitude of $x(t) - \chi(t)$. Thus, if the values of the difference signal that lie outside of the interval $[\beta_-, \beta_+]$ are outliers, the output $\chi(t)$ will be insensitive to further increase in the amplitude of such outliers. In this chapter, an effective value of the interval $[\beta_-, \beta_+]$ is obtained as the *Tukey's range*[69], a linear combination of 1st (Q_1) and the 3rd (Q_3) quartiles of the linear-regime difference signal

$$[\beta_-, \beta_+] = [Q_1 - \beta_0(Q_3 - Q_1), Q_3 + \beta_0(Q_3 - Q_1)], \tag{4.4}$$

where β_0 is a constant coefficient (e.g. $\beta_0 = 3$). Then the quartiles $Q_1(t)$ and $Q_3(t)$ are obtained as output of the QTFs described in the next subsection.

4.3.2 Quartile Tracking Filters (QTFs)

Let $y(t)$ be a quasi-stationary bandpass (zero-mean) signal with a finite interquartile range (IQR), characterised by an average crossing rate $\langle f_0 \rangle$ of the threshold equal to the third quartile of $y(t)$. (See[70] for discussion of quantiles of continuous signals, and[71] for discussion of threshold crossing rates.) Let us further consider the signal $Q_3(t)$ related to $y(t)$ by the following differential equation

$$\frac{\mathrm{d}}{\mathrm{d}t} Q_3 = \frac{A_0}{T_0} \left[\mathrm{sgn}(y - Q_3) + \frac{1}{2} \right], \tag{4.5}$$

where A_0 is a constant (with the same units as y and Q_3), and T_0 is a constant with the units of time. According to equation (4.5), $Q_3(t)$ is a piecewise-linear signal consisting of the alternating segments with positive $(3A_0/(2T_0))$ and negative $(-A_0/(2T_0))$ slopes. Note that $Q_3(t) \approx \text{const}$ for a sufficiently small A_0/T_0 (e.g. much smaller than the product of the IQR and the average crossing rate $\langle f_0 \rangle$ of $y(t)$ and its third quartile), and a steady-state solution of equation (4.5) can be written implicitly as

$$\overline{\theta\,(Q_3 - y)} \approx \frac{3}{4}, \tag{4.6}$$

where the over-line denotes averaging over some time interval $\Delta t \gg \langle f_0 \rangle^{-1}$. Thus, Q_3 approximate the *third quartile* of $y(t)$ in the time interval Δt. Similarly, for

$$\frac{\mathrm{d}}{\mathrm{d}t} Q_1 = \frac{A_0}{T_0} \left[\mathrm{sgn}(y - Q_1) - \frac{1}{2} \right], \tag{4.7}$$

a steady-state solution can be written as

$$\overline{\theta\,(Q_1 - y)} \approx \frac{1}{4}, \tag{4.8}$$

and thus Q_1 would approximate the *first quartile* of $y(t)$ in the time interval Δt. Fig. 4.3 provides an illustration of the QTFs' convergence to the steady state for different initial

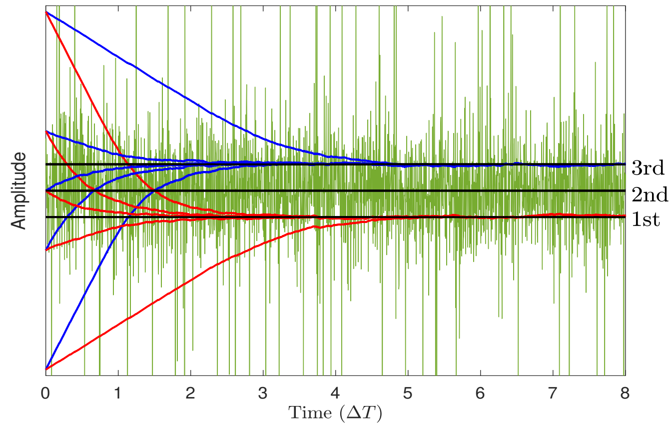

Fig. 4.3: Convergence of QTFs to steady state for different initial values. Eb/N0 = 0 dB, SIR = 0 dB. Adapted from[2].

conditions. In Fig. 4.3 signal $y(t)$ plotted by green line, first (red line) and third (blue line) quartiles, in comparison with the exact quartiles of $y(t)$ computed in the full shown time interval (black lines).

Since the proposed ACDL should not have any negative impact when there is no impulsive noise, it is essential to modify the matched filter to compensate for the CMTF in a linear chain and this modification is performed based on 2.13.

4.4 Simulation results

As a specific example, we simulate an OFDM-based PLC in accordance with the PRIME standard. The sampling frequency is chosen as $f_s = 250$ kHz and the FFT size is $N = 512$, i.e, the subcarrier spacing $f = 488$ Hz. As carriers 86-182 are used for data transmission, the PRIME signal is located in the frequency range 42-89 kHz[28]. The system is studied in a noise environment and it consists of three components: (i) a thermal noise (ii) periodic cyclostationary exponentially decaying component with the repetition frequency at twice the AC line frequency ($2 \times 60Hz$) $\tau_{\text{cs}} = 200\mu s$ (one tenth of OFDM symbol), and (iii) asynchronous random impulsive noise with normally distributed amplitudes captured by a Poisson arrival process with parameter λ and $\tau_{\text{as}} = 2\mu s$. Based on IEEE P1901.2 standard[27] the PSD of noise components (i) and (ii) decay at a rate of 30 dB per 1 MHz. Since the

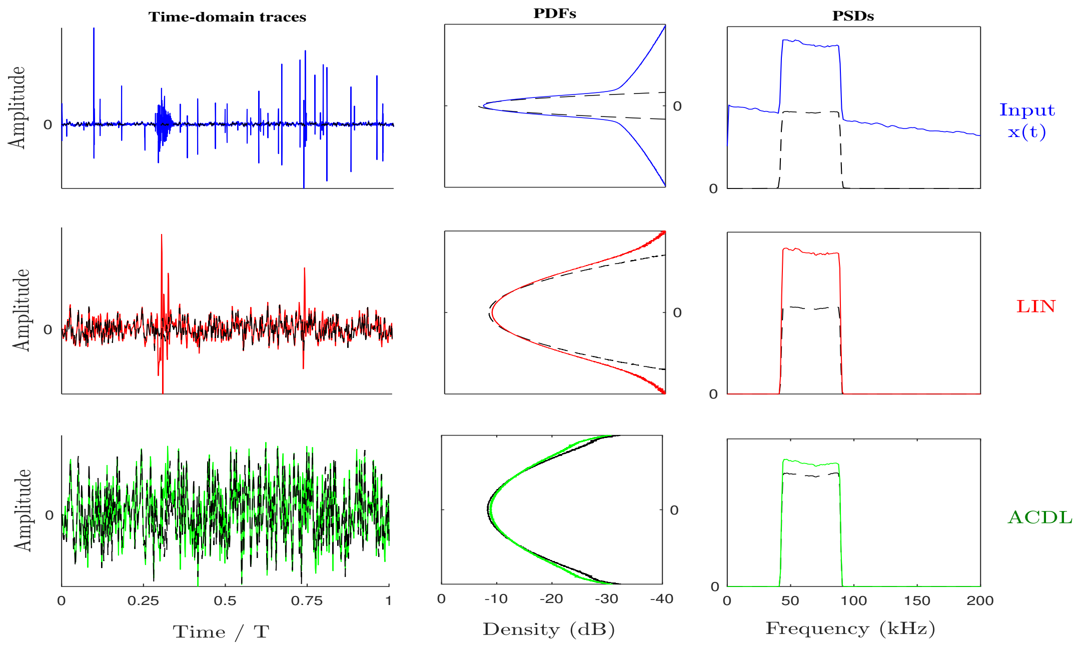

Fig. 4.4: Comparison of Linear and ACDL in time and frequency domain. Eb/N0 = 10 dB, SIR = 1 dB.

cyclostationary noise is dominant in the NB-PLC, we set the power of this component three times higher than the asynchronous impulsive noise. To emulate the analog signals in the simulation, the digitization rate is chosen to be significantly higher (by about two orders of magnitude) than the ADC sampling rate. In the following, SNR and BER of an OFDM system with BPSK modulation are used as two metrics to evaluate the performance of the proposed analog nonlinear filter in comparison with other conventional approaches such as linear filtering, blanking and clipping.

Fig. 4.4 shows an informative illustration of the changes in the signal's time and frequency domain properties, for both linear and ANDL receiver. In Fig. 4.4, the black dashed lines correspond to the desired signal (without noise), and the colored solid lines correspond to the signal+noise mixtures based on the PRIME standard. The leftmost panels show the time domain traces, the rightmost panels show the PSDs, and the middle panels show the PDF of amplitudes. The value of parameter β_0 for Tukey's range is set to $\beta_0 = 3$. From the panels of row ACDL, it is clear that CMTF disproportionately affects signals with different temporal and/or amplitude structures and then reduces the spectral density of the impulsive noise in the signal passband without significantly affecting the signal of interest. By comparing the output of linear (LIN) filter and the output of ACDL (specially PSDs panels), one can see the achieved improvement due to ACDL in the quality of the baseband signal is significant. In the following, we show the aforementioned improvement in terms of SNR and BER.

Fig. 4.5 compares the output SNR performance for the linear processing chain and ACDL for various signal+noie compositions. As one can see in Fig. 4.5, for an effective value $\beta_0 = 3$ both linear and ACDL provide effectively equivalent performance when thermal noise dominates the impulsive noise. However, the ACDL shows its potency when the impulsive noise is dominant and in low SNR (SNR less than zero) its performance is insensitive to further increase in the impulsive noise. The robustness of the ACDL in different types of impulsive noise is demonstrated by considering the case when both asynchronous and cyclostationary impulsive noise impact the signal simultaneously. The BER performance of the ACDL for different values of SIR versus Eb/N0 is shown in Fig. 4.6. The performance of the ACDL is compared with linear filter, blanking and clipping when the optimum thresholds for blanking and clipping are found based on an exhaustive numerical search. Fig. 4.6 shows that ACDL outperform other approaches, especially at high SNR. It is important to mention

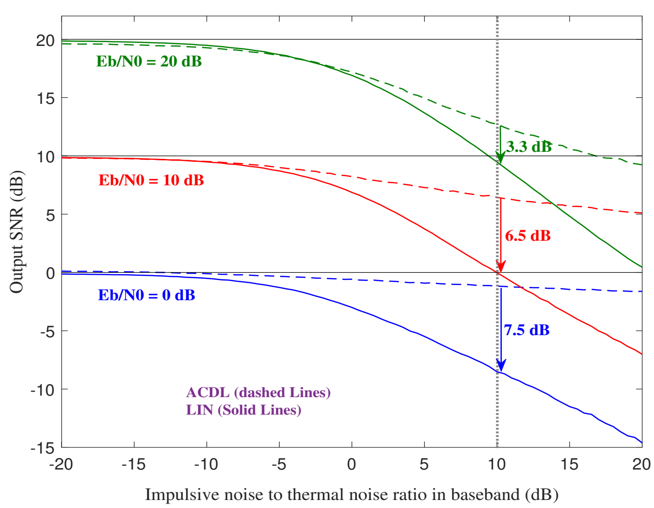

Fig. 4.5: Comparison of output SNR for the linear processing chain (solid lines) and ACDL (dashed lines). $1/\lambda = 2e^{-5}s$.

that the range $[\beta_-, \beta_+]$ in Fig. 4.6 are determined by QTFs module and $\beta_0 = 3$ which is an

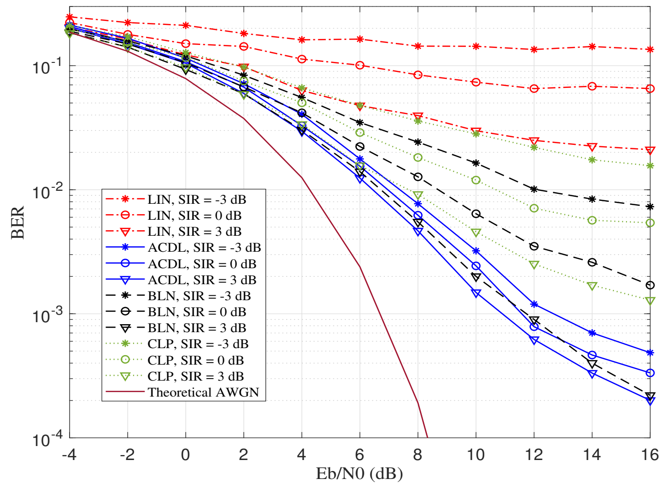

Fig. 4.6: BER versus Eb/N0 with fixed SIR. $1/\lambda = 2e^{-5}s$.

effective value for range β but not the optimum one. It is clear that a fixed value of β can not guarantee the optimum value of β for all kinds of noise, but an effective value of β_0 for a specific application can be easily found by training the ACDL in a short duration of time.

The effect of β_0 on the performance of the ACDL is illustrated in Fig. 4.7. As it can be seen the value of β_0 is critical especially at high SNR but selecting a value near the optimum one (e.g. $\beta_0 = 2.5, 3.5$ in Fig. 4.7) can ensure a reasonable performance. Using inefficient β_0, i.e., with high deviation from the effective value, may cause considerable performance degradation at higher SNR. Such behavior is due to inappropriate elimination of the impulsive noise or cropping the desired signal in large or small β_0 values, respectively.

4.5 Summary

In this chapter, a practical implementation of adaptive analog nonlinear filter, referred to ACDL is proposed to mitigate impulsive noise. The ACDL consists of two modules: CMTF and QTFs, which take care of outliers mitigation and finding a real-time range for parameter β, respectively. We demonstrate the performance of the ACDL considering an OFDM-based PLC system with both asynchronous and cyclostationary impulsive noises. The results

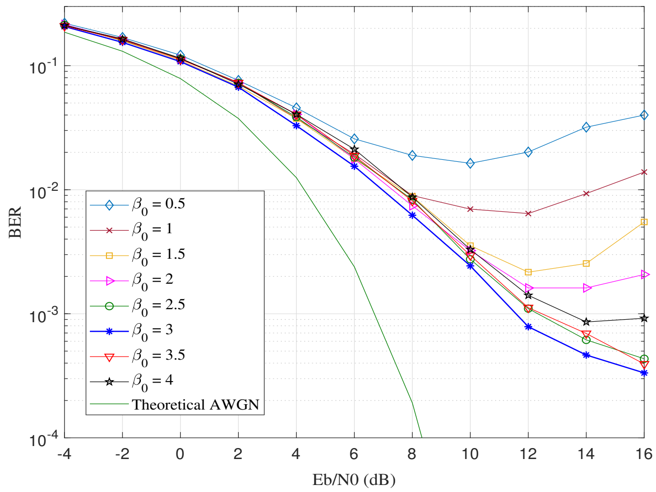

Fig. 4.7: Effect of β_0 on ACDL performance. SIR = 0 dB, $1/\lambda = 2e^{-5}s$.

show that the ACDL can provide improvement in the overall signal quality ranging from distortionless behavior for low impulsive noise conditions to significant improvement in SNR or BER performance in the presence of a strong impulsive component. Moreover, the ACDL outperforms other approaches such as blanking and clipping in reducing the BER in impulsive noise environments. It is important to note that the ACDL can be deployed either as a stand-alone low-cost real-time solution for impulsive noise mitigation, or combined with other interference reduction techniques.

Chapter 5

Intermittently Nonlinear Impulsive Noise Mitigation and Doppler Shift Compensation in UWA-OFDM Systems

Unlike previous chapters, in this chapter a realization of BAINFs is designed for a coded-OFDM system with channel impairment in UWA communication. Impulsive noise and Doppler shift can significantly degrade the performance of OFDM-based UWA communication systems. We propose a receiver structure that deals efficiently with both these channel impairments in a coded OFDM-based UWA system. First, an Analog Nonlinear Preprocessor (ANP) is proposed to efficiently detect and mitigate impulsive noise in analog domain. The proposed ANP exhibits intermittent nonlinearity when there is impulsivity. Next, the impact of impulsive noise on a two-step Doppler shift compensation approach is quantified. Specifically, the ability of the ANP to improve robustness of Doppler shift compensation in the presence of impulsive noise is highlighted. The performance improvement of the proposed receiver is due to the fact that, unlike other nonlinear methods, the ANP is implemented in the analog domain where the outliers are still broadband and distinguishable. Simulation results also demonstrate the superior BER performance of our approach relative to classic approaches that use blanking and/or clipping for impulsive noise mitigation.

5.1 Introduction

UWA communication is the most widely used technique for transmission in shallow water environments due to the low attenuation of sound in water[72;73]. Limited bandwidth, multipath fading, significant Doppler shifts, and strong impulsive noise are the major channel impairments in UWA communications[68;72;74;75]. The slow speed of sound, platform motion and instability of water medium result in significant frequency-dependent Doppler shifts and fast channel variations[75;76]. Fast time varying channel can limit the use of equalizers to compensate for frequency-selective fading. In order to cope with the frequency selectivity of the propagation channel, OFDM has been proposed[26]. In fact, by ensuring flat fading in each subcarrier, OFDM simplifies the equalizer structure and provides robustness against time-varying frequency-selective fading. While cyclic prefix (CP) or zero padding (ZP) is used to provide a guard interval between consecutive OFDM symbols to avoid inter-symbol interference (ISI) [77], inter-carrier-interference (ICI) limits the performance in the presence of frequency-dependent Doppler shifts[75]. A computationally efficient Doppler scaling factor estimation, based on preamble and postamble, is proposed in[78] for single carrier transmissions. Assuming the UWA channel has a common Doppler scaling factor on all propagation paths, authors in[75] extend the work in[78] and provide a two-step Doppler mitigation approach to deal with frequency-dependent Doppler shifts in OFDM system. In the first step a resampling technique is used to remove nonuniform Doppler effect[75] and then, in the second step, a high resolution uniform compensation of the residual Doppler is performed based on modification of the null subcarrier methods[79;80].

In addition, the UWA channel is rich in impulsive noise induced by snapping shrimp in shallow warm waters[9;10;81] or manmade noise near the shores[11]. Impulsive noise mitigation has been extensively explored in prior efforts in wired and wireless communications. The impact of channel coding on impulsive noise cancelation has been investigated in[30] and[31].

It has been shown that coding is effective only in single carrier schemes and there is no gain in OFDM systems in the presence of impulsive noise[32]. Doppler shift compensation and impulsive noise mitigation in UWA systems can be performed sequentially one after another or jointly. An iterative joint Doppler shift and impulsive noise estimation based on nonlinear least squares (LS) formulation is proposed in[68], which is computationally complex.

In this chapter, we investigate the performance of the ANP in the coded OFDM-based UWA channel. The proposed ANP offers a compromise between clipping and blanking in response to the impulsivity level which is determined based on outlier amplitude. Unlike previous chapters, which are based on uncoded OFDM in additive noise channel, in this chapter, coding, fading channel, and Doppler shift in the presence of impulsive noise are considered to model a realistic channel in UWA systems. Once the impulsive noise is mitigated by ANP in analog domain, the Doppler shift compensation and channel estimation can be accomplished by using null and pilot subcarriers, respectively, in the digital domain. We compare our proposed approach to the conventional methods such as blanking and clipping and highlight the advantage of the ANP for impulsive noise suppression. Simulation results show improvement in BER, due to the fact that, unlike classic impulsive noise mitigation methods, ANP is implemented in the analog domain where the outliers are still broadband and distinguishable.

5.1.1 Notations

Re(.) denotes the real part of a complex number. $\delta(.)$ and $\theta(.)$ represent the Dirac delta and Heaviside unit step functions, respectively. Bold upper/lower-case letters denote matrices/column vectors; $(.)^T$ and $(.)^{\mathcal{H}}$ denote the transpose and Hermitian of matrices, respectively. Finally, min(.) and $\mathbb{E}[.]$ are used to denote the minimum value and the expected value of the argument, respectively.

5.2 Transmitter, Channel, and Noise Models

5.2.1 Transmitter Model

Fig. 5.1 shows a simplified block diagram of the coded OFDM-based UWA system considered in this work. At the transmitter, information bits are channel coded and then the encoded bits are interleaved. Subsequently, the interleaved data is modulated and passed through an IDFT module to generate OFDM symbols over orthogonal subcarriers. A cyclic prefix is inserted at the beginning of each OFDM symbol. Finally, the OFDM symbols are shaped by a root raised cosine waveform with roll-off factor ρ and transmitted through the channel.

Let T and T_g denote the OFDM symbol duration and the length of the guard interval, respectively. The subcarrier spacing is $\Delta f{=}1/T$ and the total OFDM block duration is $T_{\text{bl}}{=}T + T_g$. Therefore, an OFDM signal with N subcarriers has the signal bandwidth of $B_s{\approx}N\Delta f$ and its k^{th} subcarrier is located at the frequency

$$f_k = f_c + k\Delta f, \quad k = -\frac{N}{2}, ..., \frac{N}{2} - 1, \tag{5.1}$$

where f_c is the carrier frequency. In general, an OFDM symbol can be constructed with M non-data subcarriers and $N - M$ data subcariers. The non-data subcarriers are either pilots for channel estimation and synchronization, or nulled for spectral shaping and ICI reduction. Let the nonoverlapping sets of data, pilot, and null subcarriers be defined as S_D, S_P, and S_N, respectively. Therefore, the transmitted passband analog signal envelope in time domain can be expressed as

$$\tilde{s}(t) = 2\text{Re}\left\{\sum_{k\in S_A} s_k \text{e}^{j2\pi f_k t} p(t)\right\}, \;\; 0 < t < T_{\text{bl}} \tag{5.2}$$

where $S_A = S_D \cup S_P$ represents the set of active subcarriers, s_k is the modulated symbol on the k^{th} subcarrier, and $p(t)$ denotes the pulse shaping filter.

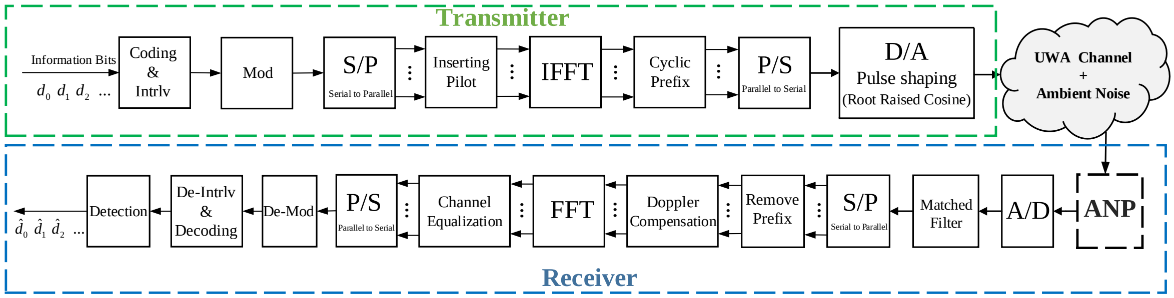

Fig. 5.1: System model block diagram.

5.2.2 Channel Model

The UWA channel can be modeled as a linear time-varying system which is described by the channel impulse response[75;78]

$$c(\tau;t) = \sum_p b_p(t)\, \delta(\tau - \tau_p(t)), \tag{5.3}$$

where $b_p(t)$ and $\tau_p(t)$ are the time-varying amplitude and delay of the p^{th} multipath component, respectively. Assuming the signal duration is short compared to the coherence time of the channel, the following assumptions may be adopted[75],[68].

- Assumption 1): The delay variation can be approximated by its first-order Taylor series expansion

$$\tau_p(t) \approx \tau_p - a_p t, \tag{5.4}$$

  where τ_p and a_p are the delay and Doppler scaling factor of the p^{th} path, respectively. In general different paths have different Doppler scaling factor; but, if the Doppler fluctuations remain relatively constant over a signal period (T_{bl}), the Doppler scaling factor can be considered as a constant value $a_p = a$ for all paths.

- Assumption 2): The path amplitudes b_p, and the delays τ_p are constant over T_{bl}. This is a reasonable assumption as channel coherence time is on the order of seconds and usually larger than the duration of a typical OFDM symbol in UWA system[75].

Based on assumptions 1 and 2, the received passband signal which is the convolution of the transmitted signal with the channel impulse response in the presence of impulsive noise, is given by

$$\begin{aligned}\tilde{x}(t) &= \int \sum_p A_p\, \delta(\tau - (\tau_p - at))\, \tilde{s}(t-\tau)\, d\tau + \tilde{n}(t) \\ &= \sum_p A_p\, \tilde{s}((1+a)t - \tau_p) + \tilde{n}(t),\end{aligned} \tag{5.5}$$

where $\tilde{n}(t)$ is passband ambient noise which is dominated by snapping shrimp impulsive noise. The equivalent baseband received signal $x(t)$ corresponds to

$$\begin{aligned}x(t) &= \sum_{k\in S_A} \left\{ s_k \mathrm{e}^{j2\pi(af_k + k\Delta f)t} \Big[\sum_p A_p \mathrm{e}^{-j2\pi k f_k \tau_p} p(t + at - \tau_p) \Big] \right\} + n(t) \\ &= x_s(t) + n(t),\end{aligned} \tag{5.6}$$

where $x_s(t)$ and $n(t)$ are desired signal and ambient noise in baseband, respectively.

5.2.3 Ambient Noise Model

In this chapter we will adopt two commonly used models for ambient noise in UWA environments as outlined below. *Bernoulli-Gaussian Model:* Ambient noise can be considered as composition of thermal noise $w(t)$ and impulsive noise $i(t)$. Here, $w(t)$ is complex Gaussian noise and $i(t)$ is modeled as a Poisson shot noise that consists of short duration high power impulses with random arrivals and is given by 3.2. The resulting time and frequency domain representation of ambient noise with BG underling impulsive noise is depicted in Fig. 5.2.

Alpha sub-Gaussian Noise with memory: In general ambient noise can be modeled based on heavy-tailed distributions as they assign large probability to outliers. It has been shown that symmetric alpha-stable (SαS) family of distributions have a good fit to ambient noise in warm shallow waters, which is impulsive and bursty [82]. In practice, this kind of noise is not

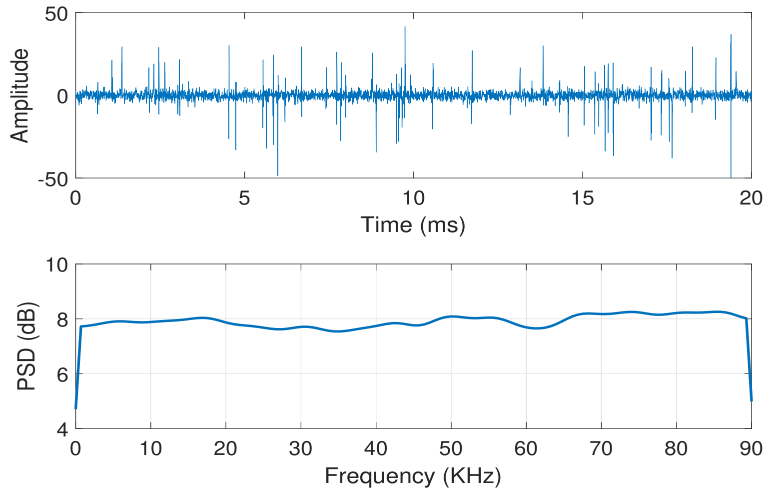

Fig. 5.2: Ambient noise with BG impulsive noise.

white and it is not possible to exploit white symmetric alpha-stable noise (WSαSN) model, which only incorporates the amplitude distribution of the noise process without considering the dependency between adjacent noise samples[82;83]. Therefore, we model the ambient noise as stationary alpha sub-Gaussian noise with memory order m (αSGN(m))[81;83] which considers both the amplitude distribution and dependency across the noise samples. Let n_k be the random samples of an αSG(m) process at index k. Then $\mathbf{n}_{k,m}$=$[n_{k-m},\, n_{k-m+1},\, ...,\, n_k]^T$ is a $(m+1)$-dimensional αSG random vector for all $k \in \mathbb{Z}$ and can be expressed as[81;83]

$$\mathbf{n}_{k,m} = A_k^{1/2}\mathbf{G}_{k,m}, \tag{5.7}$$

where $A \sim \quad S\left(\alpha/2, 1, 2(\cos(\pi\alpha/4))^2, 0\right)$ is a stable random variable with parameter α and $G_{k,m} = [G_{k-m},\, G_{k-m+1},\, ...,\, G_k]^T$ is Gaussian with distribution $\mathcal{N}(\mathbf{0}, \mathbf{R}_m)$ and $\mathbf{R}_m \in \mathbb{R}^{(m+1)\times(m+1)}$. Since αSGN(m) is stationary, the covariance matrix $\mathbf{R}_m = [r_{ij}]$ is independent of k and symmetric Toeplitz matrix, which is also positive-semi-definite[83]. The resulting time and frequency domain representation of ambient noise with αSGN(4) underling impulsive noise is illustrated in Fig. 5.3. Note that, WSαSN is a special case of αSGN(m) with $m = 0$. More details on the αSGN(m) model can be found in[81;83]. Although, the αSGN(m) in[81] model the ambient noise in digital domain, one can find the analog counter part of this

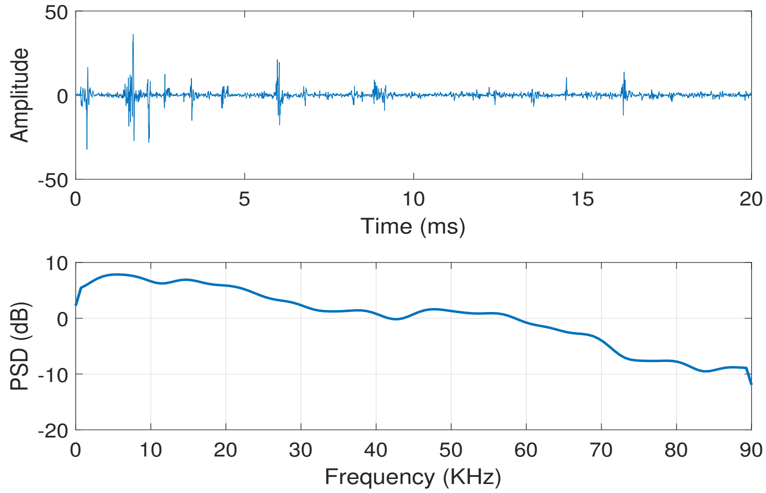

Fig. 5.3: Ambient noise with αSGN(4) impulsive noise.

model by exploiting interpolation techniques.

5.3 Receiver Structure

The block diagram of the proposed receiver is shown in Fig. 5.1. Here, in order to deal with the impulsive noise, the ANP module is implemented in analog domain before the ADC, as a front end preprocessor. In addition, the Doppler compensation is performed after cyclic prefix removal and OFDM symbol demodulation. This is followed by frequency domain equalization that depends on channel estimation. Viterbi soft decoding is used to decode the demodulated signal and then detection is performed based on the modulation scheme used. In this section, we first introduce the proposed ANP. Secondly, the Doppler effect compensation technique is introduced and, finally, the channel estimation approach is highlighted.

5.3.1 Analog Nonlinear Preprocessor (ANP) Design

It is well known that locally optimum detection of signals in non-Gaussian noise exploits nonlinear kernels[84]. For easier implementation we propose a suboptimal threshold-based nonlinear suppressor that is linear when there is no outliers. The ANP is an intermittently

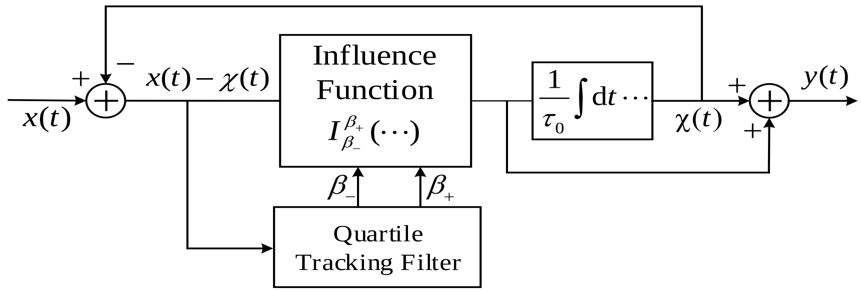

Fig. 5.4: Block diagram of generalized ANP. Adapted from[2].

nonlinear preprocessor that goes to nonlinear regime in response to incoming outliers. The general block diagram of ANP is depicted in Fig. 5.4. Here, $x(t)$ and $y(t)$ are the input and output of the ANP, respectively. The output of the ANP can be represented as

$$\begin{cases} y(t) = \chi(t) + \tau_0 \dot{\chi}(t) \\ \dot{\chi}(t) = \dfrac{1}{\tau_0} \mathcal{I}_{\beta_-}^{\beta_+} \left(x(t) - \chi(t)\right) \end{cases}, \tag{5.8}$$

where $\tau_0 = 1/(4\pi B_s)$ is fixed time constant, $\dot{\chi}(t)$ denotes the first time derivative of $\chi(t)$, and $\mathcal{I}_{\beta_-}^{\beta_+}(x)$ is the influence function. We will require that $\mathcal{I}_{\beta_-}^{\beta_+}(x)$ is effectively linear for $\beta_- \leq x \leq \beta_+$, and its absolute value monotonically decays to zero for x outside of the range $[\beta_-, \beta_+]$. For example, particular realization of influence function for ANP can be given by

$$\mathcal{I}_{\beta_-}^{\beta_+}(x) = \begin{cases} \beta_+ \exp\left(-\gamma \left(\dfrac{x - \beta_+}{\Delta\beta}\right)^2\right), & x > \beta_+ \\ \beta_- \exp\left(-\gamma \left(\dfrac{\beta_- - x}{\Delta\beta}\right)^2\right), & x < \beta_- \\ x, & \text{otherwise} \end{cases}, \tag{5.9}$$

where $\Delta\beta = \beta_+ - \beta_-$ and γ is a constant that determine how fast the proposed influence function transitions from clipping ($\gamma = 0$) to blanking ($\gamma \to \infty$). Note that, the value of γ will differ based on the application (e.g., $\gamma = 1$ is considered in this work). In other words, this influence function changes the nonlinearity from clipping to blanking based on the amplitude

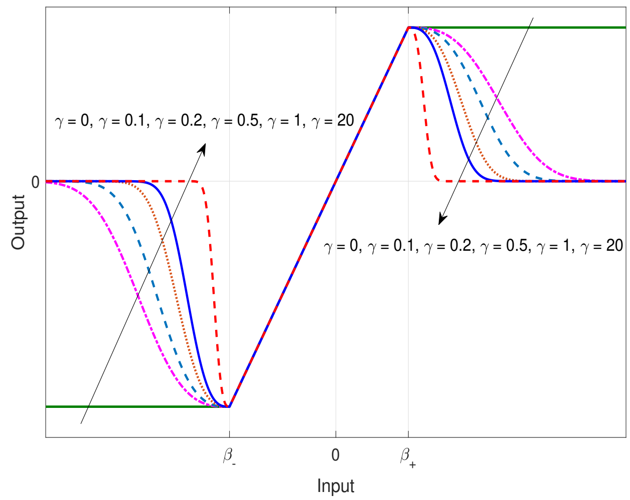

Fig. 5.5: Relation between input and output of influence function.

of incoming signal. The relation between input and output of the influence function for different values of γ is illustrated in Fig. 5.5. The expression in (5.9) demonstrates that ANP aggressively depreciate high amplitude impulsive noise and the nonlinear response of the ANP suppresses the magnitude of the respective outliers in the output signal. On the other hand, as follows from (5.8), when $\beta_- \leqslant x(t) - \chi(t) \leqslant \beta_+$ the output $y(t)$ of the ANP simply equals to its input $x(t)$ which means the proposed ANP does not harm the desired signal when there is no impulsive noise.

The proper selection of sensitivity range $[\beta_-, \beta_+]$ ensures the quality of the ANP. In this work, an effective value of the interval $[\beta_-, \beta_+]$ is obtained by using *Tukey's range*[69], which is a linear combination of the first (Q_1) and the third (Q_3) quartiles of the difference signal $x(t) - \chi(t)$ and is given by

$$[\beta_-, \beta_+] = [Q_1 - \beta_0(Q_3 - Q_1), Q_3 + \beta_0(Q_3 - Q_1)], \tag{5.10}$$

where β_0 is a constant coefficient of order unity (e.g. $\beta_0 = 3$). We direct the reader to[1;64] for details on obtaining the quartile values $Q_1(t)$ and $Q_3(t)$ in analog domain.

5.3.2 Doppler Effect Compensation

The ANP is followed by cyclic prefix removal and then the Doppler effect in the signal can be mitigated through a two step Doppler compensation technique described in [75]. The nonuniform Doppler effect of the received signal is removed through polyphase-interpolation-based resampling factor $\hat{a}$, resulting in a resampled signal. The estimate $\hat{a}$ of the Doppler scaling factor a, is calculated by comparing the time duration of the received packet $\hat{T}_{\mathrm{rx}}$ with the known time duration of the transmitted packet T_{tx}, given by [78]

$$\hat{T}_{\mathrm{rx}} = \frac{T_{\mathrm{tx}}}{1+\hat{a}} \quad \Rightarrow \quad \hat{a} = \frac{T_{\mathrm{tx}}}{\hat{T}_{\mathrm{rx}}} - 1, \tag{5.11}$$

where the received packet time duration $\hat{T}_{rx}$ is estimated in the receiver by cross-correlating the received signal with the known preamble and postamble. After impulsive noise mitigation and resampling by factor $\hat{a}$, the received resampled baseband signal $r[n]$ in digital domain can be expressed as

$$\begin{aligned} r[n] &= y\left[\left(\frac{n}{1+\hat{a}}\right)T_c\right] \\ &\approx \mathrm{e}^{j2\pi\epsilon n T_c}\big\{s[n] * h_{\mathrm{eff}}[n] + v[n]\big\}, \end{aligned} \tag{5.12}$$

where $h_{\mathrm{eff}}[n]$ and $v[n]$ are the effective channel impulse response and residual noise, respectively. Here, ϵ denotes the residual Doppler effect that can be considered to be the same for all subcarriers. Note that ϵ is similar to the carrier frequency offset (CFO) in radio frequency (RF) communication. The compensation of the CFO in (5.12) can be performed by

$$\begin{aligned} d[n] &= r[n]\mathrm{e}^{-j2\pi\hat{\epsilon} n T_c} \\ &\approx s[n] * h_{\mathrm{eff}}[n] + v[n], \end{aligned} \tag{5.13}$$

where $\hat{\epsilon}$ is the estimated value of CFO and is generated for each OFDM block. The CFO estimation is done by minimizing the leakage energy in the null subcarriers. In fact, if the receiver compensates the CFO, the null subcarriers will not see the ICI spilled over from neighbouring subcarriers. Define the cost function

$$J(\epsilon) = \sum_{k \in S_N} \left| \mathbf{f}_k^{\mathcal{H}} \mathbf{\Gamma}^{\mathcal{H}}(\epsilon) \mathbf{r} \right|^2, \tag{5.14}$$

where, $\mathbf{f}_k$, $\mathbf{\Gamma}$, and $\mathbf{r}$ can be defined as

$$\begin{aligned}
\mathbf{f}_k &:= \left[1, \mathrm{e}^{j2\pi k/N}, ..., \mathrm{e}^{j2\pi k(N-1)/N}\right]^T \\
\mathbf{\Gamma}(\epsilon) &:= \mathrm{diag}\left(1, \mathrm{e}^{j2\pi T_c \epsilon}, ..., \mathrm{e}^{j2\pi T_c (N-1)\epsilon}\right) \\
\mathbf{r} &:= [r(0), ..., r(N-1)]^T.
\end{aligned} \tag{5.15}$$

Considering (5.15), by sampling with rate B_s, we obtain N samples for each OFDM block. Therefore, the estimate of ϵ is given by

$$\hat{\epsilon} = \arg\min_{\epsilon} J(\epsilon), \tag{5.16}$$

which can be solved by a 1-D search for ϵ or using standard gradient method[80]. The mean square error (MSE) is used as a measure to quantify the performance of the CFO compensation technique in the impulsive noise environment. Thus, the MSE of Doppler compensation approach corresponds to

$$MSE_{\mathrm{CFO}} = \mathbb{E}\left[(\epsilon - \hat{\epsilon})^2\right]. \tag{5.17}$$

5.3.3 Channel Estimation

In order to estimate the channel response at the receiver, pilot subcarriers are used. Define the channel frequency response as

$$C(f) := \sum_p b_p \mathrm{e}^{-j2\pi f \tau_p}, \tag{5.18}$$

the received signal in the k^{th} subcarrier is given by

$$r_k = \mathbf{f}_k^{\mathcal{H}} \mathbf{\Gamma}^{\mathcal{H}}(\hat{\epsilon})\mathbf{r} = s[k]H[k] + v_k, \tag{5.19}$$

where $H[k] = C(f_k)$ is the channel frequency response at k^{th} subcarrier and v_k is the residual noise. Given that the channel has $L+1$ taps in discrete time, the channel estimation can be done using N_p pilot tones (at subcarrier indices $\{p_1, ..., p_{N_p}\} \in S_P$) based on least squares (LS) method as long as $N_p \geq L+1$. Assuming that ISI is eliminated by the CP or guard interval, we obtain

$$\mathbf{r}_p = \mathbf{D}_s \mathbf{F} \mathbf{h} + \mathbf{v}, \tag{5.20}$$

where

$$\begin{aligned}
\mathbf{r}_p &:= \big[r_{p_1}, ..., r_{p_{N_p}}\big] \\
\mathbf{D}_s &:= \operatorname{diag}\big(s_{p_1}, ..., s_{p_{N_p}}\big) \\
\mathbf{h} &:= \big[h_0, ..., h_L\big] \\
\mathbf{F} &:= \begin{bmatrix} 1 & \mathrm{e}^{-j\frac{2\pi}{N}p_1} & \cdots & \mathrm{e}^{-j\frac{2\pi}{N}p_1 L} \\ \vdots & \vdots & \ddots & \vdots \\ 1 & \mathrm{e}^{-j\frac{2\pi}{N}p_{N_p}} & \cdots & \mathrm{e}^{-j\frac{2\pi}{N}p_{N_p} L} \end{bmatrix}.
\end{aligned} \tag{5.21}$$

For the sake of simplicity and avoiding matrix inversion operation, we assume that pilot symbols are equally spaced within N subcarriers and they are PSK signals with unit amplitude. Thus, the matrix-vector representation of the equivalent system is obtained by

$$\begin{aligned}
\mathbf{F}^{\mathcal{H}}\mathbf{F} &= N_p \mathbf{I}_{L+1} \\
\mathbf{D}_s^{\mathcal{H}}\mathbf{D}_s &= \mathbf{I}_{N_p},
\end{aligned} \tag{5.22}$$

and the LS estimate of $\mathbf{h}$ is represented by

$$\hat{\mathbf{h}}_{\mathrm{LS}} = \frac{1}{N_p}\mathbf{F}^{\mathcal{H}}\mathbf{D}_s^{\mathcal{H}}\mathbf{r}_p. \tag{5.23}$$

Having time domain channel estimate $\hat{\mathbf{h}}_{\mathrm{LS}}$, the estimate of the channel at all subcarriers is obtained by[85]

$$\hat{H}[k] = \sum_{l=0}^{L} \hat{h}_l \mathrm{e}^{\frac{-j2\pi lk}{N}}. \tag{5.24}$$

In order to quantify the performance of channel estimation, the relative MSE of channel estimation corresponds to

$$MSE_{\mathrm{CE}} = \mathbb{E}\left[\frac{\left(\mathbf{h}-\widehat{\mathbf{h}}_{\mathrm{LS}}\right)^{\mathcal{H}}\left(\mathbf{h}-\widehat{\mathbf{h}}_{\mathrm{LS}}\right)}{\mathbf{h}^{\mathcal{H}}\mathbf{h}}\right]. \tag{5.25}$$

5.4 Simulation Results

In this section, an UWA system with quadrature phase shift keying (QPSK) modulation in the presence of impulsive noise is studied. The BER performance is used to compare the proposed ANP with other conventional approaches such as blanking and clipping. In addition, the MSE of Doppler compensation and channel estimation are investigated to highlight the impact of impulsive noise mitigation in estimation fidelity.

For a quick reference, the simulation parameters of the considered coded OFDM system in UWA channels are listed in Table 5.1. A total of 1024 subcarriers are used with 672 carrying data, 256 pilot, and 96 null subcarriers. Channel estimation is done based on pilot subcarriers which are equally spaced between 1024 subcarriers. The CFO is compensated based on null subcarriers which are placed between data and pilot subcarriers. To emulate analog signals in the simulation, the digitization rate is chosen to be significantly higher (by about two orders of magnitude) than the ADC sampling interval T_c. A 10-path fading channel is considered with path arrival times following a Poisson distribution with mean 1 ms. The path amplitudes are Rayleigh distributed with exponentially decreasing average

TABLE 5.1
SIMULATION PARAMETERS

Parameters	**Values**
Bandwidth (B_s)	6 kHz
Carrier Frequency(f_c)	17 kHz
No. of Subcarriers (N)	1024
Subcarrier Spacing (Δf)	5.88 Hz
Symbol Duration (T)	170.7 ms
Guard Interval (T_g)	79.3 ms
ADC Sampling Interval (T_c)	20.8 μs
Modulation Scheme	QPSK
Channel Length (L)	10
Convolution Code Rate (CR)	1/2
Code Constraint Length	7
Generator Polynomial	[171,133]
Roll-off Factor (ρ)	0.25

power. The Doppler shift ϵ is uniformly distributed in $[-\Delta f/2, \Delta f/2]$. The considered covariance matrices for αSGN(m) model with $m = 4$ and $m = 1$ are given by

$$\mathbf{R}_4 = \begin{bmatrix} 1.0000 & 0.5804 & 0.2140 & 0.1444 & -0.0135 \\ 0.5804 & 1.0000 & 0.5804 & 0.2140 & 0.1444 \\ 0.2140 & 0.5804 & 1.0000 & 0.5804 & 0.2140 \\ 0.1444 & 0.2140 & 0.5804 & 1.0000 & 0.5804 \\ -0.0135 & 0.1444 & 0.2140 & 0.5804 & 1.0000 \end{bmatrix},$$

$$\mathbf{R}_1 = \begin{bmatrix} 1.0 & 0.7 \\ 0.7 & 1.0 \end{bmatrix}. \tag{5.26}$$

The importance of impulsive noise mitigation in the OFDM-based receiver chain under two different settings (i) BG noise with SIR = 0 dB, $\lambda\tau_{as} = 0.03$, and (ii) αSGN(m) noise with $\alpha = 1.5$, and memory $m = 4$, are shown in Fig. 5.6a and Fig. 5.6b, respectively. As is evident from Fig. 5.6, coding alone can not deal with impulsive noise in an OFDM system. This is because of the fact that the power of impulsive noise is spread over the entire OFDM symbol

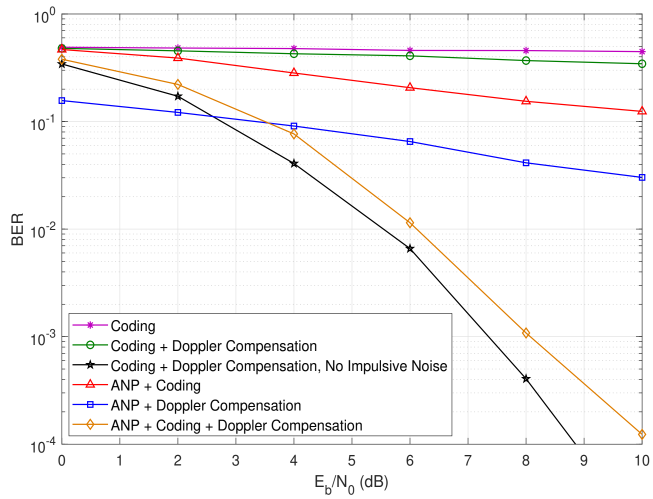

(a) BG impulsive noise, SIR = 0 dB, $\tau_{as} = 10\mu$s, $\lambda\tau_{as} = 0.03$.

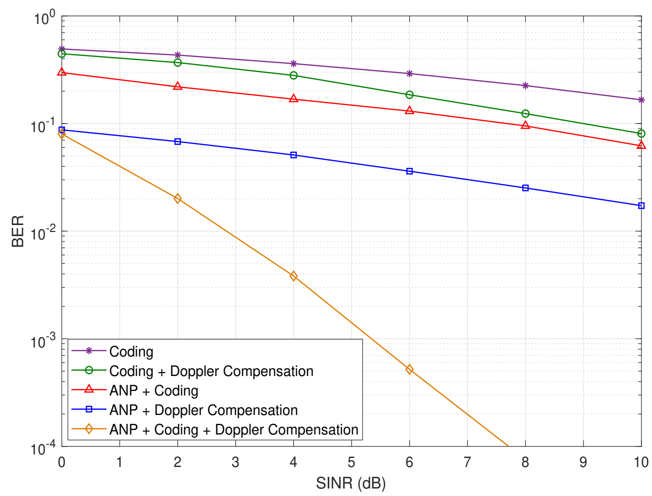

(b) αSGN(m) impulsive noise, $\alpha = 1.5$, $m = 4$.

Fig. 5.6: BER performance for different model of impulsive noise.

which makes error correction impossible.

Fig. 5.6 also shows that Doppler compensation in UWA channel is inevitable either with or without impulsive noise mitigation techniques. From Fig. 5.6 it is obvious that the best performance is achieved when the impulsive noise is suppressed by ANP with effective coding and Doppler compensation. The effect of ANP on the quality of the Doppler compensation and channel estimation are shown in Fig. 5.7 and Fig. 5.8, respectively. Fig. 5.7a and Fig. 5.7b demonstrates the effect of ANP on the MSE of Doppler compensation technique

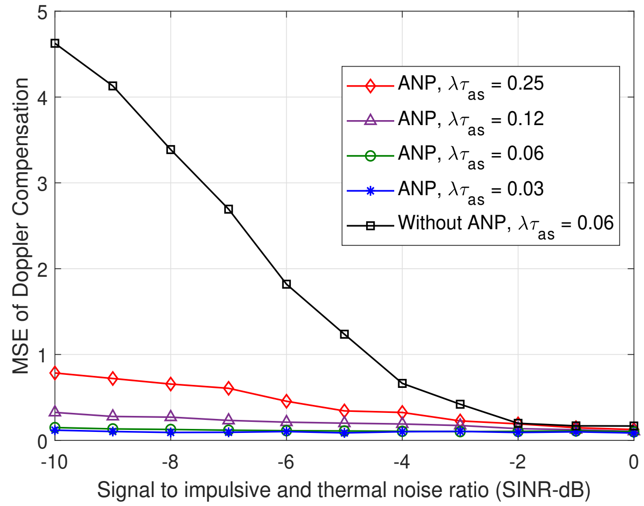

(a) BG impulsive noise, $E_b/N_0 = 2$ dB, $\tau_{as} = 10\mu$s.

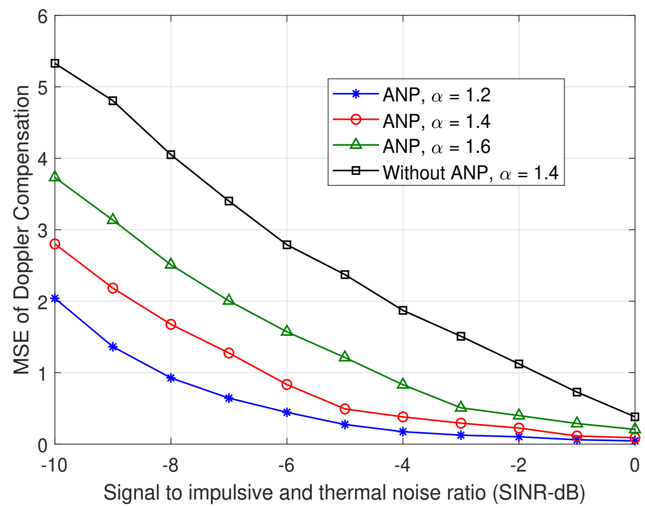

(b) αSGN(m) impulsive noise, $m = 4$.

Fig. 5.7: MSE of Doppler compensation.

for both BG and αSGN(m) impulsive noise models, respectively. As shown in Fig. 5.7, ANP improves the quality of CFO compensation technique in different levels of impulsivity.

The MSE of channel estimation in both BG and αSGN(m) impulsive noise are shown in Fig. 5.8a and Fig. 5.8b, respectively. As we are interested in quantifying the impact of impulsive noise on channel estimation, the frequency offset is set to zero for the simulations in Fig. 5.8. As illustrated in Fig. 5.8, the fidelity of channel estimation technique remains good with ANP even in the presence of severe impulsivity. It is important to remember

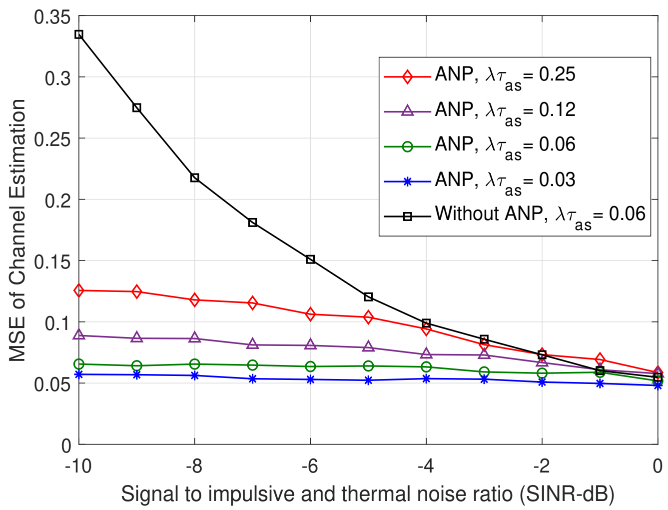

(a) BG impulsive noise, $E_b/N_0 = 2$ dB, $\tau_{as} = 10\mu$s.

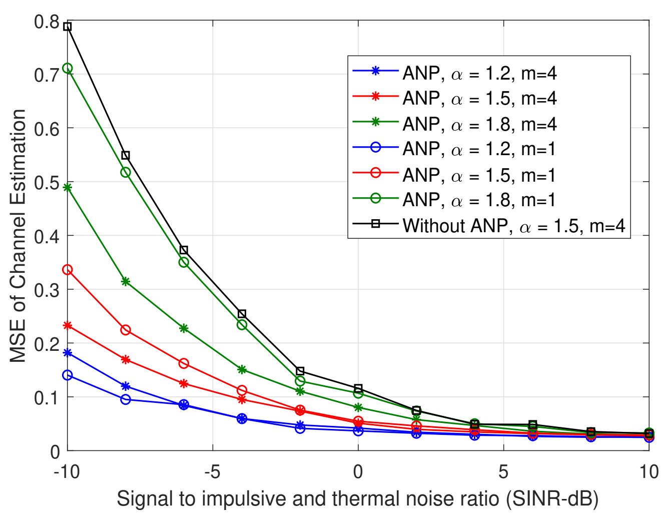

(b) αSGN(m) impulsive noise.

Fig. 5.8: MSE of channel estimation.

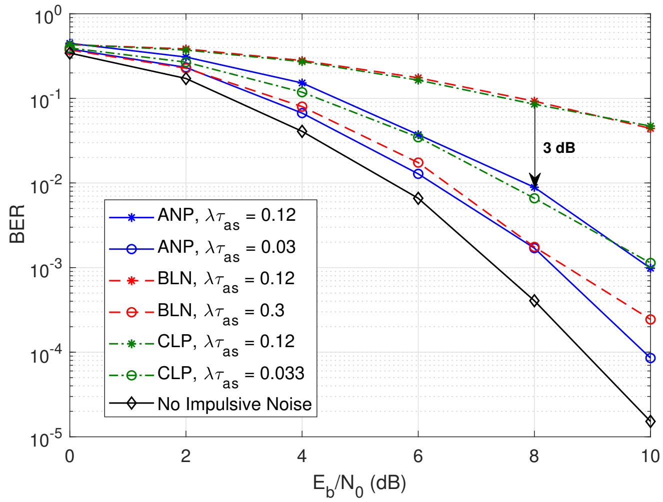

Fig. 5.9: BER comparison of ANP, BLN, and CLP versus E_b/N_0 for different values of λ. SIR = 0 dB, $\tau_{\text{as}} = 10\mu$s.

that both Doppler compensation and channel estimation are done in the frequency domain where the power of impulsive noise is spread over all OFDM subcarriers. Thus, without the ANP, the MSE is more severely impacted by the power of impulsive noise rather than its occurrence frequency.

In the following, we compare the performance of the ANP with two digital approaches of impulsive noise mitigation namely blanking (BLN) and clipping (CLP). Note that in all simulations, (i) the optimum thresholds for blanking and clipping are found based on an exhaustive numerical search, (ii) the sensitivity range $[\beta_-, \beta_+]$ for ANP is determined based on expression (6.4) with low computational complexity, and (iii) coding, Doppler compensation, and channel estimation are considered in all receivers except where it is mentioned otherwise.

Fig. 5.9 compares the BER performance of all three receivers in BG noise for different levels of impulsivity. Fig. 5.9 shows that in BG impulsive noise model, blanking and clipping are very vulnerable to the occurrence frequency of impulsive noise and their performance is poor in high impulsive environments. Although, the performance loss of the ANP with increasing the impulsivity level is also noticeable, it still outperforms other approaches in all scenarios. For example, at $E_b/N_0 = 8\,dB$, ANP provides 3 dB gain relative to blanking and

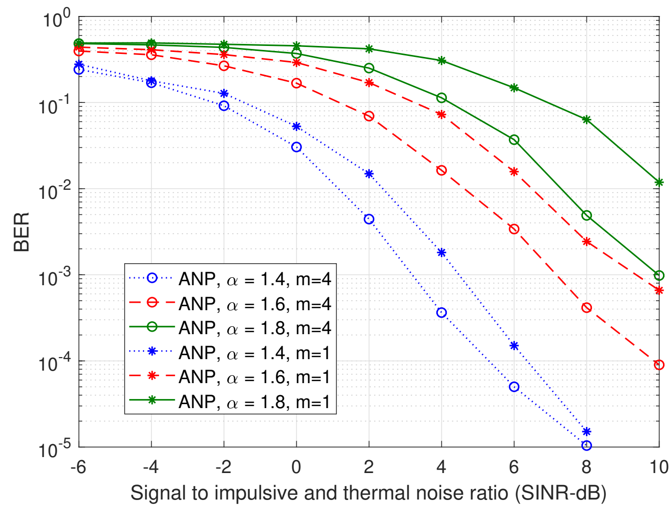

Fig. 5.10: BER performance of ANP in αSGN(m) noise

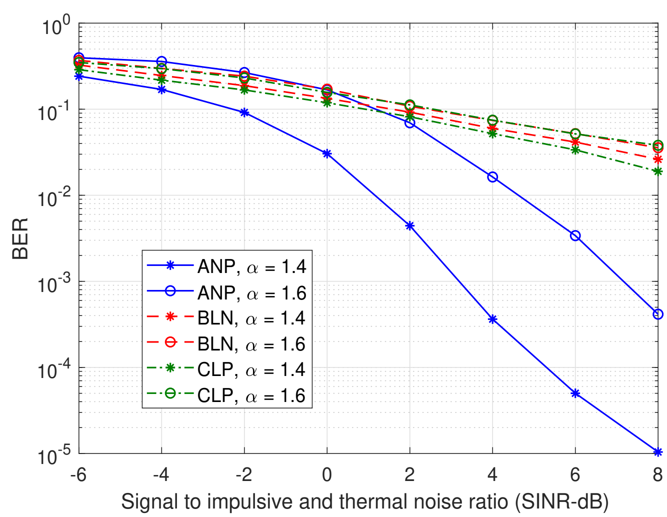

Fig. 5.11: BER comparison of ANP, BLN, and CLP in αSGN(m) noise, $m = 4$.

clipping for $\lambda\tau_{\text{as}} = 0.12$.

The BER performance of ANP in case of αSGN(m) noise for different values of α and memory size is shown in Fig. 5.10. According to αSGN(m) model, a smaller α denotes more impulsive environment which means at a given SINR the power of outliers is more than the power of thermal noise. Therefore, as shown in Fig. 5.10 we have better performance for lower values of α because ANP is able to suppress the outlier more efficiently.

Fig. 5.11 shows that the ANP considerably outperforms other methods. The potency

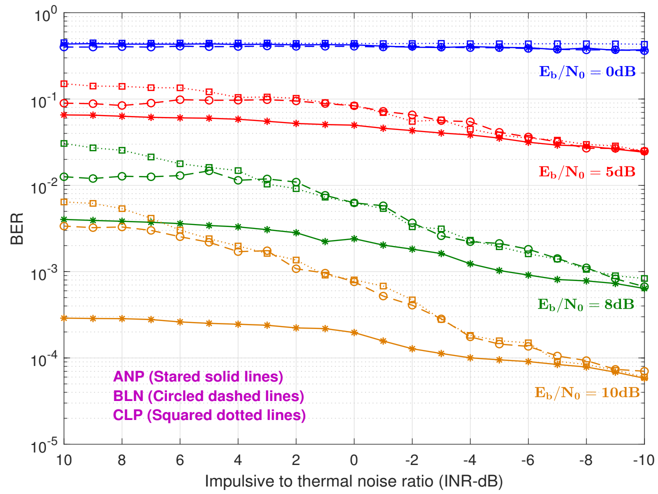

Fig. 5.12: BER comparison of ANP, BLN, and CLP versus INR for different values of E_b/N_0. $\tau_{\text{as}} = 10\mu$s, $\lambda\tau_{\text{as}} = 0.06$.

of ANP in reducing the power of impulsive noise in the signal passband is due to the fact that, unlike other nonlinear methods, ANP is implemented in the analog domain where the outliers are still broadband and distinguishable.

Fig. 5.12 illustrates the BER performance of all three impulsive noise mitigation approaches in case of BG model for various impulsive noise to thermal noise ratios (INR) in baseband. As can be seen in Fig. 5.12, all approaches provide effectively equivalent performance when thermal noise dominates the impulsive noise (right side of Fig. 5.12). However, the ANP shows its advantage when impulsive noise is dominant, specially at high SNR (SNR greater than 5 dB). Therefore, in highly impulsive environment as shown in Fig. 5.12, ANP is highly preferable to other approaches.

5.5 Summary

In this chapter, we have investigated a novel method to mitigate the effect of impulsive noise and its impact on nonuniform Doppler shift compensation in the coded OFDM-based UWA systems. After impulsive noise mitigation by the proposed ANP, the Doppler shift compensation and channel estimation are performed based on the measurements on OFDM null and pilot subcarriers, respectively. The results show that the proposed approach can provide significant improvement in BER performance of the UWA system in the presence of both strong impulsive component and nonuniform Doppler shift. In addition, the ANP-based approach outperforms other methods that use blanking or clipping for outlier suppression, specially at high levels of impulsivity.

Chapter 6

Impulsive Noise Mitigation in UWA Communication Systems: Experimental Studies

In this chapter, a simplified version of ANP as Memoryless Analog Nonlinear Preprocessor (MANP) is proposed to mitigate the effect of the impulsive noise. The proposed MANP exhibits intermittent nonlinearity only in the presence of the impulsive noise and suppresses the power of outliers based on their amplitudes. Experimental results using data collected in an under-ice environment, demonstrate the superior BER performance of our approach relative to classical nonlinear approaches such as blanking and clipping.

6.1 Introduction

As mentioned in chapter 5, the UWA communication is the most widely used technique for transmission in shallow water environments. The UWA communications are subject to multipath propagation with long delay spreading and strong Doppler effect [86;87]. In addition, impulsive noise is the main channel impairment in some underwater environments. For example, ice-cracking noise [88] is one the common sources of impulsive noise in UWA communication. With the increasing demand for high data rate applications such as environmental monitoring, sonar, and communication between underwater vehicles, modern UWA communication systems have higher bandwidth. Since impulsive noise is typically wide band, it affects certain broadband modulation techniques such as OFDM which is widely used in UWA communication. It is also widely known that impulsive noise is non-Gaussian and special care should be taken during the decoding and detection process[9;10]. Thus, impulsive noise mitigation will positively impact the performance of UWA communication systems.

In this chapter, we investigate the performance of MANP in a practical OFDM-based UWA communication system. The proposed MANP offers a compromise between clipping and blanking in response to the impulsivity level in the analog domain. The potency of the proposed MANP is evaluated based on the real data collected in Portage Lake, Michigan. We compare our proposed approach with conventional methods such as blanking and clipping and highlight the superiority of the MANP in the impulsive noise suppression.

6.2 System Model

A simplified block diagram of the zero-padded OFDM-based UWA system is shown in Fig. 6.1 and more details can be found in[89]. At the transmitter, the information bits are encoded by nonbinary low-density parity-check (LDPC) codes. Symbols are mapped from the coded bits according to the desired modulation scheme and then interleaved. After inserting pilot symbols and zeros, the data are passed through an IDFT module to generate OFDM modulated baseband signals. Zero-padding is performed to counteract multipath effects after the signals are upshifted to the passband. Lastly, preambles are added to assist signal detection and synchronization.

Let T and T_g denote the OFDM symbol duration and the length of the guard interval, respectively. As provided in chapter 5, the transmitted passband analog signal in the time

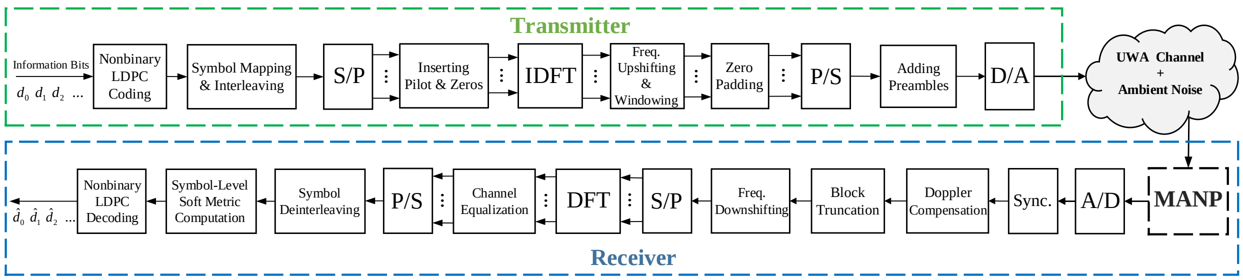

Fig. 6.1: System block diagram.

domain can be expressed as

$$s(t) = 2\mathrm{Re}\left\{ \sum_{k \in S_A} s_k \mathrm{e}^{j2\pi f_k t} p(t) \right\}, \ \ 0 < t < T_{\mathrm{bl}} \tag{6.1}$$

where S_A represents the set of active subcarriers, s_k is the modulated symbol on the k^{th} subcarrier, f_k denotes the frequency of k^{th} subcarrier, and $p(t)$ is the pulse shaping filter. Here, a rectangular window of length T is used for pulse shaping. The PSD of the transmitted waveform is shown in Fig. 6.2. As depicted in Fig. 6.2, the preambles include a linear frequency-modulated (LFM) waveform, a hyperbolic frequency-modulated (HFM) waveform, an m-sequence coded waveform, and a cyclic-prefixed (CP) OFDM block [89] to enable cross-correlation based signal detection. As it can be seen in Fig. 6.2, following the preambles, there are twenty QPSK modulated OFDM blocks followed by another twenty OFDM blocks that is 16-QAM modulated. An HFM post-amble is appended to the end of the waveform, resulting in a 14.9-second total time duration of the waveform. The synchronization and Doppler scale estimation are achieved through self-correlation of the CP-OFDM preamble. After synchronization, OFDM blocks are truncated and the symbols on the active subcarriers are obtained after the discrete Fourier transform (DFT) module. A least squared (LS) estimator follows to estimate the channel with the help of pilot symbols. Here, a linear minimum mean squared error (LMMSE) equalizer is used for symbol detection. The detected symbols are then de-interleaved, and symbol-level soft metric is computed for the LDPC decoding module.

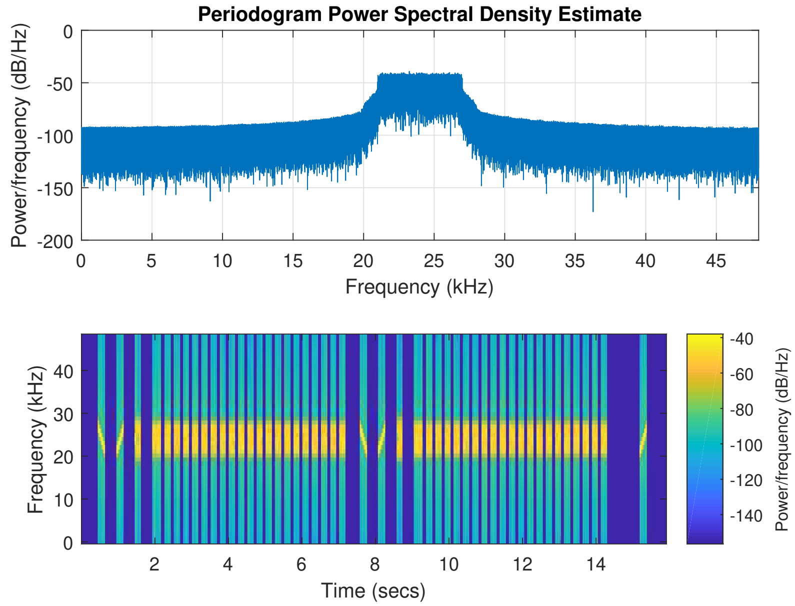

Fig. 6.2: PSD of the transmitted waveform in frequency band $[21 - 27]$ kHz[3].

6.3 Memoryless Analog Nonlinear Preprocessor (MANP) Design

The structure of the proposed receiver is shown in Fig. 6.1. The proposed MANP is implemented in the analog domain before the ADC. Since, locally optimum detection of signals in non-Gaussian noise exploits nonlinear kernels[84], the exact shape of the optimum kernel may be too complicated to be implemented by analog circuitry. Therefore, for easier implementation, a suboptimal threshold-based analog intermittent nonlinear preprocessor is proposed in this chapter.

The general block diagram of MANP is shown in Fig. 6.3. Here, $x(t)$ and $\chi(t)$ are the input and output of the MANP, respectively. The output of the MANP is represented as

$$\chi(t) = \mathcal{I}_{\beta_-}^{\beta_+}(x(t)), \tag{6.2}$$

where $\mathcal{I}_{\beta_-}^{\beta_+}(x)$ is defined as the influence function. Note that, the behavior of MANP goes to the nonlinear regime in response to the amplitude of incoming outliers. Therefore, we

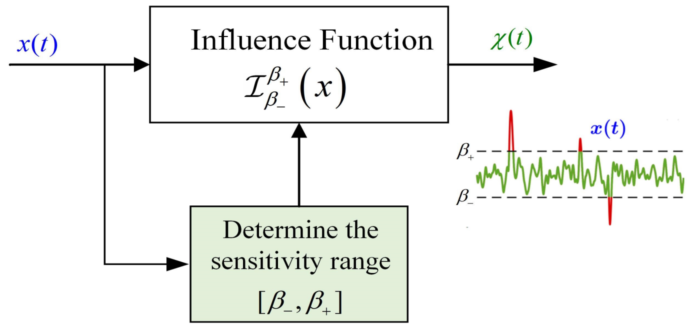

Fig. 6.3: Block diagram of generalized MANP.

will require that $\mathcal{I}_{\beta_-}^{\beta_+}(x)$ be effectively linear for $\beta_-(t) \leq x \leq \beta_+(t)$, and its absolute value monotonically decays to zero for x outside of the range $[\beta_-(t), \beta_+(t)]$. In general $|\beta_-(t)|$ and $|\beta_+(t)|$ are different, but for symmetric signals such as OFDM we can set $|\beta_-(t)| = |\beta_+(t)| = \beta(t)$. We refer to this $\beta(t)$ as the resolution parameter. Therefore, in practice we only need to find one resolution parameter $\beta(t)$ which determines the sensitivity range $[-\beta(t), \beta(t)]$. For example, one realization of the influence function for MANP can be expressed as

$$\chi(t) = x(t) \begin{cases} 1, & |x(t)| \leq \beta(t) \\ \left(\frac{\beta(t)}{|x(t)|}\right)^{\gamma+1}, & |x(t)| > \beta(t) \end{cases} \tag{6.3}$$

where γ is a constant that determines how fast the proposed influence function transitions from clipping ($\gamma = 0$) to blanking ($\gamma \to \infty$) and its value will differ based on the application (e.g., $\gamma = 1$ is considered in this work). In other words, this influence function changes the nonlinearity from clipping to blanking based on the amplitude of incoming signal.

The relationship between the input and the output of the MANP for different values of γ is shown in Fig. 6.4. The expression in (6.3) also demonstrates the disproportional behavior of the MANP on the signal of interest and impulsive noise. This nonlinear preprocessing increases the SNR in the desired frequency band by reducing the spectral density of the impulsive noise without significantly affecting the desired signal.

According to (6.3), the goal is to determine a proper resolution parameter $\beta(t)$ that enhances the quality of received signals under time-varying noise conditions. Therefore, an efficient value of $\beta(t)$ will maximize the suppression of the impulsive noise without distorting

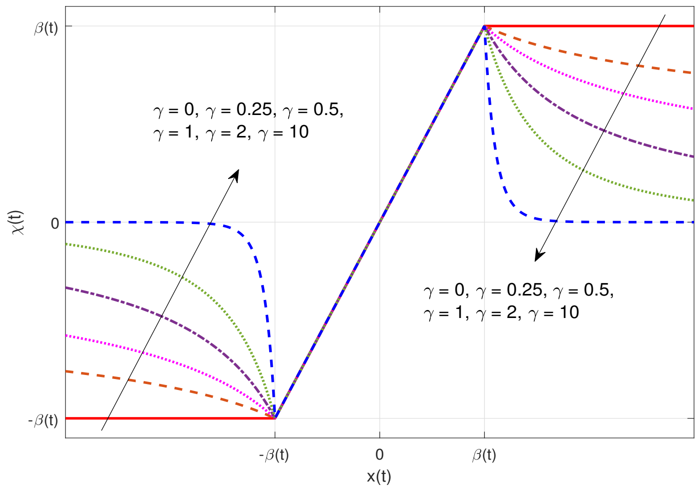

Fig. 6.4: Relation between input and output of MANP.

the signal of interest. Here, an effective value of the resolution parameter $\beta(t)$ is obtained as

$$\beta(t) = (1 + 2\beta_0)Q_2(t), \tag{6.4}$$

where $Q_2(t)$ is the second quartile (median) of the absolute value of the input signal $|x(t)|$, and β_0 is a constant coefficient (e.g. $\beta_0 = 1.5$). We direct the attention of the reader to [1] and [64] for more details on obtaining the quartile values in analog domain.

6.4 Experimental Results

On March 17, 2017, an under-ice experiment was conducted in Portage Lake, MI. The experimental setup is shown in Fig. 6.5 and the OFDM modem that is used in this experiment is depicted in Fig. 6.6. During the experiment, the Portage Lake was covered by about 40 cm thick ice. The water depth in the area varies from 8.3 to 11.3 meters. The transmitting node with an omnidirectional transducer was placed at 4.5 meters below the water surface at S_1, as illustrated in Fig. 6.5. The receiving node with 4-hydrophones was placed at S_2 at different depths and the transmission distance is 3.47 km. An example of the recorded signal contaminated with impulsive noise at the receiver is depicted in Fig. 6.7. For our

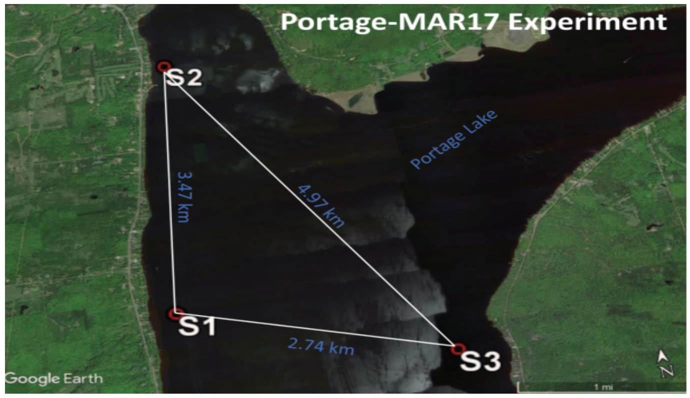

Fig. 6.5: Experiment setup[3].

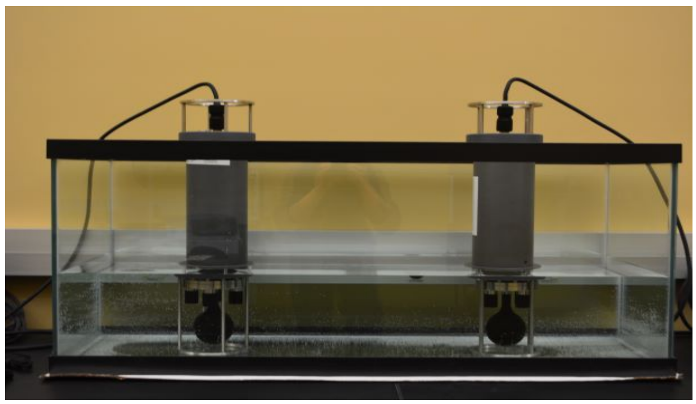

Fig. 6.6: OFDM Modem[3].

numerical experiment the recorded signal was reconditioned for analog domain processing while retaining the measured characteristic of the impulsive noise. The system parameters of the considered OFDM system in UWA channels are listed in Table 6.1. A total of 1024 subcarriers are used with 672 data subcarriers, 256 pilot subcarriers, and 96 null subcarriers. After the impulsive noise mitigation from the recorded signal, Doppler compensation and channel estimation can be done based on the measurements on null and pilot subcarriers, respectively. However, in this experiment the Doppler compensation module was taken off as the Doppler effect was negligible in the under ice situation.

In the following, the SNR and BER performance are used to evaluate the performance of the proposed MANP in this experiment. Here, we consider the time domain SNR which

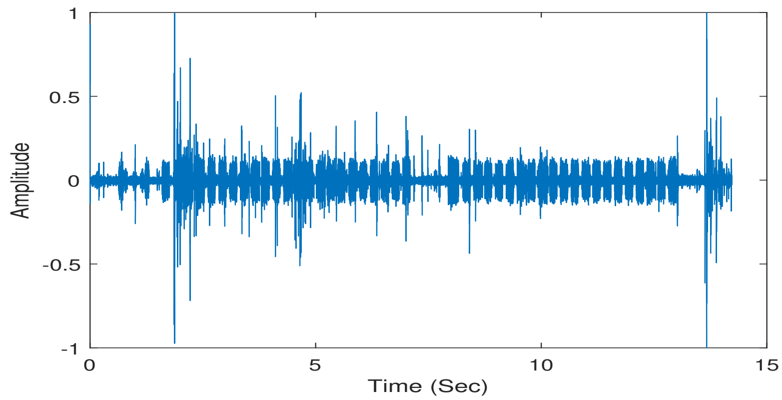

Fig. 6.7: Recorded OFDM waveform [3].

is obtained before the DFT module and can be expressed as

$$\mathrm{SNR} = \frac{P_s - P_n}{P_n} \tag{6.5}$$

where P_s and P_n are the power of OFDM block and noise, respectively. The power of the OFDM block P_s is considered as a summation of the desired signal power plus the noise power. The noise power P_n can be obtained using the silence intervals in the waveform. For example, the intervals between preambles and the interval between the last OFDM block and the postamble. As long as the silence period is longer than the channel delay spread, there will be a clean portion without interference caused by the multipath effect.

The BER and SNR performance of each OFDM block in the receiver are shown in Fig. 6.8 and Fig. 6.9, respectively. Here, we just use the received signal from the first hydrophone but in general, the received signals by all the 4 hydrophones can be combined via the maximal ratio combining for joint decoding. As it can be seen in Fig. 6.8 and Fig. 6.9, the receiver performance is improved when the impulsive noise is suppressed by MANP. Without the outlier suppression, the power of the impulsive noise will spread over the entire frequency band of the OFDM block, which introduces error in the detection process.

In the following, we compare the performance of the MANP with two nonlinear digital approaches namely blanking (BLN) and clipping (CLP). Note that in all cases the thresholds for blanking and clipping are found according to the dynamic range of the received signal in

TABLE 6.1
SYSTEM PARAMETERS

Parameters	**Values**
Modulation Scheme	QPSK-16-QAM
Bandwidth (B_s)	6 kHz
Center Frequency(f_c)	24 kHz
No. of Subcarriers (N)	1024
Subcarrier Spacing (Δf)	5.88 Hz
Sampling Frequency	96 kHz
Symbol Duration (T)	170.7 ms
Guard Interval (T_g)	79.3 ms
Silence between preambles	300 ms
Silence between preamble and OFDM blocks	100 ms
LDPC Coding Rate (CR)	1/2
Galois Field Size for QPSK and 16-QAM	GF(4), GF(16)

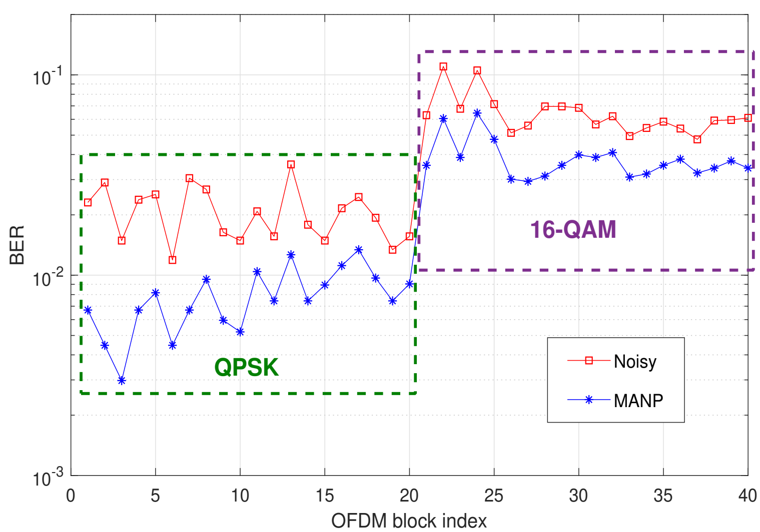

Fig. 6.8: BER of each OFDM block with and without MANP.

the desired time window.

Fig. 6.10 and Fig. 6.11 compare the average BER and the average received SNR of all three receivers, respectively. Here, the average is taken over ten recorded files. Fig. 6.10 shows that the BER performance of MANP outperforms both blanking and clipping in all investigated cases. The potency of MANP in reducing the power of impulsive noise in the signal passband is due to the fact that, unlike other nonlinear methods, MANP is implemented in the analog

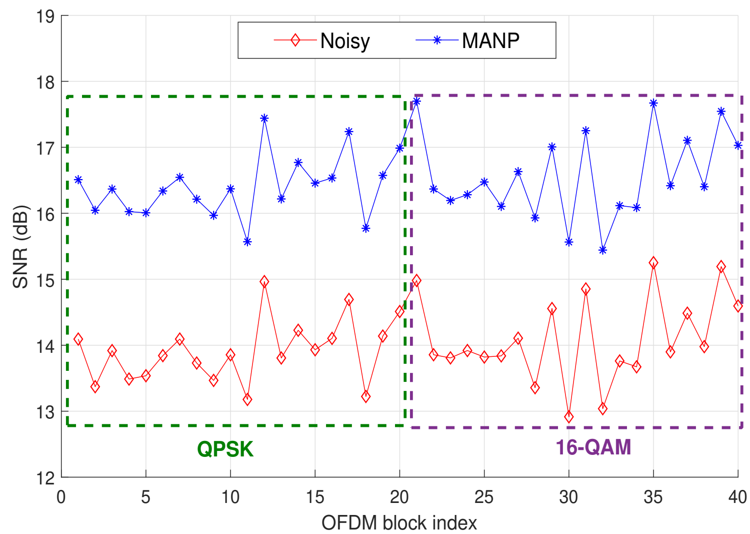

Fig. 6.9: Received SNR of each OFDM block with and without MANP.

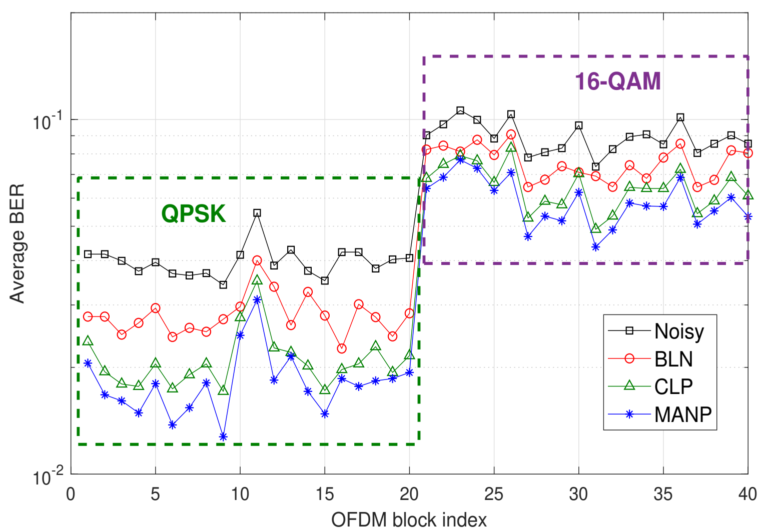

Fig. 6.10: Average BER of MANP, BLN, and CLP.

domain where the outliers are still broadband and distinguishable. As depicted in Fig. 6.11, the SNR with the proposed MANP surpasses both blanking and clipping in all studied cases. Fig. 6.11 also shows that for our case studies, clipping outperforms blanking on average. However, in some cases blanking outperforms clipping (Fig. 6.12-(a)) while in others clipping has better performance relative to blanking (Fig. 6.12-(b)).

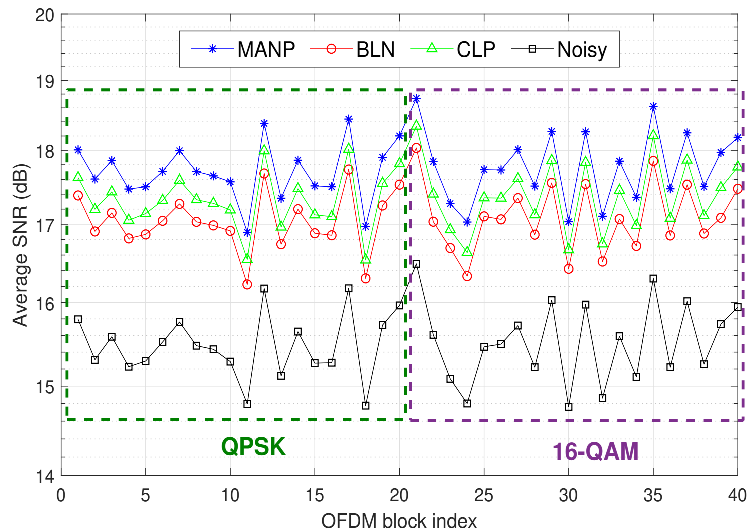

Fig. 6.11: Average received SNR of MANP, BLN, and CLP.

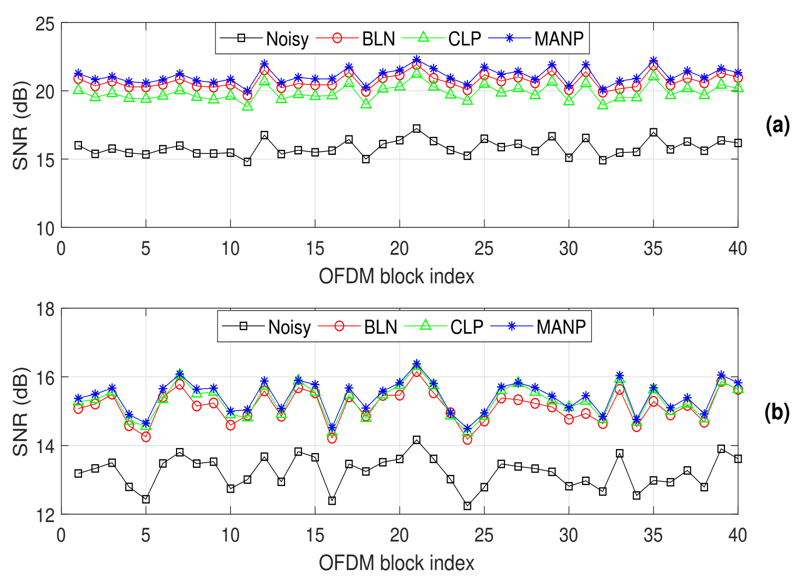

Fig. 6.12: Received SNR of MANP, BLN, and CLP.

6.5 Summary

In this chapter, the proposed MANP is used to alleviate the effect of impulsive noise in an OFDM-based UWA systems. The MANP is implemented in the analog domain as the outliers are broadband and distinguishable. We also introduced a practical schematic of MANP based on the OTAs. Experimental results based on field data collected in an under-ice environment in Portage Lake, MI show that the proposed approach can provide significant improvement in the BER performance in the presence of strong impulsive components. In addition, the MANP-based approach outperforms other methods that use blanking or clipping for outlier suppression, especially at high levels of impulsivity.

Chapter 7

Impulsive Noise Detection in OFDM-based Systems: A Deep Learning Perspective

Efficient removal of impulsive noise from received signal is essential in many communication applications. In this chapter, we propose a two stage impulsive noise mitigation approach for OFDM-based communication systems. In the first stage, a Deep Neural Network (DNN) is used to detect the instances of impulsivity. Then, the detected impulsive noise is blanked in the suppression stage to alleviate the harmful effects of outliers. Simulation results demonstrate the superior BER performance of this approach relative to classic approaches such as blanking and clipping that use threshold to detect the impulsive noise. We demonstrate the robustness of the DNN-based approach under (i) mismatch between impulsive noise models considered for training and testing, and (ii) bursty impulsive environment when the receiver is empowered with interleaving techniques.

7.1 Introduction

Machine learning methods such as deep learning are becoming popular in growing number of applications in signal and image processing[90;91], and resource allocation in wireless networks[92;93]. If appropriate network structures and processing strategies are employed, DNN may be used as powerful tools for efficient detection of impulsive noise because of their ability to learn from examples and capability to account for uncertainty that is common in the most communication applications. Additionally, in classical outlier detection approaches, determining the optimum threshold is the main challenge as this threshold will vary in response to channel conditions and model mismatches. Lastly, the high peak to average power ratio (PAPR) of OFDM signals can also degrade the performance of the classical methods. As always, there is a compromise between detection and false alarm probability in the traditional threshold based methods.

To overcome the aforementioned drawbacks, we propose a machine learning based impulsive noise suppression strategy for an OFDM-based communication system. The proposed impulsive noise mitigation approach comprises of two stages: (i) impulsive noise detection and (ii) impulsive noise suppression. In the first stage, a DNN is used to detect the impulsive noise corrupted signal instances. Then, the detected impulsive noise can be either blanked or clipped in the suppression stage to alleviate the harmful effects of outliers. The proposed DNN-based impulsive noise detection approach can be used in conjunction with any impulsive noise mitigation strategy as the operation of the detector is completely independent of the noise removal operator. The proposed DNN consists of multiple layers (input, hidden, output) with nodes in a fully connected structure that maps input data into appropriate outputs. Each node in the hidden layers has a nonlinear activation function which helps to distinguish data that are not linearly separable. Here, the DNN uses the current sample value, median deviations filter output[94], and Rank-Ordered Absolute Differences (ROAD) statistic[95] as the inputs to determine if the current sample is corrupted by impulsive noise or not. BER performance in an OFDM-based communication system is used to evaluate and compare the capability of the proposed DNN-based impulsive noise mitigation approach

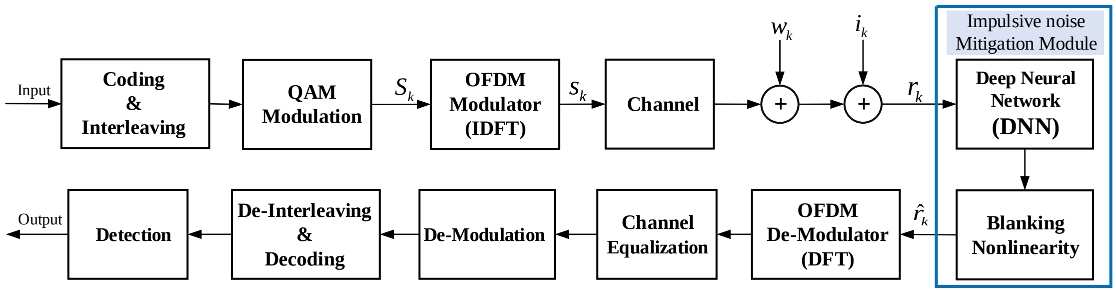

Fig. 7.1: System model block diagram.

with other conventional approaches such as blanking and clipping. The robustness of the proposed approach is highlighted by testing the performance with impulsive noise model different from the model used for training. In addition, we evaluate the robustness of our method in bursty impulsive noise when the receiver is accompanied by time domain interleaving techniques. Simulation results show that the DNN-based approach offers up to 2 dB gains relative to blanking and clipping at $BER = 10^{-3}$.

7.2 System Model

Consider the OFDM system shown in Fig. 7.1. After digital-to-analog conversion the transmitted signal envelope in the time domain can be expressed as

$$s(t) = \frac{1}{\sqrt{N}} \sum_{k \in S_A} S_k \, e^{j\frac{2\pi k t}{T_s}}, \; 0 < t < T_s, \tag{7.1}$$

where N denotes the number of subcarriers, S_A represents the set of active subcarriers; S_k is the modulated symbol on the k^{th} subcarrier; and T_s is the OFDM symbol duration. The channel can be modeled as a linear time-varying system described by the channel impulse response

$$c(\tau) = \sum_{p=1}^{L} b_p \delta(\tau - \tau_p), \tag{7.2}$$

where L is the length of the channel impulse response; b_p and τ_p are the amplitude and the delay of the p^{th} multipath component, respectively. Therefore, the received signal after down conversion, analog-to-digital conversion, guard interval removing, and synchronization can be expressed as

$$r_k = \sum_{p=1}^{L} b_p s_{k-\tau_p} + n_k\,, \quad k = 0,\, 1,\, \ldots,\, N-1 \tag{7.3}$$

where $s_k = s(kT_s/N)$; $n_k = w_k + i_k$ is the mixture of AWGN w_k and impulsive noise i_k.

Here it is assumed that the noise samples n_k are uncorrelated and their distribution can be expressed in terms of multi-component mixture-Gaussian model[48]. Corresponding to this model, the PDF of the noise samples n_k is obtained as

$$P(n_k) = \sum_{j=0}^{J-1} p_j G(n_k \left| \sigma_j^2 \right.) \tag{7.4}$$

where $G\left(n_k \left|\sigma^2\right.\right)$ is the PDF of the complex Gaussian variable with zero-mean and variance σ^2, and $\{\sigma_0, \sigma_1, ..., \sigma_{J-1}\}$ and $\{p_0, p_1, ..., p_{J-1}\}$ are the model parameters such that $\sum\limits_{j=0}^{J-1} p_j = 1$. The noise model (7.4) can support two commonly used impulsive noise models. The first impulsive noise model is a two component mixture-Gaussian noise model or Bernoulli Gaussian (BG) noise model[29] with model parameters corresponding to

$$J = 2,\;\; p_0 = 1-\varepsilon,\;\; p_1 = \varepsilon,\;\; \sigma_0^2 = \sigma_w^2,\;\; \sigma_1^2 = \sigma_w^2 + \sigma_i^2. \tag{7.5}$$

Here ε is the probability of the incoming impulse noise, σ_w^2 is the variance of AWGN component, and σ_i^2 presents the variance of the impulsive noise. The expression in (7.4) can also be used to characterize a Middleton Class A (MCA) impulsive noise model[96] with the following parameters

$$J = \infty,\;\; p_j = \frac{\mathrm{e}^{-A} A^j}{j!},\;\; \sigma_j^2 = \frac{jA^{-1} + \Gamma}{1+\Gamma}\sigma_n^2,\;\; j = 0, 1, ..., \infty \tag{7.6}$$

where σ_n^2 is the noise variance of n_k, A is the impulsiveness index designed as the product of the mean number of impulses per time unit and the mean length of an impulse (in time units), and $\Gamma = \sigma_w^2/\sigma_i^2$ denotes the background-to-impulsive noise power ratio[96]. The noise model in (7.4) is used to train the proposed DNN. In order to investigate the system performance when there is a model mismatch between training and testing, we also consider Symmetric Alpha Stable (SαS) impulsive noise which can be expressed as[97]

$$n_k \sim S(\alpha, \varsigma, \gamma, \mu) \tag{7.7}$$

where $\alpha \in (0, 2]$ denotes the stability parameter that sets the degree of the impulsiveness of the distribution; $\mu \in \mathbb{R}$ is the location parameter; $\varsigma \in [-1, 1]$ is called the skewness parameter and is a measure of asymmetry ($\varsigma = 0$ for SαS distribution); $\gamma \in (0, \infty)$ represents the scale parameter which is a measure of the width of the distribution.

7.3 Deep Neural Network (DNN) Design

In order to deal with impulsive noise, a DNN is exploited to find the instances of impulsivity. DNN is a black-box approach that can be used to model any nonlinear system if properly trained. In this section, the structure of DNN is introduced and then the input features are presented.

7.3.1 DNN Structure

As shown in Fig. 7.2, the considered neural network consists of two hidden layers with n_1 and n_2 hidden neurons in each layer, respectively. Typically, there is no analytical method to choose the number of layers and neurons, and hence they are determined experimentally on a trial and error basis. Here, $\mathbf{x} = [x_1, x_2, x_3]^T$ represents the input vector consisting of three features (as discussed in the next subsection) and $\hat{y}$ denotes the output of the DNN. There is only one node in the output layer, which generate a binary sequence of zeros and ones. Note that the soft outputs of DNN will be rounded off to a 0 or 1. An output 1 indicates that the received sample r_k is corrupted by impulsive noise and output 0 implies that the k^{th} received sample is clean. According to Fig. 7.2, the relation between layers can be expressed as

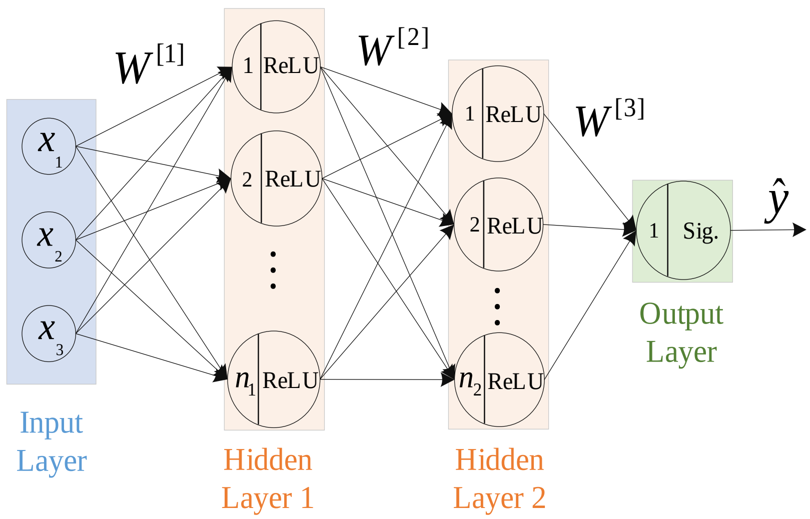

Fig. 7.2: Block diagram of the DNN.

$$\mathbf{A}^{[1]} = g^{[1]}\left(\mathbf{W}^{[1]}\mathbf{x} + \mathbf{b}^{[1]}\right)$$
$$\mathbf{A}^{[2]} = g^{(2)}\left(\mathbf{W}^{[2]}\mathbf{A}^{(1)} + \mathbf{b}^{[2]}\right)$$
$$\hat{y} = g^{[3]}\left(\mathbf{W}^{[3]}\mathbf{A}^{[2]} + \mathbf{b}^{[3]}\right), \tag{7.8}$$

where $\mathbf{W}^{[l]}$, $\mathbf{b}^{[l]}$, and $g^{[l]}$ are the parameter matrix, bias vector, and activation function of l^{th} layer that will be applied to the output of the previous layer. The activation function is a nonlinear function in general, but can also be designed to retain linearity in the transformation process. In this paper, the Rectified linear unit (ReLU) function is used for the hidden layers and a Sigmoid function is used in the output layer. The ReLU and Sigmoid functions are expressed as

$$\text{ReLU}(x) = \max(x, 0), \tag{7.9}$$

$$\text{Sigmoid}(x) = \frac{1}{1 + \mathrm{e}^{-x}}. \tag{7.10}$$

Loss or cost function is a function that returns the loss or penalty associated with a predicted value $\hat{y}$ when the true value is y over the entire training set. This loss function value decreases when the difference between the predicted value and the correct value decreases. The loss function that is used in this work corresponds to

$$\mathcal{L}(\mathbf{W}, \mathbf{b}) = -\frac{1}{m}\left[\sum_{i=1}^{m} y_i \log(\hat{y}_i) + (1-y_i)\log(1-\hat{y}_i)\right] + \frac{\psi}{2m}\sum_{l=1}^{L-1}\sum_{i=1}^{n_l}\sum_{j=1}^{n_{l+1}} W_{ij}^2, \tag{7.11}$$

where m is the number of training samples; n_l represents the number of neurons in layer l; and ψ denotes the regularization hyper parameter that is used to prevent over-fitting in the training phase. The DNN aims to determine the weights $\mathbf{W}$ and the bias vector $\mathbf{b}$ that minimize the loss function, i.e.,

$$\min_{\mathbf{W}, \mathbf{b}} \mathcal{L}(\mathbf{w}, \mathbf{b}). \tag{7.12}$$

The proposed DNN is trained using the back-propagation algorithm along with Adam optimization algorithm[98]. The Adam optimization is an extension to stochastic gradient descent and has recently seen broader adoption in deep learning applications. Adam computes adaptive learning rates for each parameter Θ at time instant k. According to the Adam algorithm, the update rule for each parameter Θ in layer l is given by

$$\Theta_{k+1}^{[l]} = \Theta_k^{[l]} - \frac{\eta}{\sqrt{\hat{\upsilon}_k^{[l]}} + \varepsilon}\hat{m}_k^{[l]}. \tag{7.13}$$

Here, η is learning rate hyper parameter and

$$\begin{aligned} m_k^{[l]} &= \beta_1 m_{k-1}^{[l]} + (1-\beta_1)\frac{\partial \mathcal{L}(\Theta)}{\partial \Theta^{[l]}} \\ \hat{m}_k^{[l]} &= \frac{m_k^{[l]}}{1-\beta_1^k}, \end{aligned} \tag{7.14}$$

$$\begin{aligned} \upsilon_k^{[l]} &= \beta_2 \upsilon_{k-1}^{[l]} + (1-\beta_2)\left(\frac{\partial \mathcal{L}(\Theta)}{\partial \Theta^{[l]}}\right)^2 \\ \hat{\upsilon}_k^{[l]} &= \frac{\upsilon_k^{[l]}}{1-\beta_2^k}, \end{aligned} \tag{7.15}$$

where the proposed default values are $\beta_1 = 0.9$, $\beta_2 = 0.999$, $\varepsilon = 10^{-8}$, and the initial value for $m_0^{[l]}$ and $\upsilon_0^{[l]}$ are randomly chosen.

7.3.2 DNN Input Features

Feature extraction is one of the most important aspects of machine learning because it turns raw data into information that is suitable for inferencing. Feature extraction eliminates the redundancy present in many types of measured data, facilitating generalization which is critical to avoiding over-fitting during the learning phase. According to Fig. 7.2, the input layer has three nodes which are (i) the current sample value, (ii) ROAD statistic, and (iii) median deviations filter output. In the following we briefly introduce the ROAD and median deviation features.

ROAD Value

The ROAD value is an efficient statistic for distinguishing between corrupted and uncorrupted samples as its value is high for noisy samples and low for uncorrupted samples[95]. In general, ROAD factor is widely used in image processing for two dimensional (2D) signals. Here, we compute the ROAD factor for a one dimensional received signal as follows:

i. The absolute difference between the centre sample and the remaining samples of a $(1 \times 2n)$ vector is calculated and denoted by $\mathbf{d}_{(k)}$ which consists of $2n$ elements:

$$\mathbf{d}_{(k)} = |r_k - [r_{k-n}, ..., r_{k-1}, r_{k+1}, ..., r_{k+n}]| \tag{7.16}$$

ii. Sort $\mathbf{d}_{(k)}$ values in increasing order:

$$\mathbf{b}_{(k)} = \mathrm{sort}(\mathbf{d}_{(k)}) \tag{7.17}$$

iii. The ROAD factor is calculated by summing up the first n values of $\mathbf{b}_{(k)}$:

$$\mathrm{ROAD} = \sum_{k=1}^{n} \mathbf{b}_{(k)}. \tag{7.18}$$

Median Deviations Filter

The median-deviations filter to obtain e_k can be expressed as

$$e_k = r_k - \text{median}\left([r_{k-n}, ..., r_k, ..., r_{k+n}]\right), \tag{7.19}$$

where the median filter used in (7.19) is a standard median filter which operates on a moving window of $2n+1$ samples.

7.4 Impulsive Noise Mitigation

After the proposed DNN determines if a received sample is contaminated with impulsive noise or not, a simple memoryless nonlinear preprocessor such as blanking can be used to alleviate the effect of impulsive noise. Therefore, the output of blanking nonlinearity can be expressed as

$$\hat{r}_k = \begin{cases} r_k, & \hat{y}_k = 0 \\ 0, & \hat{y}_k = 1 \end{cases}, \tag{7.20}$$

where $\hat{y}_k$ is the output of the DNN. It is worth mentioning that one can use other nonlinear preprocessors proposed in the literature to suppress the impact of impulsive noise. This extension is straightforward and is not the main focus of this paper. After impulsive noise mitigation a DFT module is used to transform the time domain signal to the frequency domain. The DFT module is followed by frequency domain equalization that depends on channel estimation which can be performed based on pilot subcarriers. Viterbi soft decoding is used to decode the demodulated signal and then detection is performed based on the modulation scheme used.

7.5 Simulation results

In this section, an OFDM-based communication system with QPSK modulation in the presence of channel fading, channel coding, and impulsive noise is studied. The BER performance is used to compare the proposed DNN-based impulsive noise mitigation with other conventional approaches such as blanking and clipping. Since the distribution of the received OFDM signal in case of no impulsive noise can be considered as Gaussian, the threshold value for blanking and clipping in all scenarios is obtained based on the approach provided in[47].

We set $n_1 = 20$ and $n_2 = 10$ as the number of neurons in the first and the second hidden layers, respectively. With three input features and according to Fig. 7.2, $\mathbf{W}^{(1)}$ is (20×3) matrix and $\mathbf{b}^{(1)}$ is (20×1) bias vector that connects the input layer to the first hidden layer. After applying the activation function $g^{(1)}$, the matrix $\mathbf{W}^{(2)}$ with size (10×20) and the bias vector $\mathbf{b}^{(2)}$ with size (10×1) will connect the first hidden layer to the second hidden layer. Finally, $\mathbf{W}^{(3)}$ is (1×10) matrix and $\mathbf{b}^{(3)}$ is a (1×1) bias that connects the second hidden layer to the output layer. Since the standard gradient descent from random initialization performs poorly with DNN, the initial values for all parameters is chosen based on Xavier initializer[99]. Here, the considered DNN is trained based on the signal model in (7.3) and noise model in (7.4). Specifically, the training set consists of 1000 OFDM symbols with a range of E_b/N_0 and SIR that span the operating regions of interested. The samples with different E_b/N_0 and SIR values in the training data set is randomly shuffled to remove any trend that may exist.

For a quick reference, the simulation parameters for the considered coded OFDM system in fading channel are listed in Table 7.1. A total of 1024 subcarriers are used with 672 carrying data, 256 pilot, and 96 null subcarriers. Channel estimation is done based on pilot subcarriers which are equally spaced between 1024 subcarriers. A 10-path fading channel is considered with path arrival times following a Poisson distribution with mean 1 ms. The path amplitudes are Rayleigh distributed with exponentially decreasing average power.

The BER performance of the proposed DNN-based impulsive noise mitigation approach under two different test settings (i) BG noise with SIR = 0 dB, and (ii) MCA with $\Gamma = 0.2$

Table 7.1
Simulation Parameters

Parameters	**Values**
Bandwidth (BW)	6 kHz
No. of Subcarriers (N)	1024
Symbol Duration (T)	170.7 ms
Modulation Scheme	QPSK
Channel Length (L)	10
Convolution Code Rate (CR)	1/2
Code Constraint Length	7
Generator Polynomial	[171,133]
Learning Rate (η)	0.01
Regularization Hyper Parameter (ψ)	0.1
No. of Samples (n)	5

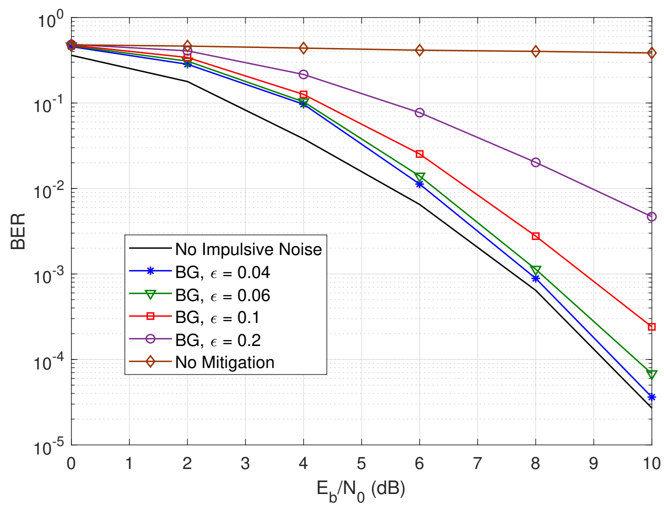

Fig. 7.3: BER in BG noise, SIR = 0 dB.

and J=10 are shown in Fig. 7.3 and Fig. 7.4, respectively. As expected the BER performance will degrade with increase in the frequency of impulsive noise occurrence.

Fig. 7.5 and Fig. 7.6 compares the BER performance of the DNN with blanking (BLN) and clipping (CLP) in BG and MCA impulsive noise models in various levels of impulsivity, respectively. From Fig. 7.5 and Fig. 7.6, it is evident that DNN outperforms both blanking and clipping in all scenarios of both BG and MCA noise models with gains close to 2 dB at BER of 10^{-3}. Fig. 7.6 shows that at high SINR, blanking and clipping are very vulnerable

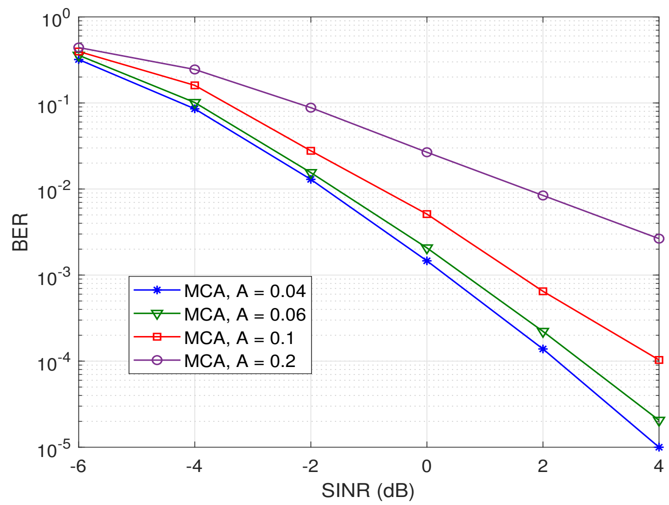

Fig. 7.4: BER in MCA noise, $\Gamma = 0.2$.

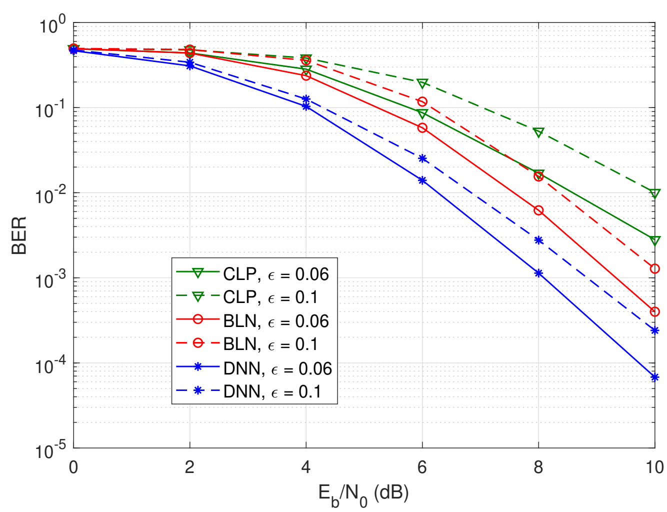

Fig. 7.5: BER comparison of DNN, BLN, and CLP in BG noise, SIR = 0 dB.

as the level of peakedness decreases and it is difficult to find a proper threshold to distinguish between desired and contaminated signals. On the other hand, a well trained DNN can handle the impulsive noise detection process even when the signal and impulsive noise peakedness is low. Although, the performance loss of DNN with increase in the frequency of impulsive noise occurrence is noticeable, it still outperforms other approaches in all scenarios. Fig. 7.7 illustrates the robustness of the proposed DNN approach under impulsive noise model mismatch. Although the proposed DNN is trained based on the noise model in

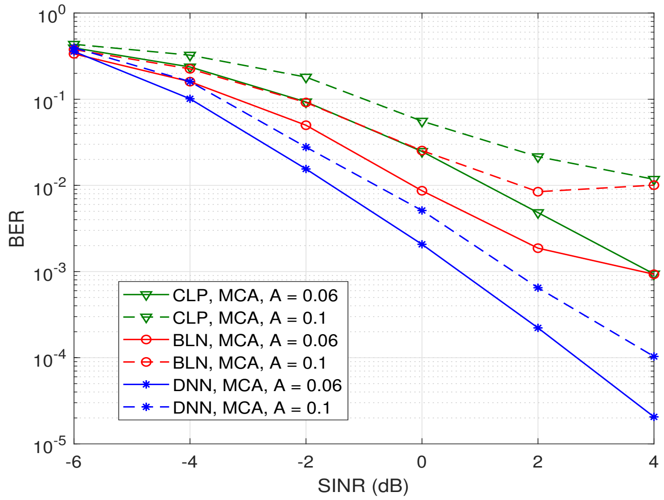

Fig. 7.6: BER comparison of DNN, BLN, and CLP in MCA noise, $\Gamma = 0.2$.

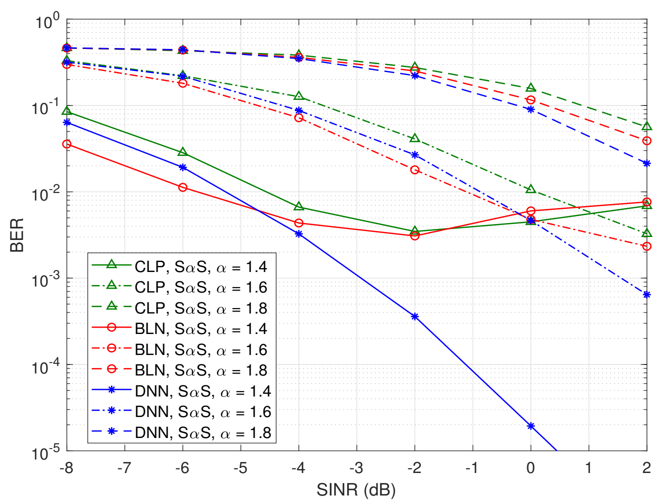

Fig. 7.7: BER comparison of DNN, BLN, and CLP in SαS noise. $\beta = 0$, γ=1, $\mu = 0$.

(7.4), the DNN-based method is the most robust technique relative to blanking and clipping in SαS noise model. The performance degradation in blanking and clipping comes from the fact that the threshold calculation is performed based on Gaussian mixture assumption for the received signal which does not hold in this scenario.

Fig. 7.8 investigates the BER performance of the considered DNN-based method in bursty impulsive noise environment when a time domain interleaver is included in the receiver. In Fig. 7.8, the parameter Num denotes the number of consecutive contaminated samples by

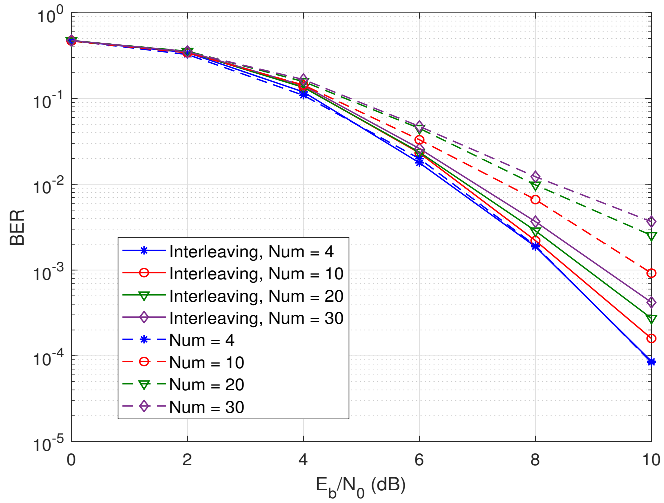

Fig. 7.8: BER performance of DNN in bursty impulsive noise, SIR = 0 dB, $\epsilon = 0.06$.

impulsive noise. As shown in Fig. 7.8, the DNN is able to find the impulsive noise instances while the level of burstiness is alleviated by time domain interleaving. From Fig. 7.8 it is obvious that the best performance is achieved when the duration of impulsive noise is short.

7.6 Summary

In this chapter, a DNN is proposed to determine if a received sample is contaminated with impulsive noise or not in an OFDM-based communication system. The ROAD value along with median deviations filter is used as input features for the DNN. In the next stage, a nonlinear preprocessor such as blanking is used to suppress the effect of impulsive noise in corrupted samples. Simulation results show that the DNN-based approach offers significant improvement in the BER performance in the presence of strong impulsive component. Moreover, the DNN-based impulsive noise mitigation outperforms other conventional threshold-based outlier mitigation methods such as blanking and clipping with providing lower BER in impulsive noise environments. We also show that DNN-based approach is robust to impulsive noise model mismatches and can effectively deal with bursty impulsive noise when the receiver includes time domain interleaving.

Chapter 8

Conclusion and Future work

In this chapter, we provide concluding remarks of this dissertation with a summary of the results and future research directions.

8.1 Conclusion

In this dissertation, two strategies for impulsive noise mitigation in OFDM-based communication system are investigated. First, a blind adaptive intermittently nonlinear filter is designed to detect and mitigate impulsive noise in the analog domain where outliers are more distinguishable.

To this end, in chapter 2, an Adaptive Nonlinear Differential Limiter (ANDL) is designed to mitigate impulsive noises in OFDM-based PLC systems without detrimental effects such as self-interference and out-of-band power leakage caused by other nonlinear approaches. The proposed ANDL is constructed from a linear analog filter by applying a feedback-based nonlinearity, controlled by a single resolution parameter. In addition, a practical and simple method is presented to find an effective value for the resolution parameter (a parameter which determines the nonlinear region of the ANDL) that ensures the mitigation of impulsive noise without impacting the desired OFDM signal. In this context, the structure of the matched filter in the receiver is modified to compensate the filtering effect of the ANDL in the linear regime. Unlike many prior approaches for impulsive noise mitigation that assume a statistical noise model, ANDL is blind to the exact nature of the noise distribution, and is designed to be fully compatible with existing linear front end filters. We demonstrate the ability of ANDL to significantly reduce the PSD of impulsive noise in the signal passband without having prior knowledge of the statistical noise model or its parameters. The simulation results show that ANDL can provide improvement in the overall signal quality ranging from distortionless behavior for low impulsive noise conditions to significant improvement in BER performance in the presence of strong impulsive component. It is important to note that ANDL can be deployed either as a stand-alone low-cost real-time solution for impulsive noise mitigation, or combined with other interference reduction techniques.

In chapter 3, an approximation of the ANDL using a piecewise combination of linear filters is provided to derive closed-form analytical expressions for the average SNR at the output of the proposed filter. The calculation is based on the idea that the ANDL can be perceived as a time-variant linear filter whose bandwidth is modified based on the intensity of the impulsive noise. In addition, by linearizing the filter time parameter variations, we treat the ANDL as a set of linear filters where the exact operating filter at a given time depends upon the magnitude of the outliers. The theoretical average BER is validated through simulations for different compositions of noise. The theoretical analysis and simulation results show that the ANDL ensures significant improvement in SNR and BER performance in the presence of strong impulsive noise component. Moreover, the proposed ANDL outperforms other conventional outlier mitigation approaches such as blanking and clipping by providing lower BER in impulsive noise environments. It is important to note that the proposed ANDL is totally blind and can be deployed in real-time applications for both sparse and bursty IN scenarios.

In chapter 4, a practical implementation of adaptive analog nonlinear filter, referred to as Adaptive Canonical Differential Limiter (ACDL) is proposed to mitigate impulsive noise in an OFDM-based systems. The proposed ACDL is constructed from a Clipped Mean Tracking Filter (CMTF) and Quartile Tracking Filters (QTFs). The QTFs help to determine a real-time range (even in non-stationary noise) that excludes outliers and is fed into the

CMTF which is responsible for impulsive noise mitigation. Note that, the CMTF is an intermittently nonlinear analog filter and its nonlinearity is controlled by the aforementioned range. Therefore, proper selection of this range ensures the improvement of the desired signal quality in impulsive environment. The performance improvement of the proposed ACDL is due to the fact that unlike other nonlinear methods, the ACDL is implemented in the analog domain where the outliers are still broadband and distinguishable. Simulation results in PRIME (OFDM-based narrowband PLC system) demonstrate the improvement in the overall signal quality and the superior BER performance of ACDL relative to other nonlinear approaches such as blanking and clipping in impulsive noise environments.

In chapter 5 and 6, an analog nonlinear preprocessor (ANP) and a memoryless analog nonlinear preprocessor (MANP) is proposed to deal with impulsive noise in coded OFDM-based UWA communication systems, respectively. In chapter 5, the impact of impulsive noise on a two-step Doppler shift compensation approach is also quantified. Specifically, the ability of the ANP to improve the robustness of Doppler shift compensation in the presence of impulsive is highlighted. We also introduced a practical schematic of MANP based on the OTAs which can be implemented in IC. Note that, the performance of the proposed MANP in chapter 6 is evaluated based on field data collected in an under-ice environment in Portage Lake, MI. The results demonstrate the superior BER performance of these approaches relative to classic approaches that use blanking and/or clipping for impulsive noise mitigation.

Secondly, in chapter 7, a machine learning based approach which consists of a deep neural network (DNN) is proposed to detect the contaminated sample with impulsive noise in OFDM-based communication system. The ROAD value along with median deviations filter is used as input features for the proposed DNN. In the next stage, a nonlinear preprocessor such as blanking is used to suppress the effect of impulsive noise in corrupted samples. Simulation results show that the DNN-based approach offers significant improvement in the BER performance in the presence of strong impulsive component. Moreover, the DNN-based impulsive noise mitigation outperforms other conventional threshold-based outlier mitigation methods such as blanking and clipping with providing lower BER in impulsive noise environments. We also show that DNN-based approach is robust to impulsive noise model mismatches and can effectively deal with bursty impulsive noise when the receiver includes time domain interleaving.

8.2 Future work

Research accomplished in this dissertation can lead to multiple follow-on efforts and possible future research directions that are highlighted in the following:

- Although, the QTFs as described in chapter 4 offer a robust means to establish the sensitivity range for the BAINFs even when the noise is non-stationary, a theoretical performance modeling and analysis effort to formulate an optimization framework for an optimal choice of the sensitivity range $[\beta_-, \beta_+]$ can further advance this idea. The optimization formulation can start with the assumption that the non-Gaussian noise distribution is known a priori. However, a distribution estimation based on measurements is needed when the distribution is unknown. A bank of N QTFs can be used to determine the sample quantiles $(Q_1, Q_2, \ldots, Q_N)$ of the signal. Then a non-parametric regression technique such as a local polynomial kernel regression strategy [100] can be used to estimate the time-dependent density function.

- An important consideration in practical networks is their dynamic nature in non-stationary noise. This challenging situation requires interference mitigation tools to adapt to the dynamically changing interference. The influence function choice determines the structure of the local nonlinearity imposed on the input signal. Based on locally most powerful (LMP) test [84], for a given noise distribution the optimal choice corresponds to $g_{LO} = -\frac{f_n'}{f_n}$, where f_n represents the technogenic noise density function and f_n' is its derivative. Then, non-stationarity in the noise distribution motivates an online adaptive strategy to design influence functions based on the updated distribution. As mentioned before a bank of N QTFs along with local polynomial kernel regression strategy can be used to estimate the distribution. Thus, we need to determine the parameters of QTFs (e.g. time window, dynamic range, and etc.) properly to guarantee the performance of the QTFs (e.g. their convergence speed and the output ripple) and consequently the performance of the estimator.

- An algorithm is needed to update the influence function periodically (period of adaption can be determined based on the coherence time of the system) or based on a mismatch parameter between current and updated distribution. Defining a proper mismatch parameter to compare two distributions precisely can be challenging but using the Kolmogorov-Smirnov (K–S) statistic quantifies a distance between two empirical distribution functions. The null distribution of this statistic is calculated under the null hypothesis that the samples are drawn from the same distribution (in two-sample case). The two-sample K–S test is one of the most useful and general nonparametric methods for comparing two samples, as it is sensitive to differences in both location and shape of the empirical cumulative distribution functions of the two samples. In order to evaluate the performance and robustness of the proposed adaptive online influence function design one can compare the results of non-stationary noise with the case when the noise is stationary.

- In chapter 7, a machine learning based approach is proposed to detect the contaminated samples with impulsive noise. However, the mitigation part of the receiver is performed by using conventional memoryless nonlinear preprocessor such as blanking which is not the optimal action on the corrupted samples. One can advance this idea by leveraging reinforcement learning (RL) to detect the corrupted samples and alleviate the impact of the impulsive noise by taking the best action based on the optimum policy. Note that, the optimum policy can be updated online in respect to variation in the environment. In this context, finding a proper reward function plays a critical role in the system performance.

Bibliography

[1] R. Barazideh, A. V. Nikitin, and B. Natarajan, "Practical implementation of adaptive analog nonlinear filtering for impulsive noise mitigation," in *IEEE Int. Conf. Commun. (ICC)*, May 2018, pp. 1–7.

[2] A. V. Nikitin and R. L. Davidchack, "Analog-domain mitigation of outlier noise in the process of analog-to-digital conversion," in *IEEE Int. Conf. Commun. (ICC)*, May 2018, pp. 1–7.

[3] R. Barazideh, W. Sun, B. Natarajan, A. V. Nikitin, and Z. Wang, "Impulsive noise mitigation in underwater acoustic communication systems: Experimental studies," in *IEEE Comput. Commun. Work. Conf. (CCWC)*, Jan 2019, pp. 0880–0885.

[4] D. Middleton, "Non-Gaussian noise models in signal processing for telecommunications: New methods and results for class A and class B noise models," *IEEE Trans. Inf. Theory*, vol. 45, no. 4, pp. 1129–1149, 1999.

[5] D. R. M. A. McHenry and R. J. Matheson., "Electronic noise is drowning out the internet of things." *IEEE Spectrum*, pp. 50–56, Sep. 2015.

[6] R. S. K. S. R. Mallipeddy, "Impact of uwb interference on IEEE 802.11a wlan system," in *National Conf. Communi. (NCC)*, 2010.

[7] J. Lin, M. Nassar, and B. L. Evans, "Impulsive noise mitigation in powerline communications using sparse Bayesian Learning," *IEEE J. Sel. Areas Commun.*, vol. 31, no. 7, pp. 1172–1183, Jul. 2013.

[8] A. V. Nikitin, R. L. Davidchack, and J. E. Smith, "Out-of-band and adjacent-channel interference reduction by analog nonlinear filters," *EURASIP J. Adv. in Signal Process.*, no. 1, p. 12, Dec. 2015.

[9] M. Chitre, S. H. Ong, and J. Potter, "Performance of coded OFDM in very shallow water channels and snapping shrimp noise," in *Proceedings of OCEANS 2005 MTS/IEEE*, Sep. 2005, pp. 996–1001 Vol. 2.

[10] M. A. Chitre, J. R. Potter, and S. H. Ong, "Optimal and near-optimal signal detection in snapping shrimp dominated ambient noise," *IEEE J. Oceanic Eng.*, vol. 31, no. 2, pp. 497–503, Apr. 2006.

[11] J. A. Hildebrand, "Anthropogenic and natural sources of ambient noise in the ocean," *Marine Ecol. Progress Ser.*, vol. 395, no. 5, pp. 1–16, 2009.

[12] S. Niknam, A. A. Nasir, H. Mehrpouyan, and B. Natarajan, "A multiband OFDMA heterogeneous network for millimeter wave 5G wireless applications," *IEEE Access*, vol. 4, pp. 5640–5648, Sep. 2016.

[13] R. Barazideh and B. Seyfe, "Cross-layer combining of adaptive pilot-symbolassisted modulation with truncated automatic repeat request in the presence of imperfect channel state information at both the receiver and the transmitter," *IET Communications*, vol. 5, no. 16, pp. 2275–2284, Nov. 2011.

[14] ——, "Cross-layer combining of adaptive modulation with truncated ARQ in SIMO systems with imperfect CSI at receiver," in *2009 ISECS International Colloquium on Computing, Communication, Control, and Management*, vol. 4, Aug. 2009, pp. 321–325.

[15] ——, "Adaptive PSAM in SIMO systems with imperfect CSI in rayleigh fading channels," in *Proceedings of the 2009 International Conference on Hybrid Information Technology*, ser. ICHIT '09. ACM, 2009, pp. 124–129.

[16] B. D. V. Veen and K. M. Buckley, "Beamforming: a versatile approach to spatial filtering," *IEEE ASSP Magazine*, vol. 5, no. 2, pp. 4–24, April 1988.

[17] L. C. Godara, "Application of antenna arrays to mobile communications. ii. beam-forming and direction-of-arrival considerations," *Proceedings of the IEEE*, vol. 85, no. 8, pp. 1195–1245, Aug 1997.

[18] S. Gollakota, S. D. Perli, and D. Katabi, "Interference alignment and cancellation," *SIGCOMM Comput. Commun. Rev.*, vol. 39, no. 4, pp. 159–170, Aug. 2009. [Online]. Available: http://doi.acm.org/10.1145/1594977.1592588

[19] O. E. Ayach, S. W. Peters, and R. W. Heath, "The practical challenges of interference alignment," *IEEE Wireless Communications*, vol. 20, no. 1, pp. 35–42, February 2013.

[20] A. Chopra, "Modeling and mitigation of interference in wireless receivers with multiple antennae," Dec. 2011.

[21] S. Niknam, B. Natarajan, and H. Mehrpouyan, "A spatial-spectral interference model for millimeter wave 5G applications," in *Proc. IEEE Veh. Tech. Conf.*, Sep. 2017, pp. 1–5.

[22] S. Niknam, B. Natarajan, and R. Barazideh, "Interference analysis for finite-area 5g mmwave networks considering blockage effect," *IEEE Access*, vol. 6, pp. 23 470–23 479, Apr. 2018.

[23] S. Niknam and B. Natarajan, "On the regimes in millimeter wave networks: Noise-limited or interference-limited?" in *IEEE Int. Conf. on Commun. Workshops*, 2018.

[24] S. Niknam, R. Barazideh, and B. Natarajan, "Cross-layer interference modeling for 5G mmwave networks in the presence of blockage," in *IEEE Veh. Tech. Conf.*, Aug. 2018, pp. 1–5.

[25] A. V. Nikitin, D. Scutti, B. Natarajan, and R. L. Davidchack, "Blind adaptive analog nonlinear filters for noise mitigation in powerline communication systems," in *Proc. IEEE Int. Symp. on Power Line Commun. and its Appl.*, Mar. 2015, pp. 1–6.

[26] J. A. C. Bingham, "Multicarrier modulation for data transmission: an idea whose time has come," *IEEE Commun. Mag.*, vol. 28, no. 5, pp. 5–14, May. 1990.

[27] *IEEE Standard for low frequency narrowband power line communications*, Std., 2012.

[28] M. Hoch, "Comparison of PLC G3 and PRIME," in *Proc. IEEE Int. Symp. on Power Line Commun. and its Appl.*, Apr. 2011, pp. 165–169.

[29] M. Ghosh, "Analysis of the effect of impulse noise on multicarrier and single carrier QAM systems," *IEEE Trans. Commun.*, vol. 44, no. 2, pp. 145–147, Feb. 1996.

[30] D. Umehara, H. Yamaguchi, and Y. Morihiro, "Turbo decoding in impulsive noise environment," in *Global Telecommun. Conf.*, vol. 1, Nov. 2004, pp. 194–198.

[31] H. Nakagawa, D. Umehara, S. Denno, and Y. Morihiro, "A decoding for low density parity check codes over impulsive noise channels," in *Proc. IEEE Int. Symp. on Power Line Commun. and its Appl.*, Apr. 2005, pp. 85–89.

[32] G. Ndo, P. Siohan, M. H. Hamon, and J. Horard, "Optimization of turbo decoding performance in the presence of impulsive noise using soft limitation at the receiver side," in *Global Telecommun. Conf.*, Nov. 2008, pp. 1–5.

[33] M. Nassar, J. Lin, Y. Mortazavi, A. Dabak, I. H. Kim, and B. L. Evans, "Local utility power line communications in the 3–500 kHz band: Channel impairments, noise, and standards," *IEEE Signal Process. Mag.*, vol. 29, no. 5, pp. 116–127, Sep. 2012.

[34] A. Al-Dweik, A. Hazmi, B. Sharif, and C. Tsimenidis, "Efficient interleaving technique for OFDM system over impulsive noise channels," in *Proc. IEEE Int. Symp. on Personal, Indoor and Mobile Radio Commun.*, Sep. 2010, pp. 167–171.

[35] S. Liu, F. Yang, and J. Song, "An optimal interleaving scheme with maximum time-frequency diversity for plc systems," *IEEE Trans. Power Del.*, vol. 31, no. 3, pp. 1007–1014, June 2016.

[36] G. Caire, T. Y. Al-Naffouri, and A. K. Narayanan, “Impulse noise cancellation in OFDM: an application of compressed sensing,” in *IEEE Int. Symp. Inform. Theory.*, Jul. 2008, pp. 1293–1297.

[37] T. Y. Al-Naffouri, A. A. Quadeer, and G. Caire, “Impulse noise estimation and removal for OFDM systems,” *IEEE Trans. Commun.*, vol. 62, no. 3, pp. 976–989, Mar. 2014.

[38] D. P. Wipf and B. D. Rao, “Sparse bayesian learning for basis selection,” *IEEE Trans. Sig. Process.*, vol. 52, no. 8, pp. 2153–2164, Aug. 2004.

[39] S. Rangan, “Generalized approximate message passing for estimation with random linear mixing,” in *IEEE Int. Symp. Inform. Theory Proc.*, Jul. 2011, pp. 2168–2172.

[40] M. Nassar, P. Schniter, and B. L. Evans, “A factor graph approach to joint OFDM channel estimation and decoding in impulsive noise environments,” *IEEE Trans. Signal. Process.*, vol. 62, no. 6, pp. 1576–1589, Mar. 2014.

[41] D.-F. Tseng *et al.*, “Robust clipping for OFDM transmissions over memoryless impulsive noise channels,” *IEEE Commun. Lett.*, vol. 16, no. 7, pp. 1110–1113, Jul. 2012.

[42] C.-H. Yih, “Iterative interference cancellation for OFDM signals with blanking nonlinearity in impulsive noise channels,” *IEEE Signal Process. Lett.*, vol. 19, no. 3, pp. 147–150, Mar. 2012.

[43] M. Korki, N. Hosseinzadeh, H. L. Vu, T. Moazzeni, and C. H. Foh, “Impulsive noise reduction of a narrowband power line communication using optimal nonlinearity technique,” in *Proc. Aust. Telecomm. Netw. and App. Conf.*, Nov. 2011, pp. 1–4.

[44] F. H. Juwono, Q. Guo, Y. Chen, L. Xu, D. D. Huang, and K. P. Wong, “Linear combining of nonlinear preprocessors for OFDM-based power-line communications,” *IEEE Trans. on Smart Grid*, vol. 7, no. 1, pp. 253–260, Jan. 2016.

[45] F. H. Juwono, Q. Guo, D. Huang, and K. P. Wong, “Deep clipping for impulsive

noise mitigation in OFDM-based power-line communications," *IEEE Trans. Power Del*, vol. 29, no. 3, pp. 1335–1343, Jun. 2014.

[46] N. Rozic, P. Banelli, D. Begusic, and J. Radic, "Multiple-threshold estimators for impulsive noise suppression in multicarrier communications," *IEEE Trans. Signal Process.*, vol. 66, no. 6, pp. 1619–1633, Mar. 2018.

[47] G. Ndo, P. Siohan, and M. H. Hamon, "Adaptive noise mitigation in impulsive environment: Application to power-line communications," *IEEE Trans. Power Del.*, vol. 25, no. 2, pp. 647–656, Apr. 2010.

[48] S. V. Zhidkov, "Analysis and comparison of several simple impulsive noise mitigation schemes for OFDM receivers," *IEEE Trans. Commun.*, vol. 56, no. 1, pp. 5–9, Jan. 2008.

[49] R. Barazideh, B. Natarajan, A. V. Nikitin, and R. L. Davidchack, "Performance of analog nonlinear filtering for impulsive noise mitigation in OFDM-based PLC systems," in *IEEE Latin-American Conf. Commun.*, Nov. 2017, pp. 1–6.

[50] R. Barazideh, B. Natarajan, A. V. Nikitin, and S. Niknam, "Performance analysis of analog intermittently nonlinear filter in the presence of impulsive noise," *IEEE Trans. Veh. Technol.*, vol. 68, no. 4, pp. 3565–3573, April 2019.

[51] R. Barazideh, S. Niknam, B. Natarajan, and A. V. Nikitin, "Intermittently nonlinear impulsive noise mitigation and doppler shift compensation in UWA-OFDM systems," *IEEE Access*, vol. 7, pp. 36 590–36 599, 2019.

[52] R. Barazideh, S. Niknam, and B. Natarajan, "Impulsive noise detection in OFDM-based system: A deep learning perspective," in *IEEE Comput. Commun. Work. Conf. (CCWC)*, Jan 2019, pp. 0937–0942.

[53] S. Galli, A. Scaglione, and Z. Wang, "For the grid and through the grid: The role of power line communications in the smart grid," *Proc. IEEE*, vol. 99, no. 6, pp. 998–1027, Jun. 2011.

[54] J. Lin and B. L. Evans, "Non-parametric mitigation of periodic impulsive noise in narrowband powerline communications," in *Proc. IEEE Global Comm. Conf.*, Dec. 2013, pp. 2981–2986.

[55] M. Zimmermann and K. Dostert, "Analysis and modeling of impulsive noise in broadband powerline communications," *IEEE Tran. Electromag. Compat.*, vol. 44, no. 1, pp. 249–258, Feb. 2002.

[56] M. Nassar, A. Dabak, I. H. Kim, T. Pande, and B. L. Evans, "Cyclostationary noise modeling in narrowband powerline communication for Smart Grid applications," in *Proc. IEEE Int. Conf. on Acoust., Speech and Sig. Process.*, Mar. 2012, pp. 3089–3092.

[57] M. Zimmermann and K. Dostert, "An analysis of the broadband noise scenario in powerline networks," in *Proc. IEEE Int. Symp. on Power Line Commun. and its Appl.*, Apr. 2000, pp. 5–7.

[58] M. Nassar, K. Gulati, Y. Mortazavi, , and B. L. Evans, "Statistical modeling of asynchronous impulsive noise in powerline communication networks," in *Proc. IEEE Global Comm. Conf.*, Dec. 2011, pp. 1–6.

[59] J. Lin and B. L. Evans, "Cyclostationary noise mitigation in narrowband powerline communications," in *Proc. Asia Pacific Signal and Info. Process. Association Annual Summit and Conf.*, Dec. 2012, pp. 1–4.

[60] Y. Yoo and J. Cho, "Asymptotic analysis of CP-SC-FDE and UW-SC-FDE in additive cyclostationary noise," in *Proc. IEEE Int. Conf. Comm.*, May. 2008, pp. 1410–1414.

[61] J. Haring and A. J. H. Vinck, "Iterative decoding of codes over complex numbers for impulsive noise channels," *IEEE Trans. Inf. Theory*, vol. 49, no. 5, pp. 1251–1260, May. 2003.

[62] Y. R. Chien, "Iterative channel estimation and impulsive noise mitigation algorithm for

OFDM-based receivers with application to power-line communications," *IEEE Trans. Power Del.*, vol. 30, no. 6, pp. 2435–2442, Dec. 2015.

[63] A. V. Nikitin, "On the interchannel interference in digital communication systems, its impulsive nature, and its mitigation," *EURASIP J. Adv. Signal Process.*, no. 1, p. 137, Dec. 2011.

[64] A. V. Nikitin and R. L. Davidchack, "Adaptive approximation of feedback rank filters for continuous signals," *Signal Process.*, vol. 84, no. 4, pp. 805–811, Apr. 2004.

[65] *IEEE Standard for low frequency narrowband power line communications*, Std., 2012.

[66] *HomePlug Green PHY The Standard For In-Home Smart Grid Powerline Communications*, Std., 2010.

[67] *IEEE Standard for Information technology-Local and metropolitan area networks-Specific requirements-Part 11: Wireless LAN Medium Access Control (MAC) and Physical Layer (PHY) Specifications Amendment 6: Wireless Access in Vehicular Environments*, Std., Jul. 2010.

[68] X. Kuai, H. Sun, S. Zhou, and E. Cheng, "Impulsive noise mitigation in underwater acoustic OFDM systems," *IEEE Trans. Veh. Technol.*, vol. 65, no. 10, pp. 8190–8202, Oct. 2016.

[69] J. W. Tukey, *Exploratory Data Analysis.* Addison-Wesley, 1977.

[70] A. V. Nikitin and R. L. Davidchack, "Signal analysis through analog representation," in *Proc. Royal Society of London A: Mathematical, Physical and Engineering Sciences*, vol. 459, no. 2033, May. 2003, pp. 1171–1192.

[71] S. O. Rice, "Mathematical analysis of random noise," *The Bell System Technical Journal*, vol. 23, no. 3, pp. 282–332, Jul. 1944.

[72] M. Chitre, S. Shahabudeen, L. Freitag, and M. Stojanovic, "Recent advances in underwater acoustic communications & networking," in *OCEANS*, vol. 2008-Supplement, Sep. 2008, pp. 1–10.

[73] M. Chitre, "A high-frequency warm shallow water acoustic communications channel model and measurements," *J. Acoust. Soc. America 122(5)*, p. 25802586, Nov. 2007.

[74] D. B. Kilfoyle and A. B. Baggeroer, "The state of the art in underwater acoustic telemetry," *IEEE J. Oceanic Eng.*, vol. 25, no. 1, pp. 4–27, Jan. 2000.

[75] B. Li, S. Zhou, M. Stojanovic, L. Freitag, and P. Willett, "Multicarrier communication over underwater acoustic channels with nonuniform doppler shifts," *IEEE J. Oceanic Eng.*, vol. 33, no. 2, pp. 198–209, Apr. 2008.

[76] M. Stojanovic, "Low complexity OFDM detector for underwater acoustic channels," in *OCEANS 2006*, Sep. 2006, pp. 1–6.

[77] B. Muquet, Z. Wang, G. B. Giannakis, M. de Courville, and P. Duhamel, "Cyclic prefixing or zero padding for wireless multicarrier transmissions?" *IEEE Trans. Commun.*, vol. 50, no. 12, pp. 2136–2148, Dec. 2002.

[78] B. S. Sharif, J. Neasham, O. R. Hinton, and A. E. Adams, "A computationally efficient doppler compensation system for underwater acoustic communications," *IEEE J. Oceanic Eng.*, vol. 25, no. 1, pp. 52–61, Jan. 2000.

[79] H. Liu and U. Tureli, "A high-efficiency carrier estimator for OFDM communications," *IEEE Commun. Lett.*, vol. 2, no. 4, pp. 104–106, Apr. 1998.

[80] X. Ma, C. Tepedelenlioglu, G. B. Giannakis, and S. Barbarossa, "Non-data-aided carrier offset estimators for OFDM with null subcarriers: identifiability, algorithms, and performance," *IEEE J. Sel. Areas Commun.*, vol. 19, no. 12, pp. 2504–2515, Dec. 2001.

[81] A. Mahmood and M. Chitre, “Modeling colored impulsive noise by markov chains and alpha-stable processes,” in *OCEANS-Genova*, May 2015, pp. 1–7.

[82] M. A. Chitre, J. R. Potter, and S. . Ong, “Optimal and near-optimal signal detection in snapping shrimp dominated ambient noise,” *IEEE J. Oceanic Eng.*, vol. 31, no. 2, pp. 497–503, April 2006.

[83] A. Mahmood and M. Chitre, “Optimal and near-optimal detection in bursty impulsive noise,” *IEEE J. Oceanic Eng.*, vol. 42, no. 3, pp. 639–653, July 2017.

[84] H. V. Poor, *An introduction to signal detection and estimation (2nd ed.).* Springer, 1994.

[85] S. Coleri, M. Ergen, A. Puri, and A. Bahai, “Channel estimation techniques based on pilot arrangement in OFDM systems,” *IEEE Trans. on Broadcasting*, vol. 48, no. 3, pp. 223–229, Sep. 2002.

[86] M. Stojanovic and J. Preisig, “Underwater acoustic communication channels: Propagation models and statistical characterization,” *IEEE Communications Magazine*, vol. 47, no. 1, pp. 84–89, January 2009.

[87] W. Sun and Z. Wang, “Online modeling and prediction of the large-scale temporal variation in underwater acoustic communication channels,” *IEEE Access*, pp. 1–1, 2018.

[88] R. F. Dwyer, “A technique for improving detection and estimation of signals contaminated by under ice noise,” *J. Acoust. Soc. Am*, vol. 74, no. 1, pp. 124–130, 1983.

[89] S. Zhou and Z. Wang, *OFDM for underwater acoustic communications.* John Wiley & Sons, 2014.

[90] G. Kaliraj and S. Baskar, “An efficient approach for the removal of impulse noise from the corrupted image using neural network based impulse detector,” *Image Vis. Comput.*, vol. 28, no. 3, p. 458466, 2010.

[91] I. Kauppinen, "Methods for detecting impulsive noise in speech and audio signals," in *14th Int. Conf. Digit. Signal Process.*, vol. 2, July 2002, pp. 967–970.

[92] R. Amiri, H. Mehrpouyan, L. Fridman, R. K. Mallik, A. Nallanathan, and D. Matolak, "A machine learning approach for power allocation in HetNets considering QoS," in *IEEE Int. Conf. on Commun. (ICC)*, May 2018, pp. 1–7.

[93] R. Amiri, H.Mehrpouyan, D.Matolak, and M.Elkashlan, "Joint power allocation in interference-limited networks via distributed coordinated learning," in *IEEE Vehicular Technology Conference, available online: arXiv:1806.02449*, 2018.

[94] H. Kong and L. Guan, "A noise-exclusive adaptive filtering framework for removing impulse noise in digital images," *IEEE Trans. Circuits Syst. II: Analog Digit. Signal Process.*, vol. 45, no. 3, pp. 422–428, March 1998.

[95] R. Garnett, T. Huegerich, C. Chui, and W. He, "A universal noise removal algorithm with an impulse detector," *IEEE Trans. Image Process.*, vol. 14, no. 11, pp. 1747–1754, Nov 2005.

[96] D. Middleton, "Canonical and quasi-canonical probability models of class A interference," *IEEE Trans. Electromagn. Compat.*, vol. EMC-25, pp. 76–106, 5 1983.

[97] C. L. Nikias and M. Shao, *Signal processing with Alpha-Stable Distributions and Applications.* New York: Chapman-Hall, 1996.

[98] J. B. Diederik P. Kingma, "Adam: A method for stochastic optimization," *arXiv:1412.6980v9.*

[99] X. Glorot and Y. Bengio, "Understanding the difficulty of training deep feedforward neural networks," in *Proceedings of the Thirteenth International Conference on Artificial Intelligence and Statistics*, vol. 9. PMLR, 13–15 May 2010, pp. 249–256.

[100] J. Fan, N. E. Heckman, and M. P. Wand, "Local polynomial kernel regression for

generalized linear models and quasi likelihood functions," *Journal of the American Statistical Association*, vol. 90, no. 429, pp. 141–150, 1995.